

**TARGETED DRUG DELIVERY FOR THE TREATMENT AND DIAGNOSIS OF
CARDIOVASCULAR DISEASE**

A Dissertation

Presented to

The Academic Faculty

By

Mario Daniel Martinez Sanchez

In Partial Fulfillment

Of the Requirements for the Degree

Doctor of Philosophy in the

Wallace H. Coulter Department of Biomedical Engineering

Emory University

Georgia Institute of Technology

December 2017

Copyright © Mario D. Martinez 2017

**TARGETED DRUG DELIVERY FOR THE TREATMENT AND DIAGNOSIS OF
CARDIOVASCULAR DISEASE**

Approved by:

Dr. Michael E. Davis, Advisor
School of Biomedical Engineering
Emory University

Dr. W. Robert Taylor
School of Biomedical Engineering
Emory University

Dr. Mark R. Prausnitz
School of Biomedical Engineering
Georgia Institute of Technology

Dr. Edward A. Botchwey, III
School of Biomedical Engineering
Georgia Institute of Technology

Dr. Luke P. Brewster
School of Medicine, Vascular Surgery
Emory University

Date Approved: December 1, 2016

This work is dedicated to all my family, whose support has been instrumental in everything I have achieved.

ACKNOWLEDGEMENTS

Many people have directly and indirectly formed part of this work through the support they have provided through the years. First of all, I want to thank my advisor, Michael E. Davis, for the opportunity to be part of his lab. Thank you for your continued enthusiasm, optimism and patience. You provided a space where I was able to grow and mature, and you have provided a great example to follow. I have learned a lot seeing the lab grow and change under your leadership through all these years.

I would like to thank my committee members Dr. Botchwey, Dr. Brewster, Dr. Prausnitz, and Dr. Taylor for the feedback and support that made the completion of this work possible. Thank you for challenging me to think from a different perspective and helping me understand the inherent risk of the ideas I proposed. Furthermore, thank you for following up not only on my research but also on other events in my life, and thank for all your advice. For each of the unique ways each member of my committee contributed to completing this work, thank you.

To all of my Davis Lab coworkers, both past and present, thank you for your friendship and support. To our current and former fellows and postdocs, thanks for the advice and perspective you have provided throughout. To our former graduate students, thanks for paving the way and setting things up for me to be successful. To our current graduate students, thanks for your continuous help and encouragement, particularly as I wrapped things up with this project. Special thanks to Milton Brown for all the help with different animal procedures, for your friendship, and for our many conversations about life. Also, a special thanks to Raffay Kahn for your friendship and mentorship during my first few years in the lab, which meant a lot.

I would also like to thank my family for all of their support throughout the years. To my parents, Mario and Alicia Martinez, thank you for always valuing my education and for pushing me to be the best that I can be in all aspects of my life. I would not be here today without your love, support and mentorship along the way. To my uncle Luis, thanks for being like a second dad to me, for your encouragement, and for constantly challenging me to grow. To my siblings, Karen, Luis, and Esther, thanks for believing in me, for loving me so well, and for being so willing to help with anything I have needed. To the Grazianos, thanks for being my family away from home and for all the support you have provided throughout the years.

To my wife, Morgan Mae Martinez, all I can say is that it has been quite an adventure. Thank you for being my partner, for your encouragement, and for your patience as we navigate this stage of life. You are the person I treasure the most, and I am glad to always have you on my side. I would also like to thank my two little ones, Noah and Mia, for being such a source of joy in my life.

Finally, I want to thank Mary Horton and the other Emory/BME support staff who have supported and encouraged me through all the aspects of this process, whether getting paperwork done or helping me navigating things outside of school. I am so thankful for your guidance and support and all you do to be there for the students going through this program. Thank you.

TABLE OF CONTENTS

ACKNOWLEDGEMENTS	iv
LIST OF TABLES	x
LIST OF FIGURES.....	xi
LIST OF SYMBOLS AND ABBREVIATIONS	xiii
SUMMARY.....	xvi
CHAPTER 1: INTRODUCTION.....	1
1.1: Motivation.....	1
1.2: Specific Aims	2
Specific Aim 1.....	2
Specific Aim 2.....	2
CHAPTER 2: LITERATURE REVIEW.....	4
2.1: Peripheral Artery Disease	4
2.1.1: Epidemiology.....	4
2.1.2: Risk Factors.....	5
2.1.3: Pathophysiology	5
2.1.4: Clinical Presentation.....	7
2.1.5: Current Therapies and Limitations	8
2.1.6: Therapeutic Angiogenesis.....	11
2.2: Vascular Endothelial Growth Factor.....	15
2.3: Hoechst	16
2.4: Myocarditis.....	16
2.4.1: Epidemiology.....	16
2.4.2: Pathophysiology	17
2.4.3: Clinical Presentation.....	18

2.4.4: Other Classifications	19
2.4.5: Current Therapies and Limitations	20
2.4.6: Current Diagnosis and Limitations	21
2.4.7: Targeted Molecular Imaging.....	24
CHAPTER 3: TARGETED DELIVERY OF VASCULAR ENDOTHELIAL GROWTH FACTOR FOR THE TREATMENT OF PERIPHERAL ARTERY DISEASE	25
3.1: Introduction.....	25
3.1.1: Peripheral Artery Disease.....	25
3.1.2: Therapeutic Angiogenesis.....	26
3.1.3: Vascular Endothelial Growth Factor	28
3.1.4: Hoechst.....	30
3.1.5: Approach	30
3.2: Methods and Results.....	30
3.2.1: Synthesis of Hoechst Compounds	30
3.2.2: Bioactivity of Hoechst Compounds	32
3.2.3: Animal Model of Peripheral Artery Disease.....	36
3.2.4: Retention of Hoechst Compounds in Animal Model of PAD.....	38
3.2.5: Targeting of Hoechst Compounds in Animal Model of PAD	46
3.3: Discussion.....	50
CHAPTER 4: IDENTIFICATION OF TARGETING PEPTIDES FOR THE DIAGNOSIS OF MYOCARDITIS	57
4.1: Introduction.....	57
4.1.1: Myocarditis	57
4.1.2: Current Diagnosis of Myocarditis	58
4.1.3: Targeted Molecular Imaging.....	60
4.1.4: Approach	60

4.2: Methods and Results.....	61
4.2.1: Animal Model of Experimental Autoimmune Myocarditis	61
4.2.2: Baseline Characteristics.....	62
4.2.3: <i>In Vivo</i> Phage Display	66
4.2.4: <i>Ex Vivo</i> Peptide Screening	70
4.2.5: Peptide Screening in Animal Model of Myocardial Infarction	76
4.2.6: <i>In Vivo</i> Peptide Screening	77
4.2.7: Immunohistochemistry	82
4.2.8: Proteomic Analysis.....	84
4.3: Discussion.....	86
CHAPTER 5: SUMMARY AND FUTURE DIRECTIONS.....	91
5.1: Targeted Delivery of VEGF for the Treatment of PAD	91
5.1.1: Summary.....	91
5.1.2: Limitations	92
5.1.3: Future Directions.....	93
5.2: Identification of Targeting Peptides for the Diagnosis of Myocarditis.....	94
5.2.1: Summary.....	94
5.2.2: Limitations	94
5.2.3: Future Directions.....	96
APPENDIX.....	97
A.1: Methods for Peripheral Artery Disease Project.....	97
A.1.1: Synthesis of Compounds.....	97
A.1.2: Methods for <i>In Vitro</i> Studies	98
A.1.3: Animal Models	101
A.1.4: Methods for <i>In Vivo</i> Studies.....	101
A.1.5: Statistical Analysis	103

A.2: Methods for Myocarditis Project	104
A.2.1: Animal Models	104
A.2.2: <i>In Vivo</i> Phage Display.....	105
A.2.3: Histology, Immunohistochemistry, and Immunofluorescence.....	108
A.2.4: Peptide Conjugation for <i>In Vivo</i> Delivery	111
A.2.5: <i>Ex Vivo</i> Fluorescent Imaging	112
A.2.6: Echocardiography	112
A.2.7: Proteomic Analysis	112
A.2.8: Statistical Analysis	117
REFERENCES.....	118

LIST OF TABLES

Table 1: Concentration of phages isolated from each treatment group for each panning.	68
Table 2: Sequences and known homology for the selected potential targeting peptides.	69
Appendix Table 1: List of genes used for enrichment analysis.....	115

LIST OF FIGURES

Figure 1: Schematic of Hoechst-thiopyridyl.....	31
Figure 2: Representative images of CPCs incubated with Hoechst compounds.	33
Figure 3: Western blot analysis of iMAECs treated with VEGFmp compounds.....	34
Figure 4: Representative images of iMAECs incubated with Hoechst compounds.....	35
Figure 5: Representative images of CECs forming tubes.....	36
Figure 6: Representative images of mouse model of HLI.	37
Figure 7: DNA levels in the serum of C57BL/6 mice.	38
Figure 8: Representative images of <i>in vivo</i> fluorescent imaging.....	39
Figure 9: Quantification of <i>ex vivo</i> fluorescent signal.	41
Figure 10: Western blot analysis of hindlimb tissue samples.	42
Figure 11: <i>In vivo</i> fluorescent imaging.	44
Figure 12: <i>Ex vivo</i> fluorescent imaging.	45
Figure 13: <i>In vivo</i> and <i>ex vivo</i> fluorescent imaging.....	47
Figure 14: <i>Ex vivo</i> fluorescent imaging of homogenized hindlimbs.	48
Figure 15: Representative <i>ex vivo</i> fluorescent images.....	49
Figure 16: Schematic of targeting peptides for the diagnosis of myocarditis.	61
Figure 17: Representative H&E images of animals with and without myocarditis.....	64
Figure 18: Echocardiography data of animals 21 days after initial immunization.....	65
Figure 19: Body weight of animals through 21 days after initial immunization.....	66
Figure 20: Flow diagram of <i>in vivo</i> phage display experiments.	67
Figure 21: Representative images of hearts stained with H&E and MyH-PhD-05.	71
Figure 22: Quantification of <i>ex vivo</i> MyH-PhD-05 staining at 21 days.....	72
Figure 23: Representative images of hearts stained with H&E and MyH-PhD-120.	73
Figure 24: Quantification of <i>ex vivo</i> MyH-PhD-120 staining at 21 days.....	74

Figure 25: Representative images of organs stained with targeting peptides.....	75
Figure 26: Representative images of hearts with MI stained with MyH-PhD-05.	76
Figure 27: Representative fluorescent images of hearts treated with S-MyH-PhD-05. ...	78
Figure 28: Quantification of S-MyH-PhD-05 signal in hearts at 21 days.....	79
Figure 29: Quantification of S-MyH-PhD-05 signal in organs at 21 days.....	80
Figure 30: Quantification of S-MyH-PhD-120 signal in hearts at 21 days.....	81
Figure 31: Representative images and quantification of immune cells in myocarditis. ...	83
Figure 32: List of major cellular components identified through proteomic analysis.	85

LIST OF SYMBOLS AND ABBREVIATIONS

AA:	Amino Acid
ACS:	Acute Coronary Syndrome
AMI:	Acute Myocardial Infarction
BSA:	Bovine Serum Albumin
CECs:	Cardiac Endothelial Cells
CFA:	Complete Freund's Adjuvant
CLI:	Critical Limb Ischemia
CMR:	Cardiac Magnetic Resonance
CPCs:	Cardiomyocyte Progenitor Cells
CVD:	Cardiovascular Disease
DAPI:	4',6-diamidino-2-phenylindole
DM:	Diabetes Mellitus
DAMPs:	Damage Associated Molecular Patterns
DCM:	Dilated Cardiomyopathy
DMEM:	Dulbecco Modified Eagle Medium
DNA:	Deoxyribonucleic Acid
EAM:	Experimental Autoimmune Myocarditis
ECs:	Endothelial Cells
EKG:	Electrocardiography
EMB:	Endomyocardial Biopsy
EPC:	Endothelial Progenitor Cells
ERK:	Extracellular Signal Regulated Kinases
FBS:	Fetal Bovine Serum
FGF:	Fibroblast Growth Factor

Flt:	Fms-like Tyrosine Kinase
Flk:	Fetal Liver Kinase
H&E:	Hematoxylin and Eosin
HbA1c:	Hemoglobin A1c
HGF:	Hepatocyte Growth Factor
HIF:	Hypoxia Inducible Factor
HLI:	Hindlimb Ischemia
HoVEGF ₁₆₅ :	Hoechst-thiopyridyl-VEGF ₁₆₅ – DyLight 800 Compound
HoVEGFmp:	Hoechst-thiopyridyl-VEGFmp Compound
IC:	Intermittent Claudication
IGF:	Insulin Growth Factor
IM:	Intramuscular
iMAECs:	Immortalized Mouse Aortic Endothelial Cells
ITS:	Insulin Transferrin Selenium
IV:	Intravenous
KDR:	Kinase Insert Domain Receptor-like
LDPI:	Laser Doppler Perfusion Imaging
LV:	Left Ventricle
MI:	Myocardial Infarction
MyH:	Myosin Heavy Chain Peptide
PAD:	Peripheral Artery Disease
PAMPs:	Pathogen Associated Molecular Patterns
PBS:	Phosphate Buffered Saline
PCR:	Polymerase Chain Reaction
PEG:	Polyethylene Glycol
PGF:	Placental Growth Factor

RV:	Right Ventricle
SDF:	Stromal Cell Derived Factor
SEM:	Standard Error of the Mean
TLRs	Toll-like Receptors
VEGF:	Vascular Endothelial Growth Factor
VEGFR:	Vascular Endothelial Growth Factor Receptor Tyrosine Kinase
VEGFmp:	Vascular Endothelial Growth Factor Mimetic Peptide
VEGF ₁₆₅ -Dy:	VEGF ₁₆₅ – DyLight 800

SUMMARY

Cardiovascular disease (CVD) has accounted for more deaths than any other major cause of death in the United States every year since 1900, with the exception of 1918. Despite improvements in the management of CVD, there is still a need for new and improved treatments and diagnostics. In peripheral artery disease (PAD), treatment with pro-angiogenic growth factors, such as vascular endothelial growth factor (VEGF), is currently being explored. However, there is a need to overcome limitations of this therapy, such as the growth factor's short half-life, inadequate delivery to target tissue, and inadequate retention at target tissue. In myocarditis, a large number of patients go undiagnosed due to the disease's heterogeneous etiology, pathophysiology, and clinical presentation. Current diagnostic techniques, such as endomyocardial biopsy and cardiac magnetic resonance, are inadequate, and there is a need for new technologies for the appropriate diagnosis and timely treatment of myocarditis. This dissertation aims to explore two different targeting technologies for the treatment and diagnosis of PAD and myocarditis.

In PAD, ischemic tissue undergoes necrosis and releases cellular contents, including DNA, into extracellular space. A modified Hoechst compound has been previously used to target extracellular DNA in an animal model of myocardial infarction. We explored using a similar modified Hoechst compound to target extracellular DNA in an animal model of PAD and deliver VEGF to ischemic tissue. Despite promising initial results, we did not observe any significant improvements in the retention or targeting of our compound to ischemic tissue when compared to controls.

Myocarditis is characterized by the presence of localized or diffuse inflammatory infiltrates in the myocardium. In an animal model of myocarditis, we used an *in vivo* phage display

library to identify peptides that preferentially targeted this diseased myocardium. *Ex vivo* screening of potential peptides was then used to identify two peptides whose binding correlated with disease severity. *In vivo* screening of these two peptides was then used to demonstrate that one of the peptide's binding correlated with disease severity. Immunohistochemistry and proteomic analysis were then used to demonstrate that this peptide colocalizes with immune cells in inflammatory infiltrates and binds to intracellular contents that are released into extracellular space during myocarditis.

Through these approaches, two different techniques for the treatment and diagnosis of CVD have been explored. These insights will advance the development of new techniques for the better treatment and diagnosis of CVD.

CHAPTER 1: INTRODUCTION

Cardiovascular disease (CVD) has accounted for more deaths than any other major cause of death in the United States every year since 1900, with the exception of 1918 [1, 2]. In fact, 1 person dies every 40 seconds due to CVD [1]. Furthermore, the direct and indirect costs of CVD were estimated to be around \$320 billion in 2011, a number that is expected to increase to \$918 billion by 2030 [1]. Despite improvements in the management of CVD, there is still a need for new and improved treatments and diagnostics, particularly for diseases such as peripheral artery disease (PAD) and myocarditis.

1.1: Motivation

PAD is characterized by the presence of ischemia and necrosis [3, 4], and treatment with pro-angiogenic growth factors, such as vascular endothelial growth factor (VEGF), is currently being explored [4-6]. However, there is a need to overcome limitations of this therapy, such as the growth factor's short half-life, inadequate delivery to target tissue, and inadequate retention at target tissue [5, 7, 8].

Myocarditis refers to localized or diffuse inflammation of the myocardium [9-11]. A large number of patients with myocarditis go undiagnosed due to the disease's heterogeneous etiology, pathophysiology, and clinical presentation [9, 12]. Current diagnostic techniques, such as endomyocardial biopsy and cardiac magnetic resonance, are inadequate, and there is a need for new technologies for the appropriate diagnosis and timely treatment of this disease.

1.2: Specific Aims

Our central hypothesis is that targeting technologies can improve current treatments and diagnosis of CVD. This dissertation aims to explore two different targeting technologies for the treatment and diagnosis of PAD and myocarditis.

Specific Aim 1: To evaluate the targeting potential of Hoechst compounds.

We hypothesized that Hoechst compounds would improve the retention and targeting of VEGF in an animal model of hindlimb ischemia (HLI). Two different targeting compounds were synthesized, HoVEGFmp and HoVEGF₁₆₅. To assess each compound's bioactivity, *in vitro* permeability assays, Western blot analysis, and tube formation assays were performed. To assess the retention and targeting of these compounds, each compound was delivered through an intramuscular or intravenous injection to animals with HLI followed by fluorescent imaging. We did not observe any improvements in the retention or targeting of our compound when compared to appropriate controls.

Specific Aim 2: To identify and evaluate targeting peptides for myocarditis.

We hypothesized that we could identify peptides that would preferentially target the hearts of animals with myocarditis. To identify potential targeting peptides, an *in vivo* phage display library was used in an animal model of myocarditis. Six of the identified peptides were then screened *ex vivo* on frozen sections from the hearts of animals with and without myocarditis. Two of these peptides were then screened *in vivo* using fluorescent imaging. Finally, the binding targets of one of these peptides were assessed using immunohistochemistry and proteomic analysis. We identified one peptide whose binding correlated with disease severity *in vivo*. We determined that this peptide

colocalized with immune cells in inflammatory infiltrates and bound to intracellular contents released into extracellular space during myocarditis.

CHAPTER 2: LITERATURE REVIEW

2.1: Peripheral Artery Disease

2.1.1: Epidemiology

Peripheral artery disease (PAD) affects between 8-10 million people in the United States, although estimates suggest that incidence could be as high as 18-21 million people with better diagnostic modalities and increased awareness [1, 13, 14]. The prevalence of PAD is estimated to be 10-25% in people over the age of 55, with higher prevalence observed among the elderly, non-Hispanic blacks and women [1, 3]. Globally, about 202 million people are living with PAD, with a 13-29% increase in the number of individuals with PAD in the last decade [1, 3, 13, 14]. In 2011, PAD any mention mortality in the United States was 62,183 people (age-adjusted death rate of 18.1 per 100,000 people), with PAD being the underlying cause of 13,484 of those deaths [1].

PAD is associated with hypertension, diabetes mellitus (DM), chronic kidney disease, and smoking [1]. It is also associated with significant morbidity. Patients with PAD report impaired function and quality of life, which is true even in patients that are currently asymptomatic [1]. Between 40-60% of patients with PAD will develop some degree of coronary or cerebrovascular disease [13, 14]. For patients with more severe critical limb ischemia (CLI), mortality rate can be as high as 20-25% at one year after presentation, and 40-70% at five years after presentation [3, 15]. It estimated that \$4.37 billion are spent every year in the treatment and management of PAD, with most expenditures associated with repeated hospitalizations and surgical procedures [14].

2.1.2: Risk Factors

Risk factors for PAD are similar to the risk factors of other cardiovascular diseases such as coronary artery disease [1, 3]. Known risk factors include male gender, age greater than 50, African American ethnicity, family history of vascular disease, smoking, hyperlipidemia, hypertension, DM, lifestyle (diet and exercise), hyperhomocysteinemia, and inflammation [1, 13, 15]. The two strongest risk factors for PAD are cigarette smoking and DM, with odds ratios of 1.88 and 2.72 respectively [1, 16]. Smoking cessation has been linked to a decrease in the incidence of PAD and improved outcomes in patients with intermittent claudication (IC) or who undergo surgical intervention [13]. For DM patients, a 1% increase in hemoglobin A1c (HbA1c) has been associated with a 26% increase in PAD risk, and even insulin resistance in the absence of DM increases the risk of PAD by 40-50% [3, 13].

2.1.3: Pathophysiology

PAD is the occlusion of peripheral arteries caused mainly by atherosclerosis and associated thrombosis, although other causes such as vasculitis and *in situ* thrombosis caused by hypercoagulable states have been reported [3]. Atherosclerosis is a chronic inflammatory process that begins with the dysfunction of vascular endothelial cells (ECs) that leads to the accumulation of lipids and the infiltration of monocytes in the intima of an artery [5, 17, 18]. Monocytes differentiate into macrophages, engulf the lipids present in the intima of the affected artery, and become foam cells [5, 17, 18]. At the same time vascular smooth muscle cells migrate to the intima, synthesize extracellular matrix, and form a fibrous cap [5, 16, 18]. Foam cells continue to release pro-inflammatory signals that enhance local inflammation and promote plaque growth [17]. Proteolysis and disruption of the atherosclerotic plaque eventually leads to the rupture of the plaque and the exposure of thrombogenic material into arterial circulation [17]. The thrombogenic

material causes platelets to adhere and aggregate, activating the coagulation cascade and creating a thrombus that prevents the blood flow through the peripheral arteries [5, 16-18].

The response to this gradually progressive limb ischemia involves the increase in blood flow through the promotion of angiogenesis and arteriogenesis, along with the activation other processes implicated in the ischemic response such as vascular remodeling, inflammation and apoptotic pathways [3]. In patients with the more severe CLI, these processes become ineffective, which leads to an on-going inadequate perfusion of tissue, depriving myocytes of oxygen and other nutrients [3, 4]. Within hours, these cells become either apoptotic and/or terminally necrotic, losing the ability to be rescued even with reperfusion therapy [19-21].

Apoptosis, which also known as the physiological pathway of cell death, is the mechanism used to clear cells that have become superfluous or aberrant in function [22]. It is characterized by a series of tightly regulated biochemical processes in which a cell becomes apoptotic bodies that contain nuclear contents and cell organelles [22]. These apoptotic bodies are then cleared by either macrophages or neighboring cells through phagocytosis, without releasing cellular contents into extracellular space [21, 22]. In contrast, necrosis, which is also known as the pathological pathway of cell death, is usually triggered by external disturbances such as hypoxia [22]. It is characterized by a slight initial cellular swelling followed by cell lysis and the release of cellular contents, including DNA, into extracellular space [21-23].

In patients with CLI, large areas of tissue damage and necrosis may be present, which may appear as ulcers and gangrene [3]. Since in the order of picograms of DNA are

present in each myocyte, these large areas of necrosis release large quantities of intracellular DNA into extracellular space [21, 23]. Although this DNA can be collected and measured in the blood of patients with PAD [24, 25], the concentration in blood is much lower than that found in the necrotic tissue itself, probably due to the diluting effect of the large volume of blood and the presence of serum nucleases [21]. Myocyte necrosis, depending on its extent, may lead to impaired healing, decreased muscle mass, disease progression, and loss of normal muscle function, causing significant morbidity and mortality [1, 26, 27].

2.1.4: Clinical Presentation

Although the two most widely described clinical presentations of PAD are IC and CLI, patients can present with a wide range of symptoms [5, 15, 28]. About 40% of PAD patients are asymptomatic, 10% present with IC, and about 50% present with symptoms different from classic claudication [1]. Only 1-3% of PAD patients present with the more severe CLI [29]. Patients with IC have insufficient blood flow during exercise [4, 5, 15], and they can be subdivided based on the degree of limitations observed. Patients with mild claudication show no limitations in walking, patients with moderate claudication show the ability to walk without stopping for more than 2 blocks or 200 meters or 4 minutes, while patients with severe claudication show the ability to only walk up to 2 blocks or 200 meters or 4 minutes [28]. In patients with the more severe CLI, blood flow is inadequate even at rest [4, 5, 15], and these patients can present with ischemic rest pain in the distal leg, ischemic ulcers on the distal leg, and ischemic gangrene [28]. It is important to note that this classification does not take into account different lesion and vessels characteristics, which may be important indicators of disease progression [28]. For example, patients can be classified based on other parameters such as the degree of peripheral artery stenosis, the length of the lesions observed, the degree of lesion

calcification, and the anatomic level of occlusions observed [28]. Understanding of the complex clinical presentation of patients with PAD is important, particularly when determining the proper clinical interventions and when comparing the efficacy of different novel therapies.

Although most asymptomatic patients will remain symptom free throughout the course of the disease, about 7-15% of these patients will progress to IC within five years [15]. Of these patients with IC, about 20-25% will experience further disease progression, with 1-3% requiring major amputation within five years [15]. A Gradual disease progression from asymptomatic to IC to CLI can be observed but is not typical, as more than 50% of patients undergoing amputation were symptom free six months earlier [3, 15]. Patients presenting with CLI have the worse prognosis, with 12% requiring amputation within 3 months, and a 40-70% mortality rate at five years after presentation [3, 15].

2.1.5: Current Therapies and Limitations

The standard treatment for PAD depends on the clinical presentation. For patients with IC, clinical interventions can be classified as risk factor control, pharmacological therapy, and surgical or catheter based interventions [5, 13, 14]. Risk factor control includes smoking cessation, weight loss, reduction of HbA1c levels, and increase in exercise [13, 14]. Cigarette smoking has been shown to have a negative impact on different risk factors for atherosclerotic disease, such as levels of triglycerides, low density lipoprotein cholesterol, high density lipoprotein cholesterol, and plasma fibrinogen [14]. Thus, smoking cessation leads to improvement in these risk factors and a decrease in the incidence and progression of PAD [13]. Weight loss has also been shown to improve risk factors associated with PAD, such as insulin resistance, dyslipidemia, and hypertension

[13]. For DM patients, a 1% increase HbA1c has been associated with a 26% increase in PAD risk [3, 13]. Thus, lifestyle modification, such as changes in diet and weight loss, along with pharmacological therapies should be considered in order to ensure HbA1c levels remain below 6-7% [13]. Finally, exercise has been linked with functional improvement in patients with IC through different proposed mechanisms, such as arterial collateralization, increased capillary density and permeability, increased vascular endothelial growth factor (VEGF) levels, increased release of nitric oxide caused by shear stress, reduced blood viscosity, increased mitochondrial function leading to enhanced oxygen extraction ratios, improved gait proficiency, reversal of metabolic myopathies, and decreased endothelial inflammation [14]. The appropriate exercise program depends on the clinical presentation of each individual patient [13, 14].

Pharmacological therapies for patients with IC can be divided into therapies that improve cardiovascular outcomes and therapies that provide symptomatic relief [14]. Medications that improve cardiovascular outcomes include antiplatelet agents, β -blockers, angiotensin converting enzymes, thiazides, and statin drugs [14, 15]. These drugs focus on controlling risk factors of PAD, such as hypertension and hyperlipidemia, and have been shown to reduce adverse cardiovascular events [14]. Medications that improve IC symptoms include cilostazol, pentoxifylline, and naftidrofuryl oxalate [14, 15]. Cilostazol has antiplatelet properties, increases vasodilation, increases plasma high density lipoprotein level and decreases triglyceride levels [5, 14]. In clinical studies, cilostazol has been shown to increase pain free walking distance by 65-83% after 24 weeks [5, 14]. Pentoxifylline improves red blood cell deformability, lowers fibrinogen levels, and inhibits platelet aggregation. However, the clinical benefit of pentoxifylline is undetermined and may not be different from placebo [5, 14]. Naftidrofuryl oxalate is believed to be a

vasoactive drug that offers modest improvement in walking distance with minimal side effects. However, there is little follow up data beyond six months and cost effectiveness remains questionable [15].

Finally, for IC patients with severe impairment in their occupational and leisure time capabilities, surgical or catheter based interventions can be considered [14, 15]. The goal of this intervention is to preserve and improve functional capacity and limb salvage [14, 15]. These procedures are not common in patients with IC, and are usually reserved for patients with CLI [14, 15].

For patients with CLI, the same risk factor control and pharmacological therapies as those given to patients with IC are administered as complements to revascularization [3, 5, 29]. Revascularization can be classified as endovascular interventions, surgical interventions, or a combination of both [3, 5, 29]. Endovascular interventions include angioplasty and stents, with many new drug eluting balloons and stents currently being explored [15, 29]. Surgical interventions include bypass surgery with a single reversed or in situ saphenous vein or other conduits, such as spliced arm and leg veins or prosthetic polytetrafluorethylene [15, 29]. Some studies suggest that outcomes in patients that undergo endovascular interventions are similar to those that undergo surgical interventions with regards to 5 year amputation free survival and mortality, thus many patients receive endovascular interventions first, followed by surgical interventions if there is a loss of patency [3, 29].

Unfortunately, a significant number of PAD patients do not respond to pharmacologic therapies and are not suitable candidates for surgery due to comorbidities or unfavorable anatomy, leaving amputation as their only treatment option [4-6, 13, 15, 16]. The prognosis of PAD patients that undergo amputation does not significantly improve, with a 30-50% mortality rate within 2 years of surgery and quality of life indices similar to those of terminal cancer patients [6].

2.1.6: Therapeutic Angiogenesis

New blood vessel formation, or neovascularization, is thought to be result of three distinct processes: angiogenesis, arteriogenesis, and vasculogenesis [5]. Angiogenesis refers to the sprouting of new capillaries from pre-existing ones, a process caused by hypoxia and mediated by hypoxia inducible factor (HIF)-1 α and VEGF [5]. Arteriogenesis refers to the maturation of pre-existing collaterals or de novo formation of mature vessels capable of carrying significant blood flow. This process is caused by shear stress and inflammation and is mediated by invasion of immune cells and the production of fibroblast growth factors (FGFs) [5]. Vasculogenesis refers to in situ formation of blood vessels from endothelial progenitor cells (EPCs) [4, 5]. All three processes are active and work together to produce new blood vessels in adults [5].

For PAD patients that remain refractory to the standard pharmacologic and surgical treatments, one novel approach being investigated is known as therapeutic angiogenesis, in which pro-angiogenic signals are delivered into ischemic tissue in order to enhance collateral circulation and blood flow [4-6, 26]. These pro-angiogenic signals can be classified into cell-based therapies and growth-factor-based therapies. Despite promising

results in animal models and phase I/II clinical studies, no new therapies for PAD patients have been successfully developed [4-6, 19, 26, 27, 30].

2.1.6.1: Cell-Based Therapies

Cell-based therapies have focused on the delivery of different stem cells to ischemic tissue in patients with PAD. Cells of interest include purified EPCs and EPC progenitor cells, such as bone marrow mononuclear cells and peripheral blood mononuclear cells. In different animal models, these cells have been shown to induce neovascularization [4-6]. In clinical studies, delivery of these cells has led to improvements in different end points such as vascularization, ulcer healing, and limb salvage. However, most of these studies enroll a low number of patients, have different clinical inclusion criteria, use different end points, and involve mostly case reports and pilot studies. Furthermore, significant adverse events such as worsening of lesions and development of arteriovenous shunts were reported [4]. It is also not clear which cell types should be used, which markers should be used to define these cells, what cell source to use in order to avoid immunogenic rejection, what number of cells should be administered due to low retention rates, what the mechanisms of action of these cells are, or what the long-term effects of these cells are [4-6, 27]. One mechanism proposed suggests that these cells exert their angiogenic effect through the secretion of different growth factors such as VEGF instead of through their incorporation into ischemic tissue, which has led to the development of different growth-factor-based therapies [4, 6, 19].

2.1.6.2: Growth-Factor-Based Therapies

Growth-factor-based therapies have focused on the delivery of growth factors to ischemic tissue using gene therapy or direct delivery of recombinant proteins. Several different pro-angiogenic growth factors have been studied, including VEGF, acidic FGF (FGF-1), basic

FGF (FGF-2), hepatocyte growth factor (HGF), and HIF-1 [4, 5, 31]. These growth factors have shown increases in blood vessel formation and myocyte regeneration when delivered as either gene therapy or recombinant proteins in different animal models [4, 7, 26, 27, 32, 33]. Despite their apparent safety in phase I/II clinical trials, several concerns remain regarding the systemic distribution of growth factors. For example, delivery of growth factors can lead to plaque growth and destabilization in patients with atherosclerotic disease, leading to thrombus formation and adverse cardiovascular events. The presence of growth factors in orbital fluid can also lead to the development of proliferative retinopathy. Finally, the presence of growth factors can lead to accelerated tumor growth or metastasis [4, 5]. Interestingly, one of the proposed mechanism of action of growth factors such as VEGF and stromal cell derived factor-1 (SDF-1) is their involvement in EPC recruitment, retention, and differentiation at the site of injury, suggesting there is a close relationship between cell-based therapies and growth-factor based therapies [4].

3.1.6.2.1: Gene Therapy

Gene therapy techniques involve the delivery of plasmid DNA or replication-defective adenovirus containing the gene of interest [4, 5]. Although other viral vectors have been utilized for gene therapy, such as adeno-associated virus and lentiviral vectors, these vectors integrate into the host genome and there are concerns regarding their safety [5]. Phase I/II clinical trials using different gene therapy techniques have shown conflicting results. For example, one clinical trial using a plasmid encoding human VEGF suggested an improvement in different endpoints such as ulcer healing and rest pain, and showed the development of new collateral vessels. However, a different clinical trial using a similar plasmid encoding human VEGF showed no decrease in amputation events [4]. This variability is probably due to the low number of patients in each study, different clinical

criteria for each study, and the different end points used for each study [4]. Furthermore, some clinical studies reported adverse events such as the development of local, moderate, or severe edema and the development of spider angiomas [4, 6]. There are also concerns about the poor efficiency of gene transfer, the variability in the level and duration of the gene expression among patients, the patient's immune and/or inflammatory response against viral vectors, and the numerous potential side effects caused by systemic distribution of the gene [4, 6-8].

2.1.6.2.2: Recombinant Proteins

Delivery of angiogenic recombinant proteins can be done systemically, intra-arterially or via direct intramuscular (IM) injection [5]. Phase I/II clinical trials using recombinant proteins have shown mixed results. A clinical trial in which recombinant FGF-2 was delivered to patients with IC showed increases in peak walking time compared to placebo; however, no functional improvements in activities of daily living or quality of life were observed [6, 31]. When compared to gene therapy, recombinant proteins offer better temporal control, more defined dosing, and no inflammatory response compared to gene therapy. However, there are concerns over the protein's short half-life, inadequate retention at target tissue, inadequate delivery, and numerous systemic side effects [5, 7, 8, 19, 26, 33-35].

2.1.6.2.3: Bioengineered Approaches for Protein Delivery

To address the limitations of direct recombinant protein administration, new techniques that provide localized, sustained delivery of protein to ischemic tissue have been developed. For example, VEGF has been packed in different nanoparticles and biodegradable polymers and shown promising results in different animal models of cardiovascular disease [19, 27, 36-40]. However, the current processing conditions to make these polymers can reduce the bioactivity of recombinant proteins such as VEGF

[41], and the delivery of some polymers and nanoparticles requires either catheterization of the unaffected femoral artery or invasive surgical implantation within ischemic tissue. Although feasible, these invasive techniques are less favored than an IM or intravenous (IV) injection [19, 26, 41-44].

2.2: Vascular Endothelial Growth Factor

The VEGF family is a family of glycoproteins that includes VEGF-1 (VEGF-A), VEGF-2 (VEGF-C), VEGF-3 (VEGF-B), VEGF-D, VEGF-E, and placental growth factor (PGF) [5, 45]. Of these, the most potent and best characterized proangiogenic factor is VEGF-1, which contains at least four different isoforms of different amino acid length: VEGF₁₂₁, VEGF₁₆₅, VEGF₁₈₉, and VEGF₂₀₆ [4, 5, 26, 46]. VEGF₁₂₁ and VEGF₁₆₅ are secreted as soluble factors into the extracellular space, while VEGF₁₈₉ and VEGF₂₀₆ are secreted but remain cell or matrix associated [5, 46]. Both of the secreted isoforms have similar angiogenic and mitogenic potency, but VEGF₁₆₅ is more predominant and retains its heparan sulfate and heparin binding capacity [4, 45, 46].

Ligands in the VEGF family bind to three different tyrosine kinase receptors: 1) Flt-1 (VEGFR-1), 2) KDR/Flk-1 (VEGFR-2), and 3) Flt-4 (VEGFR-3) [5, 45]. VEGFR-2 is thought to transduce angiogenic signals and is predominantly found on vascular ECs and their embryonic precursors [5]. VEGFR-2 has several phosphorylation sites, and activation of VEGFR-2 by its ligand induces EC survival, proliferation and migration *in vitro*, and it leads to an increase in vascular permeability and the formation of vascular tubes (i.e.: angiogenesis) *in vivo* [33, 45, 46]. Many different proteins and pathways are involved in these processes. For example, phosphorylation of Tyrosine¹¹⁷⁵ has been linked to the

activation of the protein kinase C [45, 47], which in turn activates the ERK1/2 pathway and leads proliferation of ECs [45, 48]

Structurally, VEGFs are generally homodimeric peptides stabilized into its quaternary structure through different disulfide bonds [45, 46]. The 8 different cysteine residues that are involved in intra- and inter-chain disulfide bonds are conserved among the different VEGF isomers [46]. Of particular interest for this project, VEGF₁₆₅ contains an additional 8 free cysteine residues that are not involved in disulfide bonds while VEGF₁₂₁ does not contain any.

2.3: Hoechst

Hoechst is a fluorescent molecule that has high affinity (~60nM) and high specificity for the A-T rich sequences of double stranded DNA [21, 23, 49]. Hoechst is biocompatible in humans [23, 50, 51], and it has been previously modified at its terminal phenol without losing its ability to bind with DNA [21, 23]. The incorporation of a polyethylene glycol (PEG) linker has been used to increase the compound's hydrophilicity and prevent it from crossing the cell membrane and binding to healthy tissue in *in vivo* applications [21, 23].

2.4: Myocarditis

2.4.1: Epidemiology

Cardiomyopathy and myocarditis are an increasing global medical problem, particularly in the pediatric population [52]. Due to heterogeneous clinical presentation, patient cases of myocarditis are believe to be significantly underestimated [53]. In the United States, the incidence of cardiomyopathy in infants less than 1 year of age is estimated to be 8.34

cases per 100,000 [1]. The most common form of cardiomyopathy in children is dilated cardiomyopathy (DCM), with an estimated annual incidence in infants less than 1 year of age of 4.40 cases per 100,000 [1]. Although the cause of DCM remains unidentified in 66% of cases, myocarditis accounts for 46% of the known causes [1, 52]. Globally, the prevalence of myocarditis is estimated to be about 22 per 100,000 patients, with the number of deaths attributed to cardiomyopathy and myocarditis increasing by 40.8% between 1990 and 2010 (from 286,800 to 403,900), even though the age standardized death rate decreased by 9.8% (from 6.7 to 6.1 deaths per 100,000) [1, 53]. In adolescents and young adults, myocarditis is implicated in 12% of sudden cardiac deaths [12]. In adults, myocarditis ranks as the third leading cause of sudden cardiac death in competitive athletes [53]. Myocarditis is also associated with significant morbidity. It accounts for ~11% of heart failure cases, and it is the most common cause for heart transplantation worldwide due to the lack of appropriate diagnostics and treatments [54].

2.4.2: Pathophysiology

Myocarditis refers to localized or diffuse inflammation of the myocardium [9-11]. It is a complex disease that can be caused by infections (bacterial, rickettsial, mycotic, protozoan, and viral agents), cardiotoxic agents (drugs, toxins, and alcohol), or autoimmune disease, but many cases remain idiopathic [9, 11, 12, 54-59]. Although the exact mechanisms through which myocarditis develops are not well understood for most of these causing agents, evidence suggests that myocarditis is mediated by the direct injury of the causing agent and the indirect injury of the innate and adaptive immune systems of the host [10, 12, 53, 54].

The development of myocarditis after coxsackie B3 Virus infection has been extensively studied in both animal and tissue cultures cells [11, 53]. In this model, three different

phases can be observed [11, 12, 53, 54, 56]. In the first phase, the virus infects cardiomyocytes, replicates, and induces the destruction of cardiomyocytes [11, 58]. Viral proteases are involved in both inducing apoptosis and enhancing proteolytic activity and necrosis in cardiomyocytes [11, 12, 56, 57]. The innate immune system is activated, and an invasion of natural killer cells and macrophages followed by T lymphocytes is observed [12, 53, 57]. During this phase, the innate immune system is activated through different mechanisms including pro-inflammatory cytokines, suppressors of cytokine signaling proteins, and Toll-like receptors (TLRs) [11, 54]. TLRs are able to recognize damage associated molecular patterns (DAMPs) and pathogen-associated molecular patterns (PAMPs), which may enhance cardiac cell injury or result in the efficient clearance of the virus (i.e.: asymptomatic myocarditis) [11]. This acute phase lasts a few days [56, 57]. In the second phase, the presence of the viral genome even in the absence of viral replication leads to immune dysregulation, which is characterized by maintenance of an immune response with continuous injury to the heart [11]. The adaptive immune system is activated, and autoimmune reactions develop, mediated by viral specific T-cells targeting host myocytes by molecular mimicry, as well as by cytokines and antibodies to both viral and cardiac proteins [56-58]. This second phase last weeks to months, resulting in either the pathogen being cleared or the continuation of an autoimmune process [56, 57]. In the third phase, the presence of circulating cross reacting autoantibodies in addition to the virus-induced cardiomyocyte injury and the resulting release of cytokines leads to remodeling of the heart and the development of DCM [11, 12, 53, 56-58].

2.4.3: Clinical Presentation

The clinical presentation of patients with myocarditis tends to be heterogeneous, but it can be divided based on different cluster of symptoms observed: asymptomatic, acute coronary syndromes (ACS-like), new-onset heart failure, life threatening arrhythmias, and

chronic heart failure [9, 12, 55]. The signs and symptoms of these clinical presentations are not specific to myocarditis. For patients presenting with ACS-like symptoms, myocarditis is often hard to differentiate from acute myocardial infarction (AMI) [9]. In fact, even when coronary angiography studies reveal patent coronary arteries, AMI secondary to vasospasm or embolism is assumed instead of myocarditis [9]. For patients presenting with new onset heart failure, myocarditis is assumed only when other causes, such as ischemic or valvular heart disease, are excluded [9]. Myocarditis patients can also present with a wide range of life threatening arrhythmias, including atrioventricular blocks, ventricular fibrillation/flutter, and sustained ventricular tachycardia [9]. However, myocarditis is only suspected in these patients in the absence of coronary artery disease or other electrophysiological abnormalities. Finally, although myocarditis induced DCM is one of the main causes of heart failure, there are various other causes of DCM, and in 66% of the cases the cause remains unidentified [1, 9]. Further complicating the clinical picture, pediatric patients often present with nonspecific symptoms, and infants in particular are often unable to verbalize what these symptoms are [12, 56, 59].

2.4.4: Other Classifications

Beyond the wide range of etiologies and heterogeneous clinical presentation, myocarditis can also be classified based on different parameters such as symptom onset and histological findings [9, 53]. Based on symptom onset, myocarditis can be classified as fulminant, acute or chronic. Chronic myocarditis can be further subdivided based on the level of inflammation: persistent inflammation, chronic viral infection (with or without inflammation), and healed inflammation (with or without irreversible damage to the heart) [9, 58]. Pediatric patients usually present with fulminant myocarditis [53].

The infiltration of immune cells in myocarditis can be either diffuse or focal [53]. Based on the type of infiltrative cells observed on histological samples, myocarditis can be classified into lymphocytic, giant cell, granulomatous, eosinophilic and neutrophilic myocarditis [9]. Lymphocytic myocarditis is the most commonly observed [55]. Giant cell myocarditis is characterized by the presence of multinucleated giant cells, with an autoimmune response being the probable cause [53, 55]. Giant cell myocarditis is also one of the most rapidly progressing forms of myocarditis [55]. Eosinophilic myocarditis is characterized by eosinophilic infiltrate and is sometimes referred to as hypersensitivity myocarditis [53, 55]. It has an acute onset, rapid progression, and extensive necrosis, which is why it is also sometimes referred to as necrotizing eosinophilic myocarditis [53, 55].

2.4.5: Current Therapies and Limitations

The cornerstone therapy of myocarditis is supportive therapy and symptomatic relief, as many myocarditis patients will eventually recover with little or no cardiac consequences [9, 12, 56]. The supportive therapy of choice depends on the clinical presentation, and it includes diuretics, inotropes, afterload reduction agents, β blockers, and antidysrhythmics [12, 56]. For patients with life threatening arrhythmias, the placement of a pacemaker or defibrillator may be necessary [12, 56]. For patients with new-onset heart failure and chronic heart failure that fail to improve, extracorporeal membrane oxygenation and long term ventricular assist devices may be options [12, 56]. For some patients, the cardiac damage and function impairment may be so extensive as to require heart transplantation, which is particularly true in patients presenting with DCM [53, 56].

The use of immunosuppressive agents has been met with mixed results, as most clinical evidence is based on small clinical studies with a wide range of clinical inclusion criteria [9, 53, 56]. In general, immunosuppressive therapy seems to benefit chronic patients but

not acute patients [53], although some argue that autoimmune therapy is only beneficial in autoimmune mediated myocarditis and can even be detrimental in viral myocarditis [9].

The use of antivirals and antibiotics is recommended only when treatable causes of myocarditis can be identified [56]. For example, patients with myocarditis associated with Epstein-Barr virus and varicella virus have been reported to benefit from the use of acyclovir [56]. Similarly, phase II clinical trials have demonstrated that IV delivery of Interferon- β eliminates the viral load and improves clinical symptoms of myocarditis [54]. Despite these promising results, the use of antivirals and antibiotics is limited by nonspecific targeting, unclear mechanisms, and numerous side effects [53].

2.4.6: Current Diagnosis and Limitations

The heterogeneous etiology, pathophysiology, and clinical presentation of myocarditis makes it one of the most challenging diagnosis in cardiology and leads to the under-diagnosis of cases of myocarditis [9, 12]. Patients suspected of myocarditis will undergo many different diagnostic tests, including electrocardiography (EKG), chest radiography, and echocardiography [56]. However, the two diagnostic modalities with the greatest sensitivity for myocarditis are endomyocardial biopsy (EMB) and cardiac magnetic resonance (CMR) imaging [9].

2.4.6.1: Endomyocardial Biopsy

The gold standard for the diagnosis of myocarditis is EMB, complemented by immunohistochemistry and PCR [9, 11, 12, 53, 55-57, 60]. This procedure provides information about the presence of viral genome, fibrosis, cell death, the type of inflammatory infiltration, and the deposition of iron proteins or lipids [9, 59]. The procedure is considered to be safe when performed by experienced physicians; however, it is an

invasive procedure that has some risk of serious complications, particularly in children with rates as high as 10.6% [9, 12, 57, 59, 61]. These complications include cardiac perforation with tamponade, ventricular or supraventricular arrhythmias, heart block, pneumothorax, hemothorax, puncture of central arteries, pulmonary embolization, venous hematoma, damage to the tricuspid valve, stroke, and death [9, 12, 55, 57, 61]. Furthermore, studies that compared the performance of EMB to the *ex vivo* evaluation of hearts with myocarditis found that EMB misses approximately half of the diagnoses, even when 10 biopsy samples were analyzed [9]. Due to the diffuse nature of myocarditis, it is estimated that 17 biopsies are needed to reach a sensitivity of only 80% [9, 57], and thus there is a decreased reliance on EMB particularly in pediatric populations in the United States [56-58]. The type of infiltrative cells observed in patients with myocarditis also seems to play a role in the sensitivity of EBM, with low sensitivities corresponding to lymphocytic myocarditis and high sensitivities (80-85%) corresponding to giant cell myocarditis or eosinophilic myocarditis [55].

2.4.6.2: Cardiac Magnetic Resonance

CMR is a non-invasive imaging modality that allows us to assess the structure and function of the heart [9]. It can be used to demonstrate typical features of acute myocarditis such as dysfunction, edema and necrosis [9, 53, 56, 57, 59, 60]. The use of contrast agents, such as gadolinium based contrast agent, can provide enhanced signal, particularly in regions of necrosis or fibrosis as a result of myocarditis [9, 12, 53, 59]. Studies that compared the performance of CMR to biopsy samples reported sensitivities between 47% and 74% depending on the modality used [9]. Despite improvements in the diagnostic criteria used with CMR, the diagnosis of a substantial number of patients may still be missed, particularly in patients in the chronic phase of myocarditis [9, 60]. Furthermore, CMR cannot be used to determine the underlying cause of myocarditis, to stratify the risk

of different patients, and the findings have not yet been validated in pediatric patients [9, 56, 57].

2.4.6.3: Other Diagnostic Studies

Patients with myocarditis will present with different abnormalities in various different imaging studies. Between 93-100% of patients with myocarditis will present some sort of abnormality on EKG, between 60-90% will also present with some sort of abnormality on chest radiography, and many of them will also present with left ventricular or biventricular dysfunction on echocardiography [12, 56]. These imaging modalities can be used for risk stratification, initial screening, or to eliminate other underlying causes, but they have low diagnostic value, low sensitivity, and do not provide direct evidence for a diagnosis of myocarditis [53, 56]. Troponin levels and inflammatory markers such as white blood cell count, C-reactive protein, and erythrocyte sedimentation rate, are usually elevated in patients with myocarditis, but these tests lack the sensitivity and specificity necessary to diagnose myocarditis and may be elevated due to other underlying causes such as AMI [56]. Finally, Microbiological studies have very low diagnostic yields, but samples should be obtained early in patients suspected of myocarditis [56].

2.4.6.4: Diagnostic Approach

Patients clinically suspected of myocarditis will undergo different evaluations including EKG, chest radiography, troponin levels, inflammatory markers, and echocardiography, which will eliminate other causes of cardiac clinical symptoms and provide insight as to the risk of myocarditis [9, 56]. Patients still suspected of myocarditis should always be evaluated with CMR when possible [9]. EMB should be required in all patients that are hemodynamically unstable in order to differentiate between viral and autoimmune disease and inform on the use of immunosuppressive therapy [9]. EMB should also be considered

in all patients with new onset heart failure and life threatening arrhythmias whose clinical presentation fails to improve [9]. EMB should not be performed on patients with ACS-like presentation, as these patients tend to have excellent prognosis [9].

2.4.7: Targeted Molecular Imaging

Due to the low diagnostic value, sensitivity, and specificity of current imaging techniques [9, 53, 56, 57, 60], modifications to these imaging techniques that allow for the targeted molecular imaging of myocarditis are currently being explored. For example, targeted molecular imaging using fluorine-19 in CMR has been shown to detect myocardial inflammation in an animal model of experimental autoimmune myocarditis (EAM) through the incorporation of fluorine-19 into macrophages, dendritic cells, and granulocytes [62]. However, fluoride-19 is not specific to myocarditis and can be incorporated by macrophages and monocytes in other disease processes such as pneumonia, allograft rejection, cardiac ischemia, and cerebral ischemia [62]. Similarly, microbubbles with modifications or coated with antibodies targeting leukocytes, endothelial cells, and T-lymphocytes were shown to enhance ultrasound signal in animals with EAM; however, the use of antibodies in therapies is limited by production costs, low tissue penetration, and host immune response to antibody [63, 64].

CHAPTER 3: TARGETED DELIVERY OF VASCULAR ENDOTHELIAL GROWTH FACTOR FOR THE TREATMENT OF PERIPHERAL ARTERY DISEASE

3.1: Introduction

3.1.1: Peripheral Artery Disease

Peripheral artery disease (PAD) affects between 8-10 million people in the United States, and it is associated with significant morbidity and mortality. In 2011, PAD any mention mortality in the United States was 62,183 people (age-adjusted death rate of 18.1 per 100,000 people), with PAD being the underlying cause of 13,484 of those deaths [1]. Patients with PAD report impaired function and quality of life, which is true even in patients that are currently asymptomatic [1]. It estimated that \$4.37 billion are spent every year in the treatment and management of PAD, with most expenditures associated with repeated hospitalizations and surgical procedures [14].

PAD is characterized by the occlusion of peripheral arteries caused mainly by atherosclerosis and associated thrombosis [3, 5, 16-18]. The body responds to this gradually progressive limb ischemia by increasing blood flow through the promotion of angiogenesis and arteriogenesis [3]. In patients with the more severe critical limb ischemia (CLI), these processes become ineffective, which leads to an on-going inadequate perfusion of tissue, depriving myocytes of oxygen and other nutrients [3, 4]. Within hours, these cells become either apoptotic and/or terminally necrotic, losing the ability to be rescued even with reperfusion therapy [19-21]. During necrosis, the membrane integrity of these necrotic myocytes becomes compromised, resulting in the release of cellular contents, including DNA, into extracellular space [21-23]. Myocyte necrosis, depending on

its extent, may lead to impaired healing, decreased muscle mass, disease progression, and loss of normal muscle function, causing significant morbidity and mortality [1, 26, 27]

The standard treatment for PAD depends on the clinical presentation. For patients with the less severe intermittent claudication (IC), clinical interventions include risk factor control (smoking cessation, weight loss, reduction of hemoglobin A1c levels, and increase in exercise), pharmacological therapy (antiplatelet agents, β -blockers, angiotensin converting enzymes, thiazides, and statin drugs, cilostazol, pentoxifylline, and naftidrofuryl oxalate), and in some cases surgical or catheter based interventions [5, 13-15]. For patients with CLI, risk factor control and pharmacological therapies are administered as complements to revascularization, which can be done through endovascular interventions, surgical interventions, or a combination of both [3, 5, 29]. Unfortunately, a significant number of PAD patients do not respond to pharmacologic therapies and are not suitable candidates for surgery due to comorbidities or unfavorable anatomy, leaving amputation as their only treatment option [4-6, 13, 15, 16]. The prognosis of PAD patients that undergo amputation does not significantly improve, with a 30-50% mortality rate within 2 years of surgery and quality of life indices similar to those of terminal cancer patients [6].

3.1.2: Therapeutic Angiogenesis

For PAD patients that remain refractory to the standard pharmacologic and surgical treatments, one novel approach being investigated is known as therapeutic angiogenesis, in which pro-angiogenic signals are delivered into ischemic tissue in order to enhance collateral circulation and blood flow [4-6, 26]. These pro-angiogenic signals can be classified into cell-based therapies and growth-factor-based therapies. Despite promising

results in animal models and phase I/II clinical studies, no new therapies for PAD patients have been successfully developed [4-6, 19, 26, 27, 30].

Cell-based therapies have focused on the delivery of purified endothelial progenitor cells (EPCs) and EPC progenitor cells to ischemic tissue in patients with PAD. Animal and clinical studies have shown these cells can induce angiogenesis and symptomatic improvement [4-6]. Despite these promising results, many questions remain, such as which cell types to use, which markers to use to define these cells, what cell source to use to avoid immunogenic rejection, what number of cells to administer due to low retention rates, what are the mechanisms of action of these cells, or what are the long-term effects of these cells [4-6, 27]. One mechanism proposed suggests that these cells exert their angiogenic effect through the secretion of different growth factors, such as vascular endothelial growth factor (VEGF), instead of through their incorporation into ischemic tissue, which has led to the development of different growth-factor-based therapies [4, 6, 19].

Growth-factor-based therapies have focused on the delivery of growth factors to ischemic tissue using gene therapy or direct delivery of recombinant proteins. Several different pro-angiogenic growth factors have been studied, including VEGF, acidic fibroblast growth factor (FGF-1), basic fibroblast growth factor (FGF-2), hepatocyte growth factor (HGF), and hypoxia inducible factor (HIF)-1 [4, 5, 31]. These growth factors have induced angiogenesis and myocyte regeneration when delivered as either gene therapy or recombinant proteins in different animal models [4, 7, 26, 27, 32, 33]. Furthermore, different phase I/II clinical studies have shown the safety of these approaches [4-6, 31]. Despite these results, several concerns remain regarding the systemic distribution of growth factors, such as the promotion of plaque growth and destabilization in patients with

atherosclerotic disease, the development of proliferative retinopathy, or the acceleration of tumor growth or metastasis [4, 5]. Specific to gene based therapies, there are also concerns about the poor efficiency of gene transfer, the variability in the level and duration of the gene expression among patients, and the patient's immune and/or inflammatory response against viral vectors [4, 6-8]. In contrast to gene therapy, recombinant proteins offer better temporal control, more defined dosing, and no inflammatory response; however, there are concerns over the protein's short half-life, inadequate retention at target tissue, and inadequate delivery to target tissue [5, 7, 8, 19, 26, 33-35].

To address the limitations of direct recombinant protein administration, new techniques that provide localized, sustained delivery of protein to ischemic tissue have been developed. For example, VEGF has been packed in different nanoparticles and biodegradable polymers and shown promising results in different animal models of cardiovascular disease [19, 27, 36-40]. However, the current processing conditions to make these polymers can reduce the bioactivity of recombinant proteins such as VEGF [41], and the delivery of some polymers and nanoparticles requires either catheterization or invasive surgical implantation within the ischemic tissue. Although feasible, these invasive techniques are less favored than an intramuscular (IM) or intravenous (IV) injection [19, 26, 41-44].

3.1.3: Vascular Endothelial Growth Factor

One of the most potent and best characterized pro-angiogenic factors is VEGF-1 [4, 5, 26, 45, 46]. Alternative splicing of VEGF-1 leads to the production of different isoforms, of which only VEGF₁₂₁ and VEGF₁₆₅ are secreted as soluble factors into extracellular space [4, 5, 26, 46]. Both of these secreted isoforms have similar angiogenic and mitogenic potency, but VEGF₁₆₅ is more predominant and retains its heparan sulfate and heparin

binding capacity [4, 45, 46]. Structurally, VEGFs are generally homodimeric peptides stabilized into its quaternary structure through different disulfide bonds [45, 46]. The 8 different cysteine residues that are involved in intra- and inter-chain disulfide bonds are conserved among the different VEGF isomers, including VEGF₁₂₁ and VEGF₁₆₅ [46]. Of particular interest for this project, VEGF₁₆₅ contains an additional 8 free cysteine residues that are not involved in disulfide bonds while VEGF₁₂₁ does not contain any.

It has been suggested that the use of shorter bioactive peptide sequences derived from growth factor proteins could be advantageous in certain applications, as long as these peptides retain the same bioactivity [65]. For VEGF, a mimetic peptide (QK, Sequence: Ac-KLTWQELYQLKYKGI-amide) that offers lower molecular and biological complexity than VEGF₁₆₅, but retains VEGF₁₆₅'s angiogenic activity has been previously developed and tested both *in vitro* and *in vivo* [65-67]. This peptide is easier to manipulate, and it only interacts with its specific VEGF Receptor (VEGR)-2, thus avoiding any off target effects that VEGF₁₆₅ might have [67].

Ligands in the VEGF family bind to three different tyrosine kinase receptors: 1) Flt-1 (VEGFR-1), 2) KDR/Fik-1 (VEGFR-2), and 3) Flt-4 (VEGFR-3) [5, 45]. VEGFR-2 is thought to transduce angiogenic signals and is predominantly found on vascular endothelial cells and their embryonic precursors [5]. Activation of VEGFR-2 by its ligand induces EC survival, proliferation and migration *in vitro*, and it leads to an increase in vascular permeability and the formation of vascular tubes (i.e.: angiogenesis) *in vivo* [33, 45, 46].

3.1.4: Hoechst

Hoechst is a fluorescent molecule that has nanomolar affinity for the A-T rich sequences of double stranded DNA [49, 68]. Hoechst is biocompatible in humans [50, 51], and it has been previously modified without losing its ability to bind with DNA [23, 68]. In previous studies, a modified Hoechst has been used to deliver Insulin Growth Factor (IGF)-1 to necrotic tissue in an animal model of myocardial infarction by binding to extracellular DNA [23]. Thus, a modified Hoechst should also bind to the high concentrations of DNA released into extracellular space by necrotic tissue in PAD [68].

3.1.5: Approach

We developed a novel delivery system in which a modified Hoechst compound can be used to deliver either a VEGF mimetic peptide (VEGFmp) or VEGF₁₆₅ to the necrotic tissue in PAD. We hypothesized that both of our compounds, Hoechst-VEGFmp (HoVEGFmp) or Hoechst-VEGF₁₆₅ (HoVEGF₁₆₅), would be retained in and/or target necrotic tissue in animal model of PAD. This approach could enhance the pro-angiogenic effects of VEGF therapy, reduce its side effects, and lead to improved clinical outcomes in PAD patients.

3.2: Methods and Results

3.2.1: Synthesis of Hoechst Compounds

We modified Hoechst by adding a polyethylene glycol (PEG) chain that will render the compound cell impermeable, ensuring it will only target extracellular DNA released by necrotic cells [21, 23]. Furthermore, a thiopyridyl moiety was attached to the PEG chain in order to permit the cysteine-specific incorporation of this compound to recombinant proteins or peptides by forming disulfide bonds [69] (Figure 1).

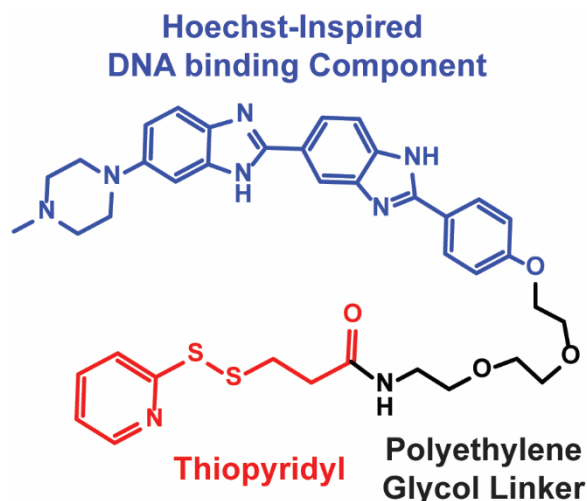


Figure 1: Schematic of Hoechst-thiopyridyl. A modified Hoechst derivative, Hoechst-thiopyridyl, was synthesized by adding a PEG linker (in black) and thiopyridyl moiety (in red) to Hoechst (in blue).

3.2.1.1: HoVEGFmp

We used the VEGF mimetic peptide (QK, Sequence: Ac-KLTWQELYQLKYKGI-amide [66]) due to its lower molecular and biological complexity, and the ability to easily modify it [65-67]. We performed two modifications on the sequence of this peptide: 1) an extra cysteine residue was added on the C terminus of the peptide to facilitate its conjugation with Hoechst-thiopyridyl, and 2) a fluorescent dye (HiLyte FluorT 647 or HiLyte Fluor 750, Anaspec) that is detectable at low concentrations (<150nM) [70] was added to the N terminus for *in vivo* and *ex vivo* imaging studies. The resulting VEGF mimetic peptide (VEGFmp, Sequence: Ac-CKLTWQELYQLKYKGIK[HiLyte FluorT 647]-NH₂ or Ac-CKLTWQELYQLKYKGIK[HiLyte Fluor 750]-NH₂, Anaspec) was then conjugated with Hoechst-thiopyridyl through the formation of a single disulfide bond with the cysteine residue, and the resulting Hoechst-thiopyridyl-VEGFmp (HoVEGFmp) compound was dialyzed using a 2kDa molecular weight cutoff to remove any excess Hoechst-thiopyridyl (MW=751.96Da) in the solution.

3.2.1.2: HoVEGF₁₆₅

The VEGF₁₆₅ isoform was used due to the 8 free cysteine residues that are available to create a disulfide bond with the Hoechst-thiopyridyl derivative [46]. Before conjugation with Hoechst, VEGF₁₆₅ was conjugated with an amine-reactive near-IR fluorescent dye (DyLight 800, Thermo Scientific #53063) that reacts with lysine residues to form stable amide bonds. The resulting VEGF₁₆₅-DyLight 800 (VEGF₁₆₅-Dy) was conjugated with Hoechst-thiopyridyl, and the resulting Hoechst-thiopyridyl-VEGF₁₆₅-DyLight 800 (HoVEGF₁₆₅) was dialyzed using a 2kDa molecular weight cutoff to remove any excess Hoechst thiopyridyl (MW=751.96Da) in the solution.

3.2.2: Bioactivity of Hoechst Compounds

3.2.2.1: HoVEGFmp

To determine if HoVEGFmp is a good therapeutic candidate for *in vivo* experiments, we evaluated the DNA binding activity and VEGF binding activity of HoVEGFmp *in vitro*.

3.2.2.1.1: In Vitro Assessment of DNA Binding Activity

Cardiomyocyte progenitor cells (CPCs) were treated with methanol (fixed) or standard tissue culture media (live) for 10 minutes. Both fixed and live cells received 2×10^{-6} M of either Hoechst-thiopyridyl or HoVEGFmp. The treatment is two times the suggested dose [66], which was done with the intent of ensuring that DNA binding would be observable in this assay. As shown in Figure 2, both HoVEGFmp and Hoechst-thiopyridyl clearly bound to DNA found in the nucleus of fixed cells with compromised cell membranes. In contrast, no Hoechst-thiopyridyl or HoVEGFmp was able to bind to intracellular DNA of live cells with intact cell membrane.

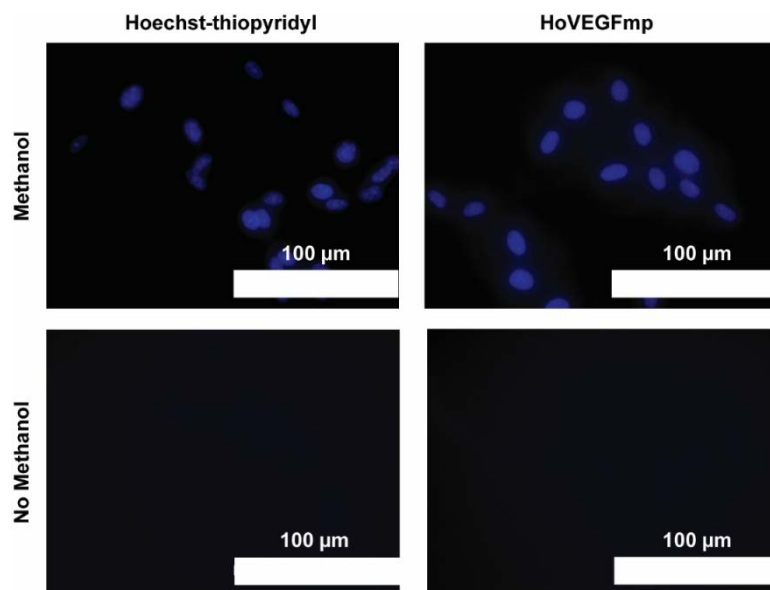


Figure 2: Representative images of CPCs incubated with Hoechst compounds. CPCs were either fixed with methanol for 10 minutes or left untreated, followed by treatment for 20 minutes with either Hoechst-thiopyridyl or HoVEGFmp. Fluorescent imaging: 40x, Blue: DAPI.

3.2.2.1.2: *In Vitro* Assessment of Angiogenic Activity

Immortalized mouse aortic endothelial cells (iMAECs), which express VEGFR-2, were treated with 1×10^{-6} M of VEGFmp or HoVEGFmp for 1, 5, 10 or 30 minutes. After treatment, cells were lysed and western blot analysis was performed using phosphorylated and total ERK 1/2 antibodies. Figure 3A shows a representative image of the Western blot membrane that was obtained. Quantification of Western blots (Figure 3B) showed that the largest increase in the phosphorylation of ERK1/2 occurred after 1 and 5 minutes of treatment with either VEGFmp or HoVEGFmp. No significant differences between groups were observed.

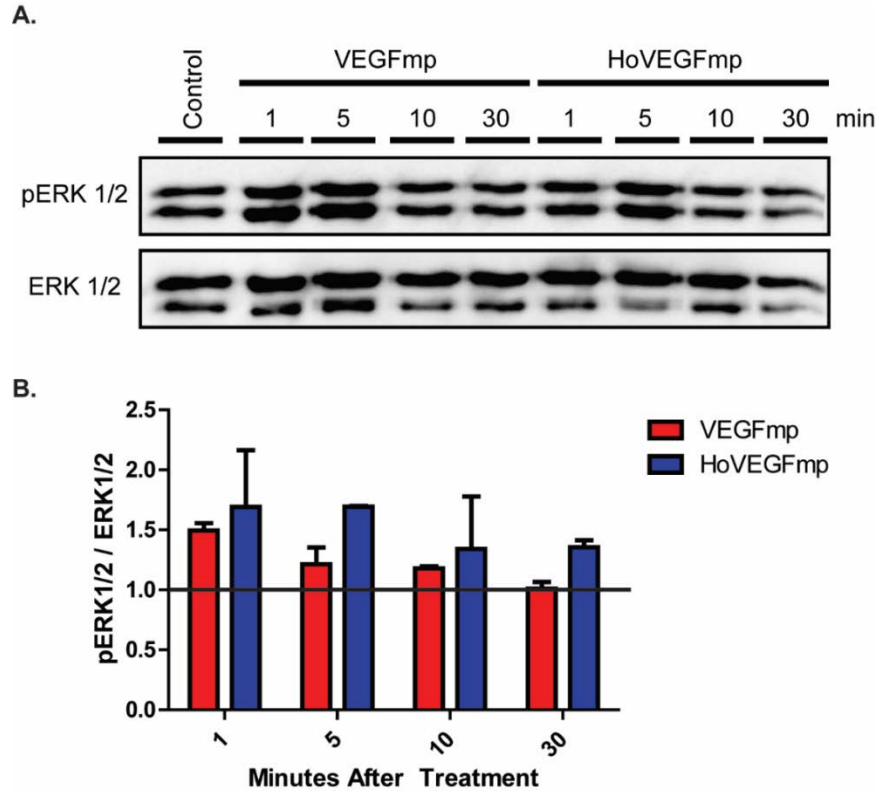


Figure 3: Western blot analysis of iMAECs treated with VEGFmp compounds. After starving iMAECs for 5-6 hours, cells were treated with either VEGFmp or HoVEGFmp for 1, 5, 10, or 30 minutes. Western blot analysis with pERK1/2 and total ERK1/2 antibodies was performed. (A) Representative image of Western blots. (B) Quantification of Western blots normalized to control (black line). (B) Two-way ANOVA not significant. Bars represent Mean \pm SEM, n=2.

3.2.2.2: HoVEGF₁₆₅

To determine if HoVEGF₁₆₅ is a good therapeutic candidate for *in vivo* experiments, we evaluated the DNA binding activity and VEGF binding activity of HoVEGF₁₆₅ *in vitro*.

3.2.2.2.1: *In Vitro* Assessment of DNA Binding Activity

Similar to the experiments with HoVEGFmp, iMAECs were treated with methanol (fixed) or standard tissue culture media (live) for 10 minutes. Both fixed and live cells received 2000ng/mL of Hoechst 33258, 2000ng/mL of Hoechst-thiopyridyl, or 500ng/mL of HoVEGF₁₆₅. The treatment is in excess of the suggested dose [66], and the differences in dosage with the HoVEGF₁₆₅ was due to limitations with the amount of compound available at the time. As shown in Figure 4, all three treatment groups successfully bound to DNA in the nucleus of fixed cells. In contrast, only Hoechst 33258 was able to bind to intracellular DNA of live cells with intact cell membranes.

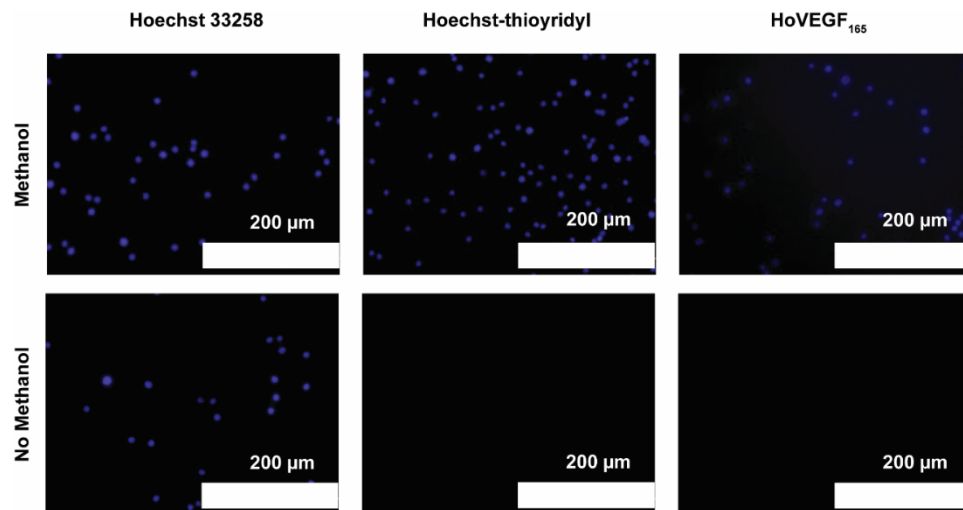


Figure 4: Representative images of iMAECs incubated with Hoechst compounds. iMAECs were either fixed with methanol for 10 minutes or left untreated, followed by treatment for 20 minutes with either Hoechst 33258, Hoechst-thiopyridyl, or HoVEGF₁₆₅. Fluorescent imaging: 20x, Blue: DAPI.

3.2.2.2.2: *In Vitro* Assessment of Angiogenic Activity

Rat cardiac endothelial cells (CECs) were treated with 500ng/mL of VEGF₁₆₅, VEGF₁₆₅-Dy, or HoVEGF₁₆₅ after being starved in low serum media for 24 hours. After 24 hours of

treatment, cells were re-plated on Geltrex coated plates at a density of 30,000 cells/cm². Six hours after plating, the cells were treated with calcein green fluorescent dye and imaged. Figure 5 shows representative images obtained. All treatments led to tube formation.

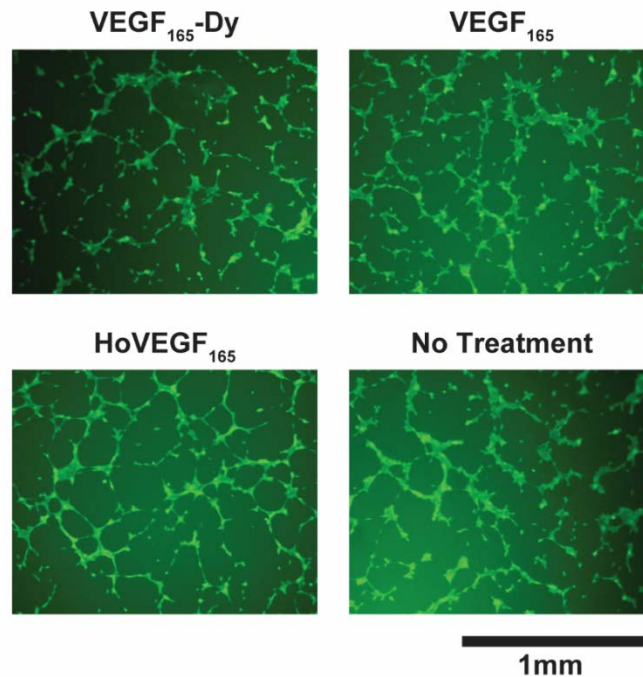


Figure 5: Representative images of CECs forming tubes. After starving Rat CECs overnight, cells were treated with HoVEGF₁₆₅, VEGF₁₆₅-Dy or VEGF₁₆₅ for 24 hours. 30,000 cells/cm² were then plated on 96 well plates covered with Geltrex and allowed to form tubes for 6 hours. Fluorescent Imaging: 2x, Green: FITC.

3.2.3: Animal Model of Peripheral Artery Disease

We used a validated model of hindlimb ischemia (HLI) in male BALB/c mice, in which the femoral artery of one hindlimb was ligated at two different locations [26, 27, 38, 71-74] (Figure 6A). This model is reproducible and leads to the formation of large areas of necrotic tissue. Laser Doppler Perfusion Imaging (LDPI) was used to assess the success rate of the femoral ligation procedure by measuring the signal intensity of both the

ischemic and non-ischemic hindlimbs (Figure 6B). About 90% of animals tested in our preliminary studies had a perfusion ratio ≤ 0.2 , indicating the procedure was successful. Any animal with an unsuccessful femoral ligation was excluded from our studies and immediately euthanized.

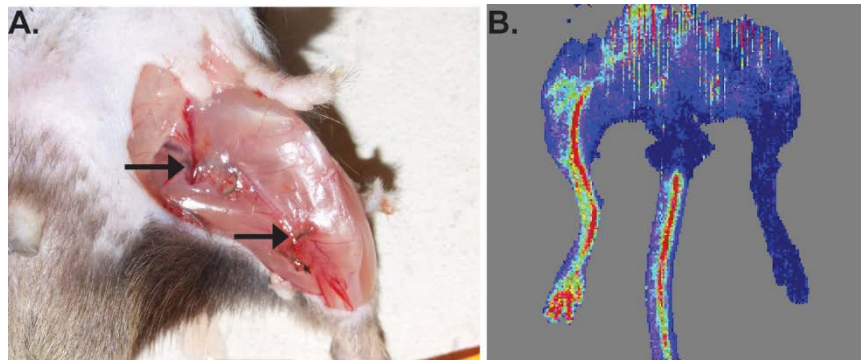


Figure 6: Representative images of mouse model of HLI. Femoral ligation was performed at two different sites to induce ischemia. (A) Representative image of femoral ligation. (B) Representative image of LDPI performed 24 hours after femoral ligation. Black arrows represent the sites where the femoral artery was ligated, at the origin of the deep femoral artery and saphenous artery.

The time course of DNA release following femoral artery ligation was measured. Briefly, C57BL/6 mice underwent one of three different surgical procedures: (1) femoral ligation (hindlimb ischemia model, HLI), (2) myocardial ischemia-reperfusion (myocardial infarction model, MI), or (3) no surgery (No Sx). Blood samples were obtained for each animal at 2, 24, and 48 hours after surgical procedure, and DNA concentration was measured using SYBR Gold Nucleic Assay Gel Stain and a plate reader [75]. As shown in Figure 7, DNA levels for both HLI and MI double by 24 hours after surgical procedure when compared to controls, although none of the differences observed between groups were statistically significant. For all subsequent animal studies involving HLI, treatment was delivered 24 hours after surgery.

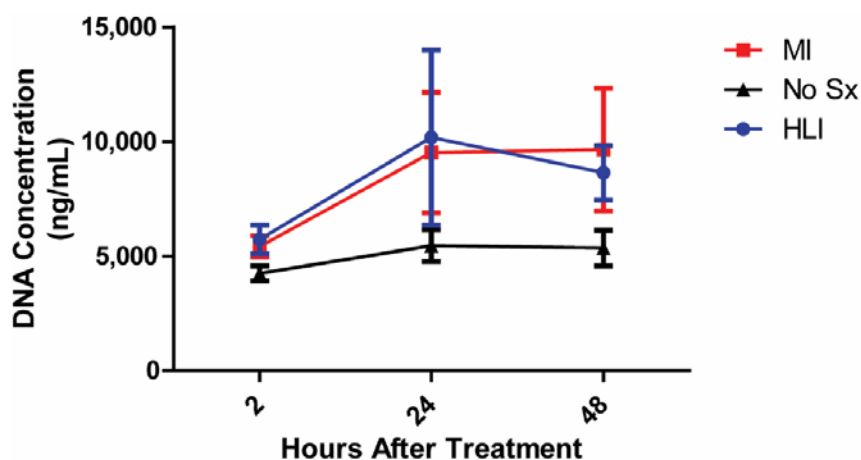


Figure 7: DNA levels in the serum of C57BL/6 mice. C57BL/6 mice underwent different surgical procedures: Hindlimb Ischemia (HLI), Myocardial Infarction (MI) and No surgery (No Sx). DNA levels in serum were measured at 2, 24, and 48 hours after surgical procedure. Two-way ANOVA not significant. Points represent Mean \pm SEM, n=2-4.

3.2.4: Retention of Hoechst Compounds in Animal Model of PAD

To determine the effectiveness of our targeted delivery approach, the retention of our compound was evaluated after an IM injection to ischemic tissue in a HLI model using BALB/c mice.

3.2.4.1: HoVEGFmp

The appropriate dosing was based on levels reported using a similar VEGF mimetic peptide (QK) dissolved into hydrogels to study this peptide's angiogenic response when implanted into mouse corneas [65]. That study delivered 0.005nmol of peptide to each animal [65]. However, previous studies in our lab delivering a similar Hoechst-IGF-1 compound IV to ischemic hearts have shown a targeting of 2-5% [23]. Thus, we chose to

start with a dose 50x higher than what was previously reported for peptide QK for our retention (IM) and targeting (IV) experiments [65].

BALB/c mice underwent femoral ligation followed by an IM injection of either VEGFmp or HoVEGFmp (55 μ L, 4.64 μ M, 1000ng, 0.255nmol total) 24 hours after surgery. Animals were imaged *in vivo* at 0 and 2 hours after treatment to determine the feasibility of *in vivo* fluorescent imaging with the Xenogen IVIS 100 imaging system. As shown in Figure 8, both VEGFmp and HoVEGFmp produced a detectable fluorescent signal immediately after IM injection (0 Hours). However, two hours after treatment a fluorescent signal was observed in the bladder area. We were unable to quantify the amount of peptide remaining in the ischemic limbs due to the interference caused by the fluorescent signal in the bladder area.

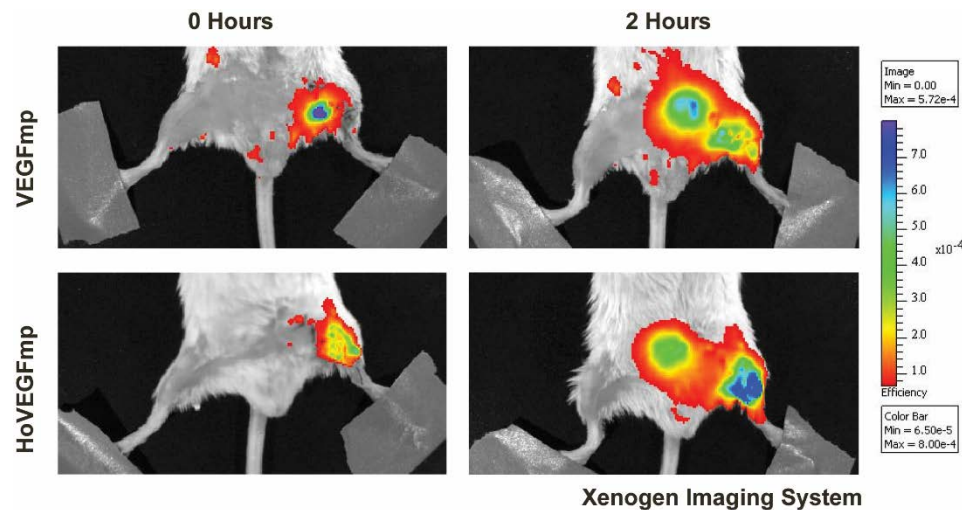


Figure 8: Representative images of *in vivo* fluorescent imaging. BALB/c mice received IM treatment of VEGFmp or HoVEGFmp. At 0 and 2 hours after treatment, *in vivo* fluorescent imaging was done. Scale represents arbitrary fluorescent units.

To determine the biodistribution of HoVEGFmp, a second set of BALB/c mice underwent femoral ligation followed by an IM injection of either VEGFmp or HoVEGFmp (55 μ L,

4.64 μ M, 1000ng, 0.255nmol total) 24 hours after surgery. Animals were then sacrificed at 2, 6, and 18 hours after treatment, and the following organs were dissected and imaged using the Xenogen IVIS 100 imaging system: ischemic hindlimb, non-ischemic hindlimb, liver, lung, spleen, and kidney. The fluorescence levels of each organ were quantified, and the fold change in fluorescence (i.e.: ischemic hindlimb/non-ischemic hindlimb, liver/non-ischemic hindlimb, etc.) was reported. As shown in Figure 9A, no differences were observed between the ischemic hindlimbs of animals treated with VEGFmp or HoVEGFmp at any time point. Two hours after treatment, large increases in fluorescent levels were observed (257.4 fold change for VEGFmp, 156.1 fold change for HoVEGFmp), but by 18 hours after treatment, most of the fluorescent signal had been cleared (72.2 fold change for VEGFmp, 6.6 fold change for HoVEGFmp). Similarly, off target organs showed no differences between VEGFmp and HoVEGFmp treatments at any time points (Figure 9B-E). The largest signals were observed in the kidneys (fold changes between 3.7 and 14.9), while the lowest signals were observed in the liver (fold changes between 0.05 and 0.33).

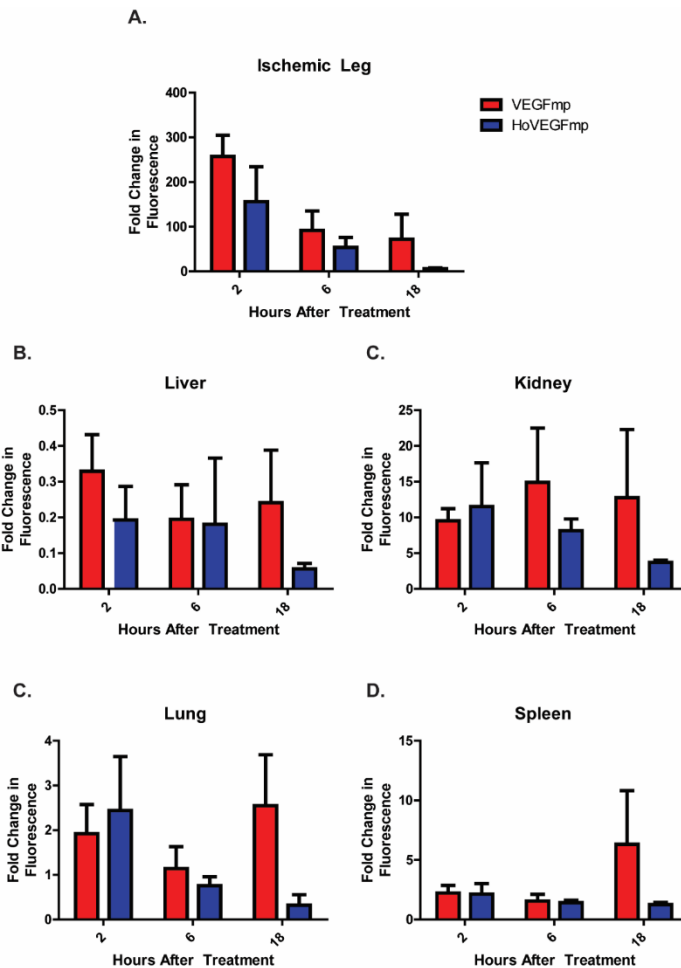


Figure 9: Quantification of *ex vivo* fluorescent signal. BALB/c mice received IM treatment of VEGFmp or HoVEGFmp. At 2, 6, and 18 hours after treatment, the organs of each mouse were dissected, *ex vivo* fluorescent imaging was done, and fluorescent signals were quantified. (A) Ischemic hindlimbs. (B) Liver. (C) Kidney. (D) Lung. (E) Spleen. (A-E) Fold change to non-ischemic hindlimb, two-way ANOVA not significant. Bars represent Mean \pm SEM, n=3-4.

Immediately after *ex vivo* imaging, the tissue obtained from the ischemic hindlimbs was flash frozen and then homogenized. Immunoprecipitation was performed using a VEGFR-2 antibody. Western blot analysis was performed using phospho-tyrosine (p-Tyr) kinase and VEGFR-2 antibodies to determine if either VEGFmp or HoVEGFmp treatment had

activated the VEGFR-2 signaling pathway. Figure 10A shows a representative image of the western blot membranes that were obtained. Figure 10B shows the quantification of the western blots. Even though higher levels of phosphorylation were observed at 18 hours after treatment, no significant differences were observed between VEGFmp, HoVEGFmp, and PBS treated controls.

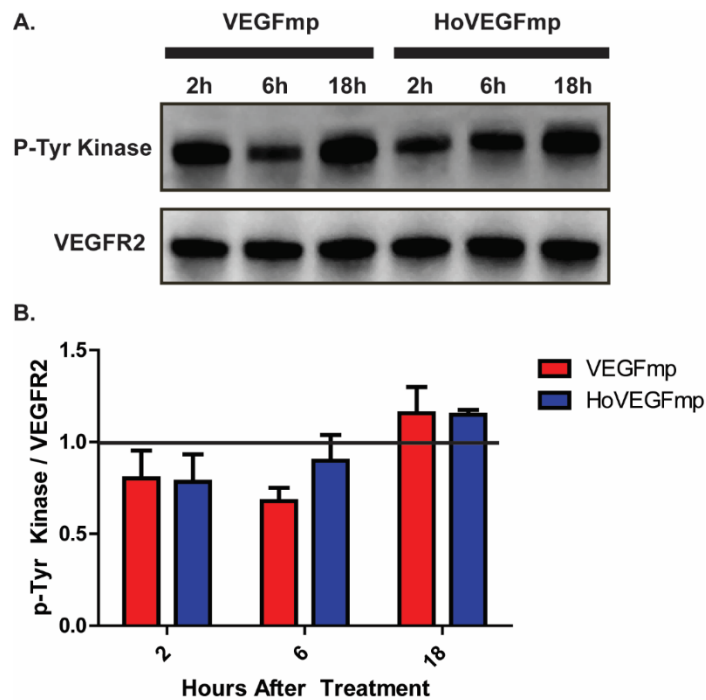


Figure 10: Western blot analysis of hindlimb tissue samples. BALB/c mice received IM treatment of VEGFmp or HoVEGFmp. At 2, 6, and 18 hours after treatment, hindlimbs were dissected, homogenized, and immunoprecipitated with VEGFR-2 antibody. Western blot analysis was performed with p-Tyrosine Kinase and VEGFR-2 antibodies. (A) Representative image of Western blots. (B) Quantification of Western blots normalized to PBS treated controls (black line). (B) Two-way ANOVA not significant. Bars represent Mean ± SEM, n=3-4.

3.2.4.2: HoVEGF₁₆₅

A new imaging system (In Vivo Xtreme, Bruker Corporation) was used for this and subsequent imaging studies. A dose of 1000ng of HoVEGF₁₆₅ or VEGF₁₆₅-Dy was used, as preliminary studies showed that this dose saturated the imager when placed on a 96 well plate, and the dose was within the range of doses reported in other *in vivo* studies with mice (0.1 to 3µg) [37, 76].

BALB/c mice underwent femoral ligation followed by an IM injection of PBS, VEGF₁₆₅-Dy, or HoVEGF₁₆₅ (55µL, 0.87µM, 1000ng, 0.049nmol total) 24 hours after surgery. Animals were imaged *in vivo* before treatment and at 0, 2, 6, 24, 48 and 168 hours after treatment. Fluorescence levels of ischemic and non-ischemic hindlimbs were quantified, and fold change in fluorescence (ischemic hindlimb/non-ischemic hindlimb) was reported for each animal. Figure 11A shows representative images obtained with the new In Vivo Xtreme fluorescent imager. Figure 11B shows analysis of *in vivo* imaging data. VEGF₁₆₅-Dy was significantly greater than PBS 2 hours (2.66 vs 1.03, p<0.01) and 6 hours (2.47 vs 1.05, p<0.01) after treatment. Similarly, HoVEGF₁₆₅ was significantly greater than PBS 2 hours (2.13 v 1.03, p<0.05) and 6 hours (2.16 vs 1.05, p<0.05). No significant differences between VEGF₁₆₅-Dy and HoVEGF₁₆₅ were observed at any time points.

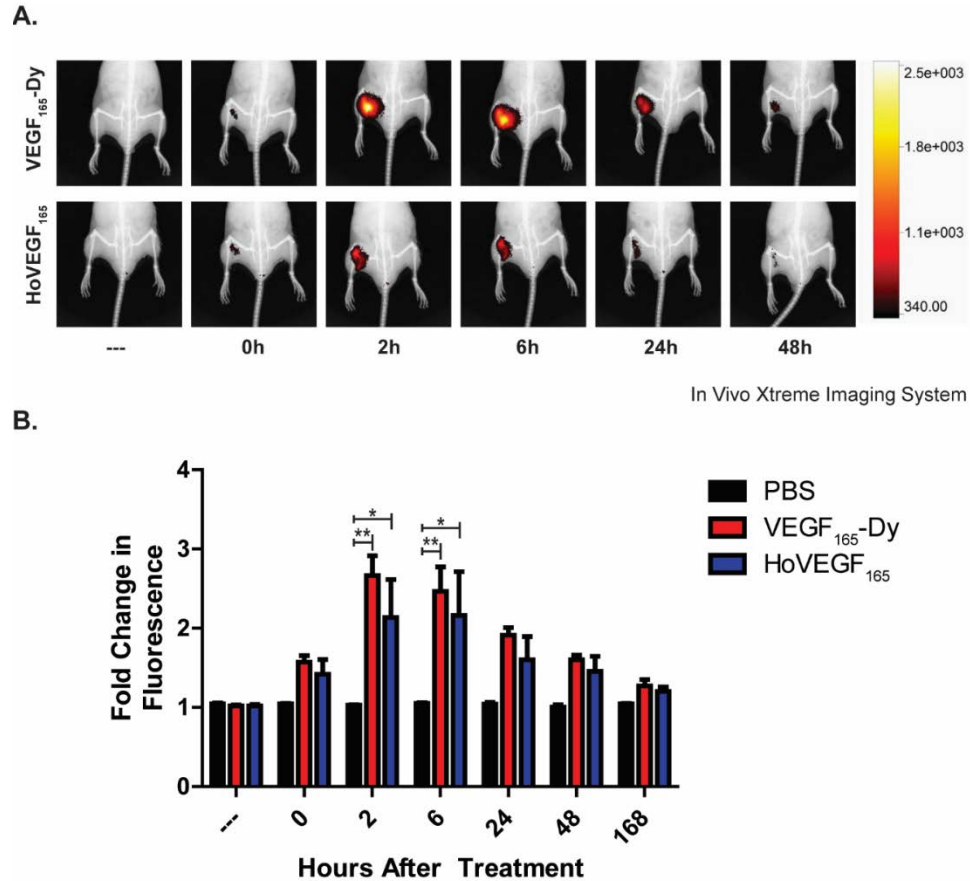


Figure 11: *In vivo* fluorescent imaging. BALB/c mice received IM treatment of PBS, VEGF₁₆₅-Dy, or HoVEGF₁₆₅. At 0, 2, 6, 24, 48 and 168 hours after treatment, *in vivo* fluorescent imaging was done, and fluorescent signals were quantified. (A) Representative *in vivo* fluorescent images. (B) Quantification of *in vivo* fluorescent signal in ischemic hindlimbs. (A) Scale represents arbitrary fluorescent units. (B) Fold change to non-ischemic hindlimb, two-way ANOVA ($p < 0.05$) with Bonferroni post hoc, * $p < 0.05$, ** $p < 0.01$. Bars represent Mean \pm SEM, $n = 3-6$.

BALB/c mice underwent femoral ligation followed by an IM injection of PBS, VEGF₁₆₅-Dy, or HoVEGF₁₆₅ (55 μ L, 0.87 μ M, 1000ng, 0.049nmol total) 24 hours after surgery. Animals were then sacrificed at 24, and 168 hours after treatment, and the following organs were dissected and imaged: ischemic hindlimb, non-ischemic hindlimb. Figure 12A shows

representative *ex vivo* images of hindlimbs 24 hours after treatment. Figure 12B shows quantification of these images. VEGF₁₆₅-Dy was significantly different than PBS at 24 (2.59 vs 1.02, $p < 0.05$) and 168 (2.43 vs 1.08, $p < 0.01$) hours after treatment. No significant differences between HoVEGF₁₆₅ and VEGF₁₆₅-Dy, or HoVEGF₁₆₅ and PBS were observed at any time point.

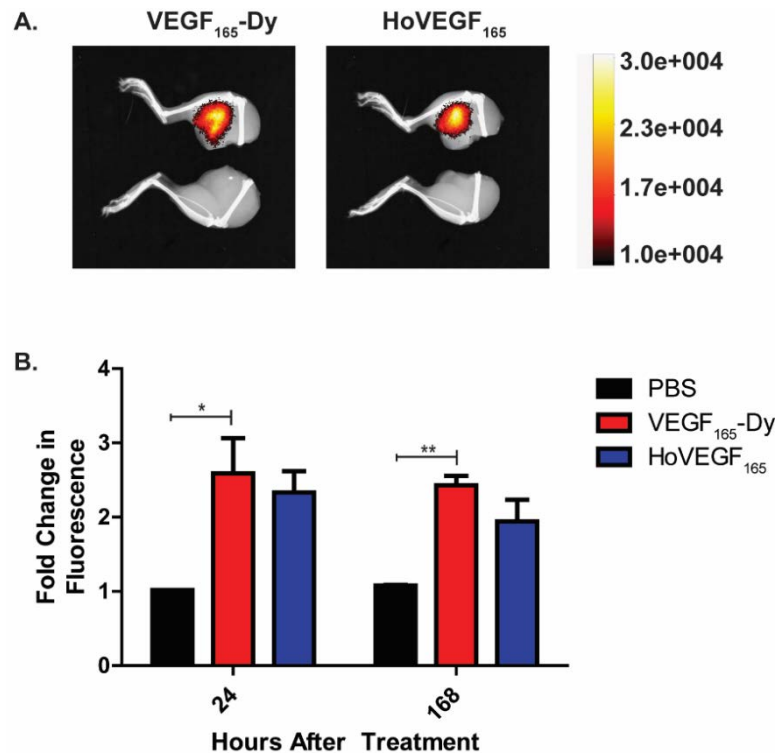


Figure 12: *Ex vivo* fluorescent imaging. BALB/c mice received IM treatment of PBS, VEGF₁₆₅-Dy, or HoVEGF₁₆₅. At 24 and 168 hours after treatment, the hindlimbs of each mouse were dissected, *ex vivo* fluorescent imaging was done, and fluorescent signals were quantified. (A) Representative *ex vivo* fluorescent images at 2 hours after treatment. (B) Quantification of *ex vivo* fluorescent signal in ischemic hindlimbs. (A) Scale represents arbitrary fluorescent units. (B) Fold change to non-ischemic hindlimb, two-way ANOVA ($p < 0.05$) with Bonferroni post hoc, * $p < 0.05$, ** $p < 0.01$. Bars represent Mean \pm SEM, $n = 3-5$.

3.2.5: Targeting of Hoechst Compounds in Animal Model of PAD

To determine the effectiveness of our targeted delivery approach, the targeting of our compound was evaluated after an IV injection in a HLI model using BALB/c mice.

3.2.5.1: HoVEGFmp

For our treatment groups, we decided to deliver 1000ng of VEGFmp or HoVEGFmp in 110 μ L of PBS IV. This treatment is the same as the one used for retention studies, with a molarity of 2.32 μ M and total of 0.255nmol being delivered. In pilot studies, as little as 10 μ L of compound at this concentration was visible using the In Vivo Xtreme fluorescent imager when injected directly to leg of mouse cadavers.

BALB/c mice underwent femoral ligation followed by an IV injection of PBS, VEGFmp, or HoVEGFmp (110 μ L, 2.32 μ M, 1000ng, 0.255nmol total) 24 hours after surgery. Animals were imaged *in vivo* before treatment and at 0 and 24 hours after treatment. As shown in Figure 13A, no detectable levels of the compound were found in the ischemic legs at any time point after treatment (only 2 hour time point shown). At 2 hours after treatment, fluorescent signal was observed over the bladder of animals imaged. Fluorescent levels *in vivo* were not quantified due to the absence of signal. Animals were then sacrificed at either 2 or 24 hours after treatment, and the ischemic and non-ischemic hindlimbs were imaged. As shown in Figure 13A, a weak signal was observed in the ischemic hindlimbs compared to the contralateral non-ischemic hindlimb of animals treated with HoVEGFmp and VEGFmp (VEGFmp treated animal not shown). Quantification of this signal (Figure 13B) showed the VEGFmp was significantly greater than HoVEGFmp (1.64 vs 1.33, $p < 0.01$) and PBS (1.64 vs 1.16, $p < 0.05$) at 2 hours after treatment. However, no significant differences between any of the treatment groups were observed at 24 hours after treatment.

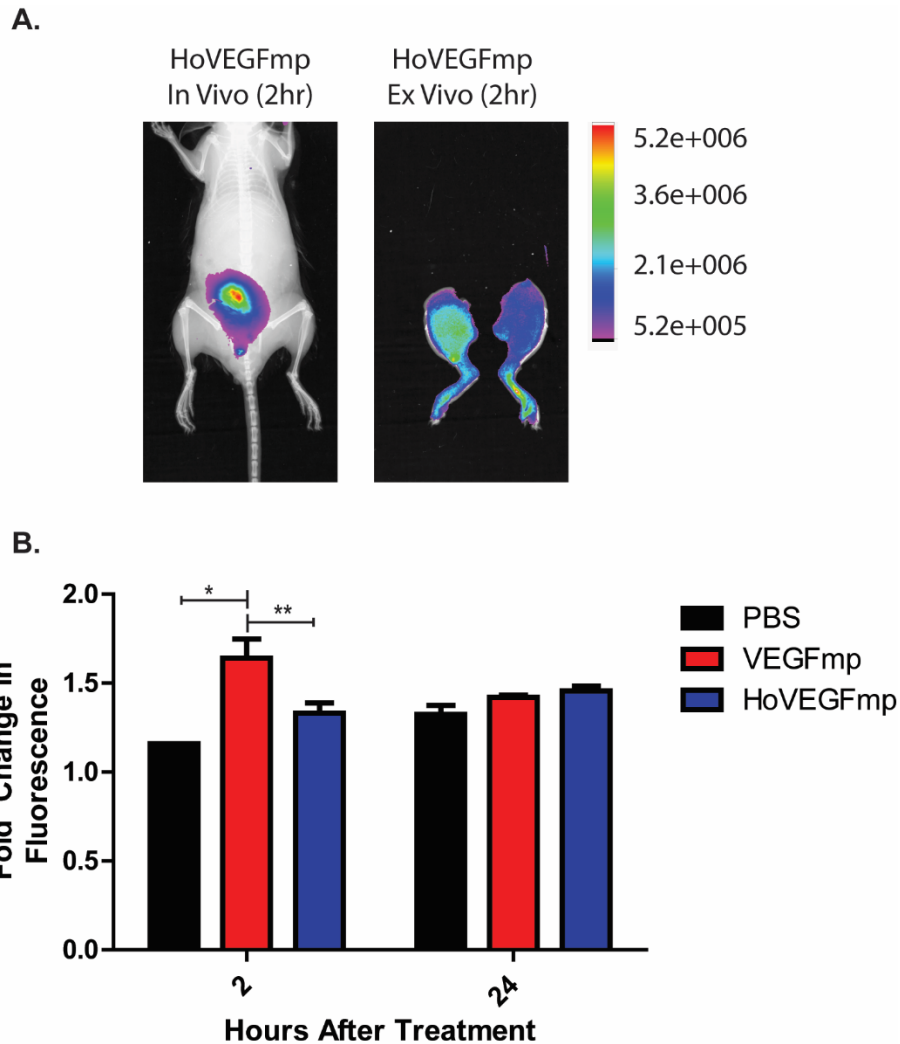


Figure 13: *In vivo* and *ex vivo* fluorescent imaging. BALB/c mice received IV treatment of PBS, VEGFmp, or HoVEGFmp. At 2 hours after treatment, *in vivo* fluorescent imaging was done. At 2 and 24 hours after treatment, the hindlimbs of each animal were dissected, *ex vivo* fluorescent imaging was done, and fluorescent signals were quantified. (A) Representative *in vivo* and *ex vivo* fluorescent images. (B) Quantification of *ex vivo* fluorescent signal in ischemic hindlimbs. (A) Scale represents arbitrary fluorescent units. (B) Fold change to non-ischemic hindlimb, two-way ANOVA ($p < 0.05$) with Bonferroni post hoc, * $p < 0.05$, ** $p < 0.01$. Bars represent Mean \pm SEM, $n = 7-9$ for VEGFmp and HoVEGFmp groups, $n = 1-2$ for PBS groups.

Immediately after *ex vivo* imaging, the tissue obtained from the ischemic and non-ischemic hindlimbs was flash frozen and then homogenized. Two repeats of 200 μ L of homogenate were placed on each well of a black 96 well plate with a clear bottom for each sample. Each plate was imaged using the In Vivo Xtreme imager and the resulting images were quantified. Figure 14A shows a representative image of four different animals treated with HoVEGFmp and sacrificed 2 hours after treatment. Slightly stronger signal seems to be present in Ischemic hindlimbs (Isch) when compared to non-ischemic hindlimbs (N-Isch). Figure 14B shows the quantification of the fluorescent signal in these plates. No differences between any treatment groups were observed at either 2 or 24 hours after treatment.

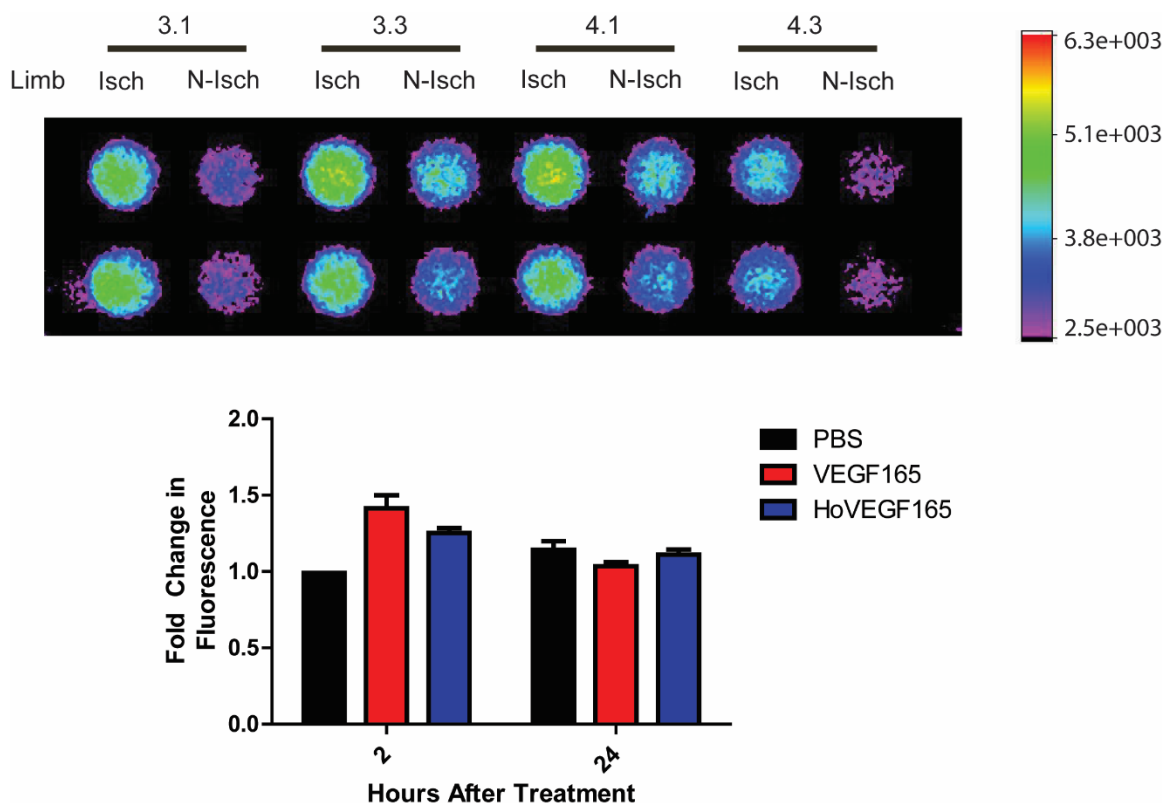


Figure 14: *Ex vivo* fluorescent imaging of homogenized hindlimbs. BALB/c mice received IV treatment of PBS, VEGFmp, or HoVEGFmp. At 2 and 24 hours after treatment,

hindlimbs were dissected, homogenized, and *ex vivo* fluorescent imaging was done on a black, clear bottom, 96 well plate. Fluorescent signals were then quantified. (A) Representative *ex vivo* fluorescent images. (B) Quantification of *ex vivo* fluorescent signal of homogenized hindlimbs. (A) Scale represents arbitrary fluorescent units. Isch: ischemic hindlimb, N-Isch: non-ischemic hindlimb. Numbers 3.1, 3.3, 4.1, and 4.3 represent four different animals treated with HoVEGFmp. (B) Fold change to non-ischemic hindlimb, two-way ANOVA not significant. Bars represent Mean \pm SEM, n=7-9 for VEGFmp and HoVEGFmp groups, n=1-2 for PBS groups.

3.2.5.2: HoVEGF₁₆₅

During pilot studies, we were unable to detect any signal after IV treatment with 1000ng of either VEGF₁₆₅-Dy or HoVEGF₁₆₅ *in vivo* or *ex vivo*, as shown in Figure 15. Thus, we decided not to proceed with a targeting study for HoVEGF₁₆₅ compound.

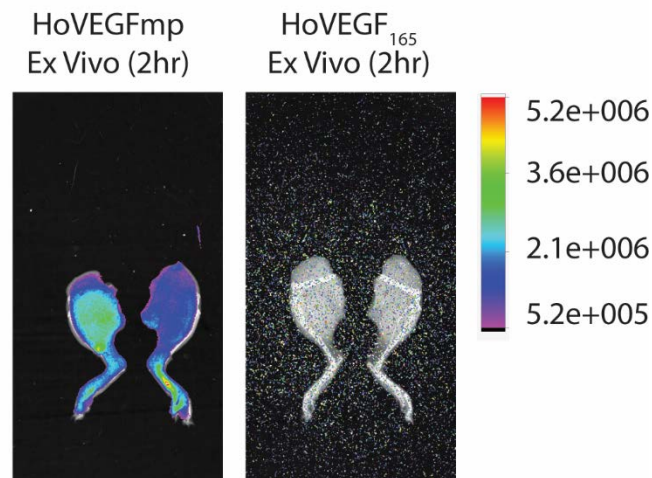


Figure 15: Representative *ex vivo* fluorescent images. BALB/c mice received IV treatment of HoVEGFmp or HoVEGF₁₆₅. At 2 hours after treatment, hindlimbs were dissected and

ex vivo fluorescent imaging was done. No signal was observed in animals treated with HoVEGF₁₆₅. Scale represents arbitrary fluorescent units.

3.3: Discussion

The delivery of VEGF recombinant protein for the treatment of PAD has been widely explored in pre-clinical and clinical studies [5, 7, 26, 27, 31, 36-39, 44, 67]. Despite promising results in different animal models, clinical studies have shown limited success [5, 7, 31, 44], probably due to the proteins short half-life, inadequate retention and targeting to target tissue, and numerous systemic side effects [5, 44]. To address these limitations, new techniques that provide localized, sustained delivery of protein to ischemic tissue have been developed [19, 26, 36, 37, 39, 40, 65, 77]. For example, VEGF has been packed in injectable hydrogels [26, 27, 36, 38, 39], implantable hydrogels [37, 65], immunoliposomes [19], and nanoparticles [40]. However, the current processing conditions to make these hydrogels and nanoparticles can reduce the bioactivity of recombinant proteins such as VEGF [41], and although IM injection and surgical implantation are clinically feasible, the use of a non-invasive IV injection is preferred [19, 21, 23, 26, 41-44]. Additionally, the use of VEGF mimetic peptides instead of full length VEGF has also been explored, since such peptides offer the same bioactivity and are easier to manipulate and package than full length VEGF [26, 65-67].

In this project we explored the use of a novel targeted delivery system using a modified Hoechst compound to deliver either VEGFmp or VEGF₁₆₅ to necrotic tissue in an animal model of PAD. A similar modified Hoechst had previously been used in our lab to deliver IGF-1 to ischemic tissue in an animal model of myocarditis after an IV injection [23]. We hypothesized that these modified Hoechst compounds would bind to extracellular DNA

present in necrotic tissue, deliver VEGFmp or VEGF₁₆₅ to the ischemic tissue, and promote angiogenesis and functional recovery.

After the successful synthesis of our compounds (HoVEGFmp and HoVEGF₁₆₅) we sought to verify that the bioactivity of our compounds was not compromised during the conjugation reactions. Using a permeability assay, we were able to evaluate if our compound would remain cell membrane impermeable and bind only to extracellular DNA. Similar to other modified Hoechst compounds used in our lab [21, 23], we confirmed that both of our compounds remained impermeable to the intact cell membranes of live cells, but both compounds were able to bind to DNA after these cell membranes were disrupted using methanol (Figure 2 and Figure 4). Using Western blot analysis and a tube formation assay, we were able to evaluate if our compound retained the angiogenic activity of VEGF. Western blot analysis showed slight increases in phosphorylation of ERK1/2 after 1 minute of treatment with VEGFmp (1.49 fold) or HoVEGFmp (1.69 fold) when compared to untreated controls, although these results were not significant (Figure 3). Western blot analysis has been previously used to evaluate the bioactivity of VEGF and VEGF mimetic peptides [26, 66, 76, 78], with the reported phosphorylation of VEGFR-2 being only 1.58 fold higher than that of untreated controls [26]. Thus, increasing our sample size from n=2 would allow us to accurately identify the slight changes in phosphorylation that are expected. The Tube formation assay showed extensive tube formation after treatment with HoVEGF₁₆₅, VEGF₁₆₅-Dy, VEGF₁₆₅, and control (Figure 5). Although tube formation assays have been successfully used to evaluate tube formation after angiogenic treatment [38, 40, 76, 79], it is possible that either our treatment media or Geltrex contained growth factors that promote tube formation even in the absence of VEGF, as has been reported by others in our lab. Thus, better control of treatment factors would allow us to properly evaluate the angiogenic activity of our compound using a tube formation assay. In

summary, we were able to verify the bioactivity of the DNA binding component of our compound, but the evaluation of the bioactivity of the angiogenic component of our compound remains inconclusive.

We proceeded to study the retention and targeting effects of our compounds in an *in vivo* model of HLI (Figure 6) [26, 27, 36-39, 67, 71-74, 80, 81]. Despite this model being extensively used, different levels of ischemia have been reported depending on the strain of mice used and the extent of femoral vessel damage [71, 72, 74, 80, 81]. We used BALB/c mice and a partial femoral ligation at two sites, near the origin of the deep femoral artery and near the origin of the saphenous artery, to induce moderate levels of ischemia. To evaluate the extent of necrosis, we measured the levels of DNA present in the serum of mice up to 48 hours after femoral ligation. We compared our results to a different model of ischemia (MI), since we had previously been successful in targeting necrosis in this model [23]. We observed increases in the blood levels of DNA by 24 hours after either HLI and MI surgical procedures (Figure 7), although these changes were not significantly different than control probably due to the low number of animals used for this study (n=2-4). Although serum DNA levels do not necessarily correlate with the extent of necrosis, they indirectly suggest that necrosis is indeed present by 24 hours.

We performed two sets of *in vivo* studies for each compound: (1) a retention study after IM injection of our compound, and (2) a targeting study after IV injection of our compound.

For HoVEGFmp, retention studies demonstrated that our compound was not preferentially retained in ischemic tissue when compared to VEGFmp control (Figure 8, Figure 9). The presence of fluorescent signal in the bladder in *in vivo* images (Figure 8) and the large fold increases in fluorescence in the kidneys (3.7 to 14.9 fold) when compared to other off

target organs in *ex vivo* analysis (Figure 9C) suggests that the peptide was probably excreted through the renal system. Furthermore, treatment with either VEGFmp or HoVEGFmp did not lead to further activation of VEGFR-2 in ischemic hindlimbs *in vivo* (Figure 10). It is possible that this is due to the angiogenic activity of our compound being compromised after the addition of a fluorophore and/or the conjugation with Hoechst-thiopyridyl. Targeting studies using HoVEGFmp, demonstrated that our compound did not preferentially target ischemic hindlimbs when compared to VEGFmp (Figure 13, Figure 14). *In vivo* images demonstrated fluorescent signal in the bladder, similar to that observed in retention studies (Figure 13A). In contrast to retention studies, the fluorescent signal of HoVEGFmp treated animals in *ex vivo* analysis was not significantly different than that of PBS treated control animals (Figure 13B). One possible reason for this is that perhaps our compound was only present in low quantities deep in the muscle tissue. In order to extract our compound from the muscle tissue, we homogenized the tissue and measured the fluorescent signal of the resulting homogenate (Figure 14); however, no differences between HoVEGFmp, VEGFmp or PBS treated animals were observed. In summary, our HoVEGFmp compound did not show improvements in retention or targeting when compared to controls.

For HoVEGF₁₆₅, retention studies demonstrated that our compound was not preferentially retained in ischemic tissue when compared to VEGF₁₆₅-Dy control (Figure 11, Figure 12). Interestingly, *in vivo* fluorescent imaging showed no signal over the bladder of any of the animals imaged (Figure 11A). The fold change in fluorescence observed in *ex vivo* studies (Figure 12B) was lower than that observed in retention studies with HoVEGFmp (Figure 9). This could be due to differences in dosing (HoVEGFmp: 1000ng=0.255nmol; HoVEGF₁₆₅: 1000ng=0.049nmol of compound) or imaging system used. Targeting studies for HoVEGF₁₆₅ were not performed, as a pilot study showed that no signal was observed

after IV injection of the compound (Figure 15). In summary, our HoVEGF₁₆₅ did not show improvements in retention or targeting when compared to controls.

One possible explanation for the lack of retention and targeting of our compounds is the rapid breakdown of our compounds at the site of injury or in blood plasma. Blood plasma contains a number of different proteinases (serine-, cysteine-, aspartic-, and metallo-) whose activity is usually kept in check by proteinase inhibitors (α 1 antitrypsin, α 2 antiplasmin and α 2 macroglobulin) [82-84]. In sites inflammation, the presence of macrophages and neutrophils leads to an increase in the amount of proteinases and results in the rapid breakdown of circulating proteins and peptides [82, 83]. Interestingly, the breakdown of peptides has been observed to be much faster than that of proteins even in the absence of inflammation, with many peptides having a half-life in the order of seconds in human plasma [82, 83].

In our retention experiments, it is possible that an inflammatory response to the femoral ligation surgery increased the levels of proteinases present, particularly at the injury site. This, in turn, lead to the rapid breakdown of both peptides (HoVEGFmp) and proteins (HoVEGF₁₆₅) delivered to the injury site for retention studies. Since peptides tend to be hydrolyzed much faster than proteins, we would expect to see our HoVEGFmp compound being cleared from the injury site much faster than HoVEGF₁₆₅. Unfortunately, an accurate comparison between our two compounds was not possible due to the use of different doses, fluorescent imaging systems, and end points. In our targeting experiments, it is possible that both of our compounds were broken down by proteinases before reaching our target tissue. To circumvent these limitations, both peptide and protein based compounds could be modified. For example, glycosylation, PEGylation, substitution of peptide cleavage sites, modification to secondary peptides structures, or binding to carrier

proteins such albumin has been proposed [82-85]. In our lab, conjugation to streptavidin (~50kDa) improved the half-life of IGF-1 after IV delivery [23].

A second possible explanation for the lack of retention and targeting of our compounds is the rapid breakdown and excretion of our compound through the kidneys. It is known that filtration of peptides and proteins through the kidneys depends on their size, shape and charge [82-84, 86, 87]. Peptides (<5kDa) usually pass into the ultrafiltrate unimpaired, with a peptide clearance/inulin clearance of almost 1 (range is from 0 for albumin to 1 for small peptides) [82, 84, 86]. Peptides can then be excreted unchanged or they can be hydrolyzed by brush border membrane proteinases, with the resulting peptide fragments and amino acids being reabsorbed [82, 84, 86]. For proteins of ~20kDa size, clearance ranges from 0.5 to 0.8 depending on their charge [82]. Here, proteins are collected in endocytic vacuoles that fuse with lysosomes, breakdown proteins, and return amino acids into circulation [82, 84, 86].

In our retention and targeting experiments, we were able to observe the presence HoVEGFmp but not HoVEGF₁₆₅ in the anatomical areas that correspond to the bladder (Figure 8, Figure 11A, Figure 13A). This suggests that our HoVEGFmp was being broken down in the brush border membrane of the kidneys, with the resulting amino acids being reabsorbed while the fluorophore was excreted through the renal system. HoVEGF₁₆₅, on the other hand was internalized into endocytic vacuoles, where the fluorophore was probably broken down instead of being secreted through the renal system. In either case, modification of both peptide and protein based compounds would be necessary to circumvent these limitations [82-85].

Finally, for *in vivo* studies we used an animal model of HLI with BALB/c mice. BALB/c mice have been reported to have fewer or narrower collaterals when compared to C57BL/6 mice, and we would expect to see more severe ischemia and necrosis in BALB/c mice [71]. Even though this provides more extracellular DNA for our compounds to target, the lack of collaterals could limit the amount of compound that can be delivered to areas of ischemia and necrosis.

Our studies have explored a novel targeting technique for the treatment of PAD. Although our results were not what we expected, the insights obtained here can be used to advance the development of new techniques for the treatment of PAD.

CHAPTER 4: IDENTIFICATION OF TARGETING PEPTIDES FOR THE DIAGNOSIS OF MYOCARDITIS

4.1: Introduction

4.1.1: Myocarditis

Cardiomyopathy and myocarditis are an increasing global medical problem [52]. The prevalence of myocarditis is estimated to be about 22 per 100,000 patients, with the global number of deaths attributed to cardiomyopathy and myocarditis increasing by 40.8% between 1990 and 2010 (from 286,800 to 403,900) [1, 53]. Furthermore, these diseases are also associated with great morbidity. For example, myocarditis accounts for ~11% of heart failure cases and it is the most common cause for heart transplantation worldwide due to the lack of appropriate diagnostics and treatments [54]. In pediatric populations in the United States, the incidence of cardiomyopathy in infants less than 1 year of age is estimated to be 8.34 cases per 100,000 [1]. The most common form of cardiomyopathy in children is dilated cardiomyopathy (DCM), with an estimated annual incidence in infants less than 1 year of age of 4.40 cases per 100,000 [1]. Although the cause of DCM remains unidentified in 66% of cases, myocarditis accounts for 46% of the known causes [1, 52].

Myocarditis refers to localized or diffuse inflammation of the myocardium [9-11]. It is a complex disease that can be caused by infections (bacterial, rickettsial, mycotic, protozoan, and viral agents), cardiotoxic agents (drugs, toxins, and alcohol), or autoimmune disease, but many cases remain idiopathic [9, 11, 12, 54-59]. Although the exact mechanisms through which myocarditis develops are not well understood, evidence suggests that both the innate and adaptive immune systems of the host are involved [10, 12, 53, 54]. For example, in animal models of viral myocarditis due to Coxsackie B3 Virus,

three different phases can be observed [11, 12, 53, 54, 56]. In the first phase (first few days), the virus infects cardiomyocytes, replicates, and induces the destruction of cardiomyocytes [11, 56-58]. The innate immune system is activated through different pathways (pro-inflammatory cytokines, suppressors of cytokine signaling proteins, toll-like receptors), and an invasion of natural killer cells and macrophages followed by T lymphocytes is observed [11, 12, 53, 54, 57, 58]. In the second phase (weeks to months), the presence of the viral genome leads to immune dysregulation, activation of the adaptive immune system through viral specific T-cells, the presence of inflammatory cellular infiltration, autoimmune reactions, and continuous injury to cardiomyocytes [11, 12, 56-58]. In the third phase, the presence of circulating cross reacting autoantibodies in addition to the virus-induced cardiomyocyte injury leads to remodeling of the heart and the development of DCM [11, 12, 53, 56-58].

The clinical presentation of patients with myocarditis tends to be heterogeneous. However, based on the different clusters of symptoms observed, it can be classified into different presentation types: acute coronary syndrome like, new-onset heart failure, life threatening arrhythmias, and chronic heart failure [9, 12, 55]. However, patients often present with nonspecific symptoms or without any symptoms at all, and infants in particular are often unable to verbalize what these symptoms are [12, 56, 59].

4.1.2: Current Diagnosis of Myocarditis

The heterogeneous etiology, pathophysiology, and clinical presentation of myocarditis makes it one of the most challenging diagnosis in cardiology and leads to the under-diagnosis of cases of myocarditis [9, 12]. The gold standard for the diagnosis of myocarditis is endomyocardial biopsy (EMB) complemented by immunohistochemistry and PCR [9, 11, 12, 53, 55-57, 60]. This procedure is considered to be safe when

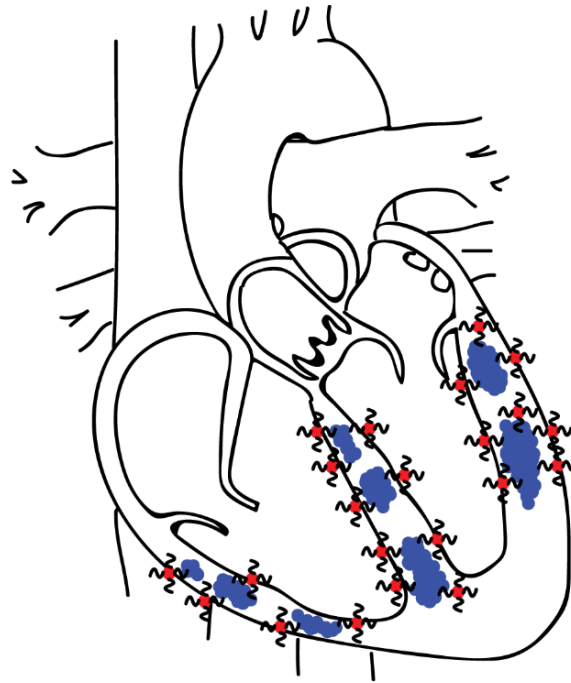
performed by experienced physicians; however, it is an invasive procedure that has some risk of serious complications, particularly in children with rates as high as 10.6% [9, 12, 57, 59, 61]. These complications include cardiac perforation with tamponade, ventricular or supraventricular arrhythmias, heart block, pneumothorax, hemothorax, puncture of central arteries, pulmonary embolization, venous hematoma, damage to the tricuspid valve, stroke, and death [9, 12, 55, 57, 61]. Furthermore, studies that compared the performance of EMB to the *ex vivo* evaluation of hearts with myocarditis found that EMB misses approximately half of the diagnoses, even when 10 biopsy samples were analyzed [9]. Due to the diffuse nature of myocarditis, it is estimated that 17 biopsies are needed to reach a sensitivity of only 80% [9, 57], and thus there is a decreased reliance on EMB particularly in pediatric populations in the United States [56, 57]. Due to these limitations, other noninvasive diagnostic modalities have been explored. For example, cardiac magnetic resonance (CMR) can be used to demonstrate typical features of acute myocarditis such as dysfunction, edema and necrosis [9, 53, 56, 57, 59, 60]. Studies that compared the performance of CMR to biopsy samples reported sensitivities between 47% and 74% depending on the modality used [9]. Despite improvements in the diagnostic criteria used with CMR, the diagnosis of a substantial number of patients may still be missed, particularly in patients in the chronic phase of myocarditis [9, 60]. Furthermore, CMR cannot be used to determine the underlying cause of myocarditis, to stratify the risk of different patients, and the findings have not yet been validated in pediatric patients [9, 56, 57]. Other noninvasive diagnostic modalities, such as electrocardiogram, chest radiography, or echocardiography have low diagnostic value, sensitivity, and specificity [53, 56].

4.1.3: Targeted Molecular Imaging

Modifications to noninvasive imaging techniques that allow for the targeted molecular imaging of myocarditis are currently being explored. For example, targeted molecular imaging using fluorine-19 in CMR has been shown to detect myocardial inflammation in an animal model of experimental autoimmune myocarditis (EAM) through the incorporation of fluorine-19 into macrophages, dendritic cells, and granulocytes [62]. However, fluoride-19 is not specific to myocarditis and can be incorporated by macrophages and monocytes in other disease processes such as pneumonia, allograft rejection, cardiac ischemia, and cerebral ischemia [62]. Similarly, microbubbles with modifications or coated with antibodies targeting leukocytes, endothelial cells, and T-lymphocytes were shown to enhance ultrasound signal in animals with EAM; however, the use of antibodies in therapies is limited by production costs, low tissue penetration, and host immune response to antibody [63, 64]. Thus there is still a need for improved technologies for the appropriate diagnosis and timely treatment of myocarditis.

4.1.4: Approach

Using an *in vivo* phage display library [88-92], we identified potential peptides that can be used for molecular imaging or targeted drug delivery in patients with myocarditis. We hypothesized that these peptides can be used to target hearts with myocarditis after intravenous (IV) delivery (Figure 16). These peptides would address the limitations of previous targeted molecular imaging studies and would provide another tool to improve the diagnosis and potential treatment of myocarditis.





-  Fluorescent Streptavidin coated with Targeting Peptides
-  Inflammatory Infiltrates in acute Myocarditis

Figure 16: Schematic of targeting peptides for the diagnosis of myocarditis. Biotinylated targeting peptides binding to fluorescent streptavidin can be used for the diagnosis of myocarditis *in vivo*.

4.2: Methods and Results

4.2.1: Animal Model of Experimental Autoimmune Myocarditis

We used an animal model of EAM in which male BALB/c mice (6-8 weeks old) were immunized at 0 and 7 days with subcutaneous injections containing 150 μ g of myosin heavy-chain α peptide (MyH: Ac-SLKLMATLFSTYASAD-OH, New England Peptide) dissolved in 100 μ L of PBS and emulsified with 100 μ L of complete Freund's adjuvant (CFA, Sigma) [62, 64, 93-99]. For control groups, animals were either immunized at 0 and 7 days with subcutaneous injections containing 100 μ L of PBS emulsified with 100 μ L of CFA, or

were not treated at all. In this animal model, it is expected that animals immunized with MyH/CFA will develop inflammatory infiltrates in their hearts at 10 days after initial immunization, and that these infiltrates will peak around 21 days and will be cleared by 56 days after initial immunization [55, 99]. However, only 40-60% of animals develop myocarditis, and these animals usually have variable disease severity as determined by the degree of infiltration observed on H&E stained sections [62, 64, 93-99].

4.2.2: Baseline Characteristics

A total of 94 animals that were used in our *ex vivo* peptide screening (n=31) and *in vivo* peptide screening (n=63) experiments were euthanized at 21 days after initial immunization and histologically scored for disease severity using H&E staining. These animals were assigned to one of the following treatment groups: untreated controls (n=14), immunized with PBS/CFA (n=16), and immunized with MyH/CFA (n=64). Scoring for disease severity was based on the amount of infiltration present. The protocols that have been used to score animals for myocarditis and myocarditis severity vary among different studies and are subject to inter- and intra-observer variability [62, 64, 93-99]. To account for this, we decided to use a well-defined protocol that is similar to ones that have been more recently published [62, 64]. Briefly, the left ventricle (LV) was divided into four quadrants. Each quadrant and the right ventricle (RV) were then scored on a scale of 0 to 4, with 0 representing no inflammatory infiltrates, 1 representing small foci of leukocytes between cells, 2 representing larger foci of > 100 leukocytes, 3 representing >10% of the quadrant cross section involved with inflammatory infiltrates, and 4 representing >30% of the quadrant cross section involved with inflammatory infiltrates. The sum of the scores for each LV quadrant and the RV (H&E Sum Score) was then used to classify the severity of myocarditis as follows: no myocarditis: H&E Sum Score ≤ 3 ; mild myocarditis: $4 \leq$ H&E Sum Score ≤ 7 ; and severe myocarditis: H&E Sum Score ≥ 8 . To prevent any bias, all

scoring was conducted and analyzed by investigators blinded to the animal's treatment group. In line with expectations, a total of 42 animals immunized with MyH/CFA (65.63%) developed myocarditis, with 28 animals being scored as mild myocarditis (43.75%) and 14 animals being scored as severe myocarditis (21.88%). None of the animals immunized with PBS/CFA or left untreated developed myocarditis, and in subsequent analyses these animals were grouped together as the Control group (n=30). Representative images of animals immunized with MyH/CFA with no myocarditis, mild myocarditis, and severe myocarditis are shown in Figure 17. Additionally, no differences in any functional parameters measured by echocardiography or body weight were observed between groups (Figure 18 and Figure 19), suggesting that the inflammatory infiltrates are present prior to the onset of any cardiac dysfunction even in animals with severe myocarditis

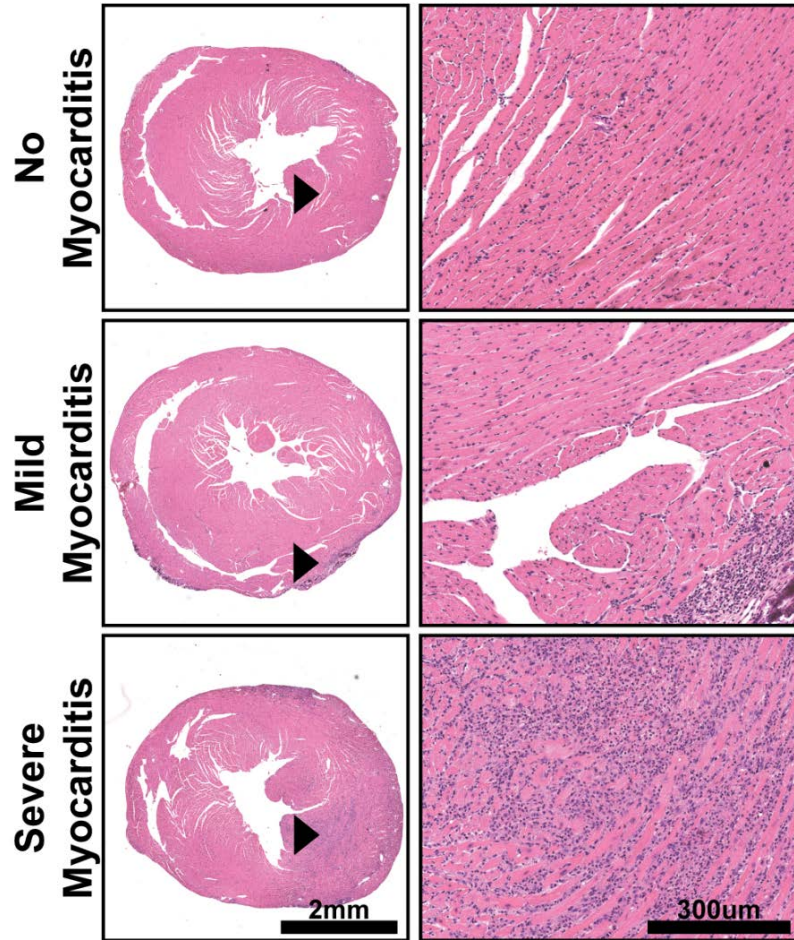


Figure 17: Representative H&E images of animals with and without myocarditis. Heart sections of animals immunized with MyH/CFA were stained with H&E, imaged, scored, and classified as no myocarditis, mild myocarditis, and severe myocarditis. Black arrowheads represent the approximate location of the areas that were amplified. Significant leukocyte infiltration was present in both animals with mild and severe myocarditis.

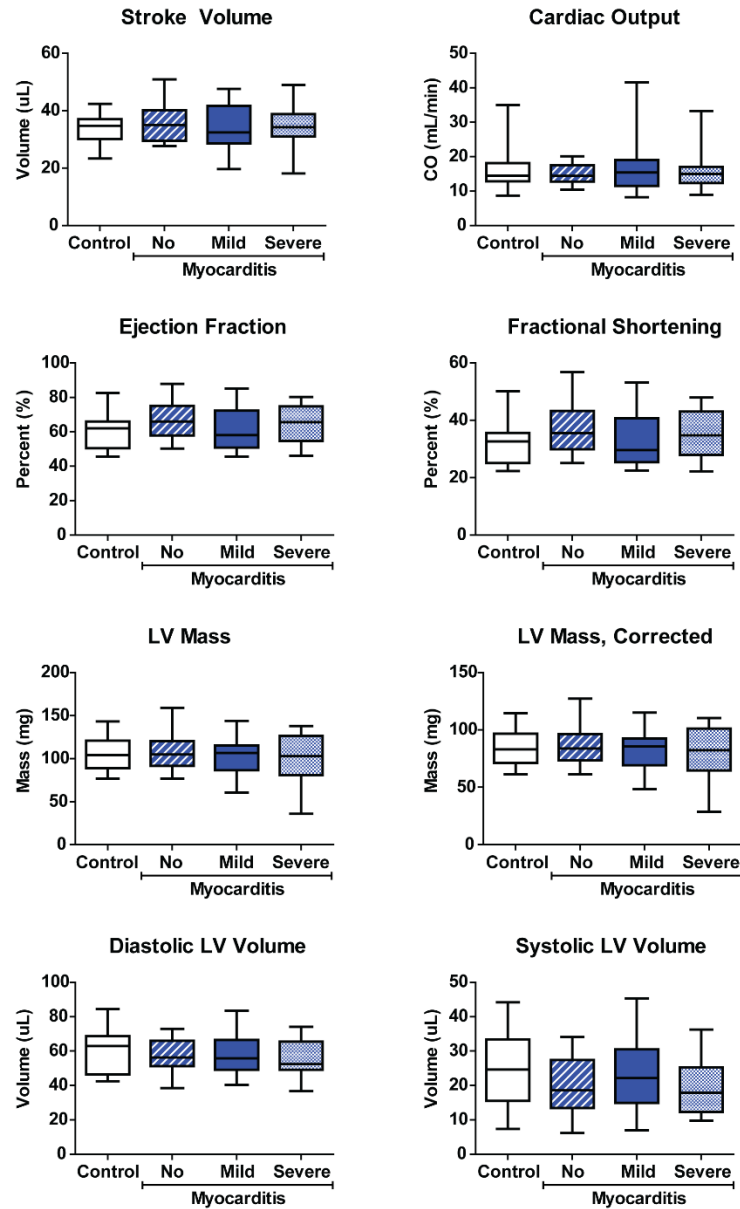


Figure 18: Echocardiography data of animals 21 days after initial immunization. Animals assigned to *ex vivo* and *in vivo* peptide screening experiments underwent echocardiography analysis 21 days after initial immunization. Data for different parameters measured is presented. Median values (horizontal line), 25% to 75% percentiles (box), and range of values (whiskers). Control, n=22; No Myocarditis: n=18; Mild Myocarditis: n=27; Severe Myocarditis: n=13. One way ANOVA ($p < 0.05$) not significant for any parameter.

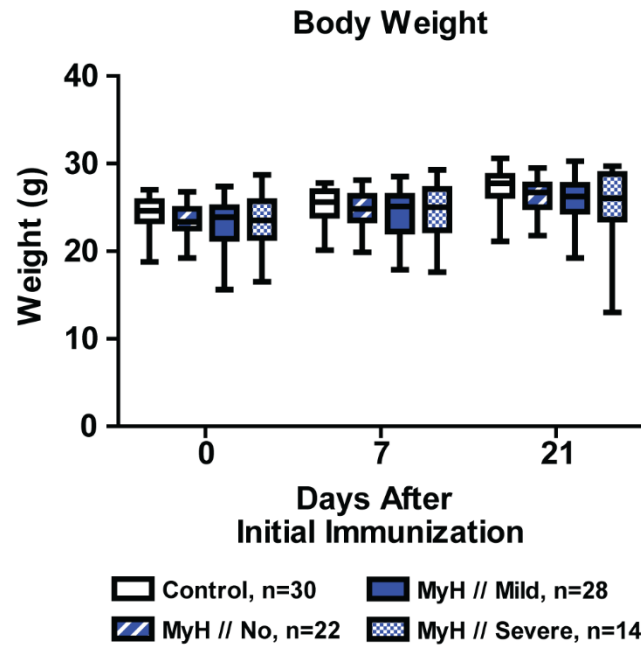


Figure 19: Body weight of animals through 21 days after initial immunization. The body weight for animals assigned to *ex vivo* and *in vivo* experiments was measured at 0, 7, and 21 days after initial immunization. Median values (horizontal line), 25% to 75% percentiles (box), and range of values (whiskers). Two-way ANOVA ($p < 0.05$) showed an effect of time but not treatment group.

4.2.3: *In Vivo* Phage Display

We used *in vivo* phage display to identify potential targeting peptides for the diagnosis of myocarditis. The experimental setup for our *in vivo* phage display experiments is shown in Figure 20. We performed a total of 3 cycles or pannings, similar to other published *in vivo* phage display experiments [88-91]. Briefly, at 21 days after initial immunization animals received an IV injection through the tail vein with either a linear 12 amino acid (AA) peptide phage library (Ph.D. 12 Phage Display Peptide Library Kit, New England BioLabs, #E8110S) or an empty control phage (M13KE, New England BioLabs, #EN0316S) at a concentration of 1×10^9 plaque-forming units (pfu)/ μL , as suggested by the manufacturer. For each panning, animals were divided into the following treatment

groups: MyH PhD: immunized with MyH/CFA and injected with the phage library (n=5 per panning); MyH Cont: immunized with MyH/CFA and injected with the control phage (n=4-5 per panning); PBS PhD: immunized with PBS/CFA and injected with the phage library (n=2-3 per panning); and PBS Cont: immunized with PBS/CFA and injected with the control phage (n=2 per panning). The phages were allowed to circulate for 10 minutes after being injected, at which point animals were euthanized and the hearts were excised, washed extensively in PBS and flash frozen. Since only 40-60% of animals were expected to develop myocarditis, the hearts for each of the four treatment groups were pooled together, and the phages were recovered through tissue homogenization and amplified in bacteria. The phages isolated in panning 1 were then reinjected to animals in the same treatment group in panning 2, and the phages isolated in panning 2 were reinjected to animals in the same treatment group in panning 3.

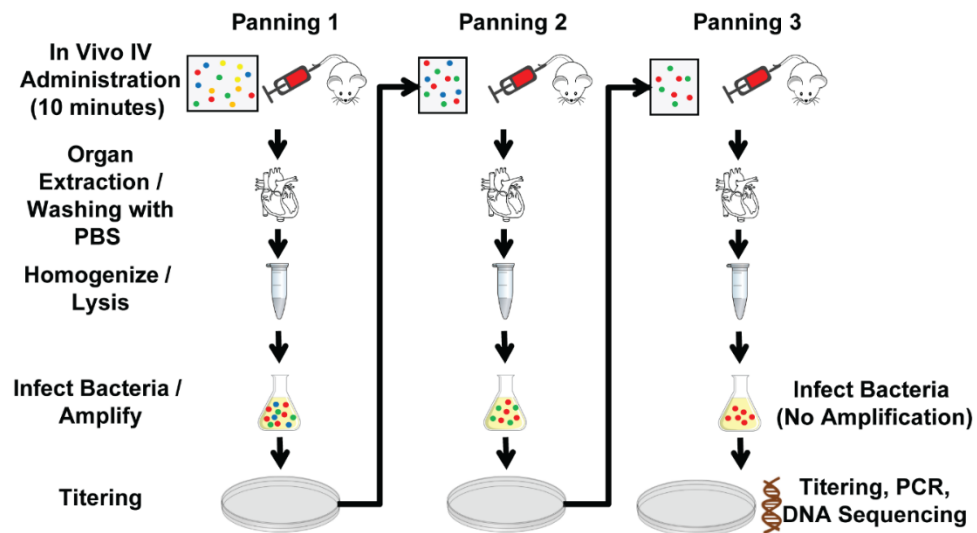


Figure 20: Flow diagram of *in vivo* phage display experiments. Animals underwent three different rounds or pannings of *in vivo* phage display. The phages isolated in panning 1 were reinjected to animals in the same treatment group in panning 2, and the phages

isolated in panning 2 were reinjected to animals in the same treatment group in the final panning 3.

Although we expected to see preferential accumulation in the number of phages binding to the hearts of animals in the MyH PhD group in each subsequent panning when compared to the other treatment groups, this was not observed (Table 1). This is probably due the variability present in the titrating process and the single data point present for each panning after pooling animals in the same treatment group together.

Table 1: Concentration of phages isolated from each treatment group for each panning.

Treatment Group	Panning 1 (pfu/10uL)	Panning 2 (pfu/10uL)	Panning 3 (pfu/10uL)
MyH PhD	3.03E+11	9.40E+10	3.60E+05
MyH Cont.	3.86E+11	1.12E+11	2.15E+05
PBS PhD	3.12E+11	1.93E+11	6.50E+04
PBS Cont.	1.78E+11	9.10E+10	4.13E+05

After the third panning, a total of 110 colonies for MyH PhD, 16 colonies for MyH Cont, 110 colonies for PBS PhD, and 16 colonies for PBS Cont were selected for DNA sequencing. Each colony was amplified using PCR with custom designed primers (sense: CACCGTTCATCTGTCCTCTTTC, antisense: TCACCGTACTCAGGAGGTTTAG). After cleaning up the PCR products, the amplicons were sent for sequencing. It is possible that screening more colonies could have yielded other promising targets, but such screening would have been both time and resource intensive. As expected, none of the colonies isolated from MyH Cont and PBS Cont treatment groups showed the presence of a 12 AA linear peptide sequence. For MyH PhD, a total of 46 colonies sequenced contained a 12 AA linear peptide sequence with a total of 36 unique sequences being identified. For PBS PhD, a total of 41 colonies sequenced contained a 12 AA linear peptide sequence with a

total of 37 unique sequences identified. Although screening of all peptides identified in the MyH PhD group would have been ideal, we selected six different peptides for further *ex vivo* and *in vivo* screening (Table 2). Peptides MyH-PhD-09 and MyH-PhD-120 were selected because each sequence was repeated 5 times, suggesting that it had a higher affinity for animals with myocarditis. Peptides MyH-PhD-04, MyH-PhD-05, MyH-PhD-13, and MyH-PhD-16 were selected after BLAST and literature review of each peptide sequence, as each had homology with a component of different cell types potentially involved in the immune response (astrocytes, T lymphocyte, endothelial cells, etc.). It is possible that some of the other peptides that were not selected for *ex vivo* and *in vivo* screening could have been good candidates for targeting myocarditis, though screening so many candidates is resource intensive. It is important to note that none of the peptides selected were also found in the peptides identified in the PBS PhD treatment group, suggesting that the selected peptides target cardiac tissue with myocarditis and not just healthy cardiac tissue. For *ex vivo* and *in vivo* screening experiments, custom biotinylated peptides of each sequence were used (New England Peptide).

Table 2: Sequences and known homology for the selected potential targeting peptides.

Peptide Name	Peptide Sequence	Frequency	Known Homologies
MyH-PhD-04	LGDLHNRDNNSA	1	pericentriolar material 1 protein; protocadherin; plexin C1
MyH-PhD-05	HSRTDYVQASYP	1	pancreatic lipase-related protein 2; cytotoxic T lymphocyte lipase; Duox 2 protein
MyH-PhD-09	GLHTSATNLYLH	5	pannexin-3; olfactory receptor 460; cubilin precursor
MyH-PhD-13	GDGNSVLKPGNW	1	trans-2-enoyl-CoA reductase, mitochondrial precursor; Dhml protein; Xrn protein
MyH-PhD-16	TASDVPRSRPHS	1	cell division cycle associated 7; plexin D1; Cell adhesion molecule 4 precursor
MyH-PhD-120	SGVYKVAYDWQH	5	helicase, mus308-like; lipase, member 01 precursor; Gm8978

4.2.4: *Ex Vivo* Peptide Screening

To assess the targeting potential of each selected peptide *ex vivo*, different frozen heart sections of 31 animals at 21 days after being either untreated (n=6), immunized with PBS/CFA (n=9), or immunized with MyH/CFA (n=16) were stained with H&E and each of the six biotinylated peptides (Table 2). Each animal was assessed for disease severity as previously described. A total of 13 out of 16 animals immunized with MyH/CFA (81.25%) developed myocarditis (mild: n=8; severe: n=5), while none of the animals that were either not treated or immunized with PBS/CFA developed myocarditis (control, n=15). Similar to disease severity scoring, each animal was also scored for the binding of each of the six targeting peptides. Briefly, the LV was divided into four quadrants. Each quadrant and the RV were then scored on a scale of 0 to 3, with 0 representing no stained cells, 1 representing few scattered stained cells, 2 representing the presence of a few stained foci, and 3 representing the continuous presence of stained tissue. The sum of the scores for each LV quadrant and the RV (Sum Score of peptide) was used to assess the degree of staining of each peptide, with a Sum Score of peptide > 2 being considered as positive staining. To prevent any bias, all scoring was conducted and analyzed by investigators blinded to the animal's treatment group and the peptide being screened.

For peptides MyH-PhD-04, MyH-PhD-09, MyH-PhD-13, and MyH-PhD-16, no positive staining was observed on any of the frozen sections of animals for any treatment group (control, no myocarditis, mild myocarditis, and severe myocarditis). These peptides were eliminated from consideration for future experiments. For peptide MyH-PhD-05, 0 out of 15 animals in the control group (untreated or immunized with PBS/CFA), 1 out of 3 animals in the no myocarditis group, 8 out of 8 animals in the mild myocarditis group, and 4 out of 5 animals in the severe myocarditis group had positive staining. Representative images show that MyH-PhD-05 staining corresponded to areas of increased leukocyte infiltration

(Figure 21), while the quantification of the Sum Score of MyH-PhD-05 shows a gradual increase in the amount of staining present as animals develop mild and severe myocarditis (Figure 22).

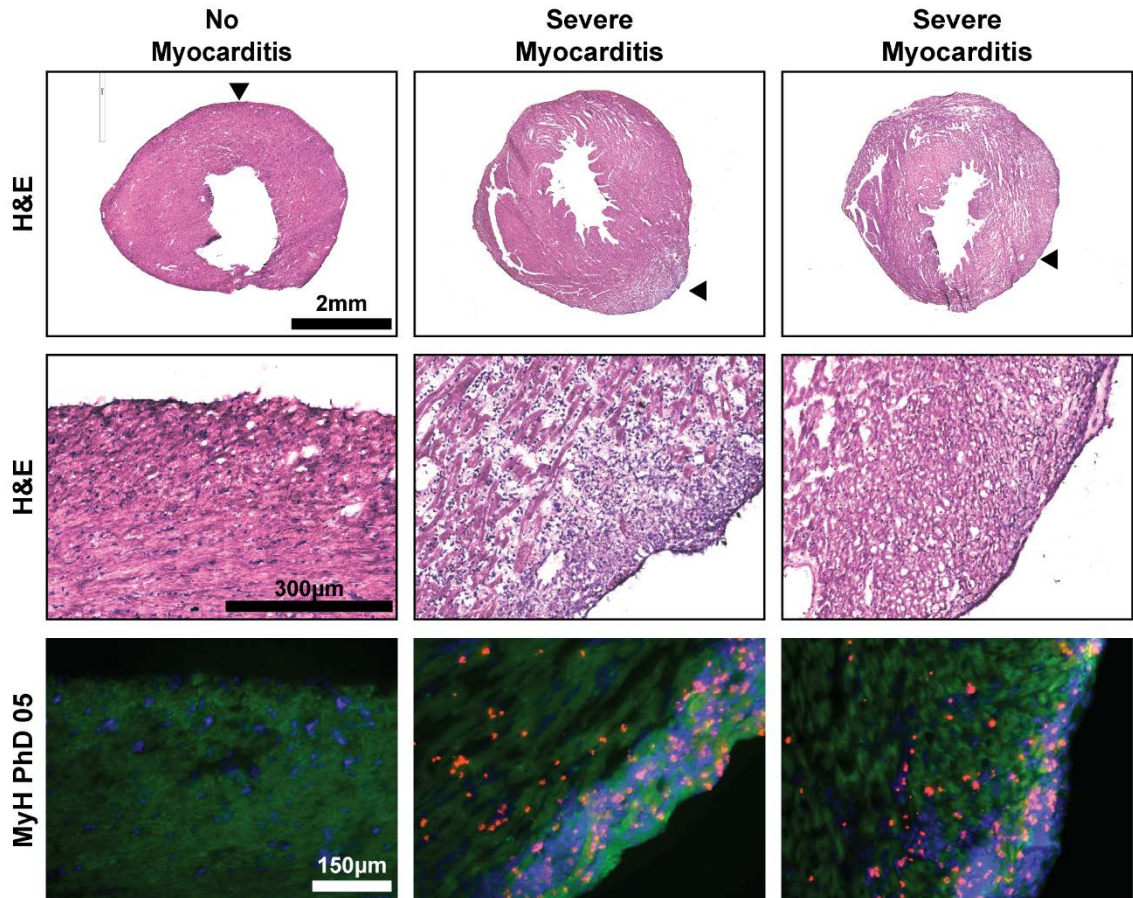


Figure 21: Representative images of hearts stained with H&E and MyH-PhD-05. Black arrowheads on the whole heart H&E images represent the approximate location of the areas that were amplified in subsequent H&E images. MyH-PhD-05 staining corresponds to areas of increased leukocyte infiltration in animals with myocarditis. Fluorescent imaging: 20x, Blue: DAPI (nuclei), Green: FITC (auto fluorescence), and Red: Cy5 (peptide).

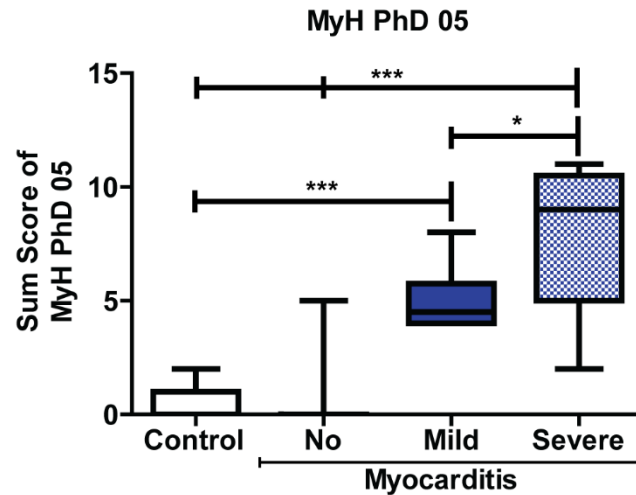


Figure 22: Quantification of *ex vivo* MyH-PhD-05 staining at 21 days. Median values (horizontal line), 25% to 75% percentiles (box), and range of values (whiskers). Control: n=15; No Myocarditis: n=3; Mild Myocarditis: n=8; Severe Myocarditis: n=5. One way ANOVA ($p < 0.05$) with Tukey multiple comparison test, *** $p < 0.001$, * $p < 0.05$.

For peptide MyH-PhD-120, 0 out of 15 animals in the control group, 1 out of 3 animals in the no myocarditis group, 3 out of 8 animals in the mild myocarditis group, and 4 out of 5 animals in the severe myocarditis group had positive staining. Similar to MyH-PhD-05, MyH-PhD-120 staining corresponded to areas of leukocyte infiltration (Figure 23); however, quantification of Sum Score of MyH-PhD-120 showed a much weaker increase in staining as animals developed mild and severe myocarditis when compared to MyH-PhD-05 (Figure 24).

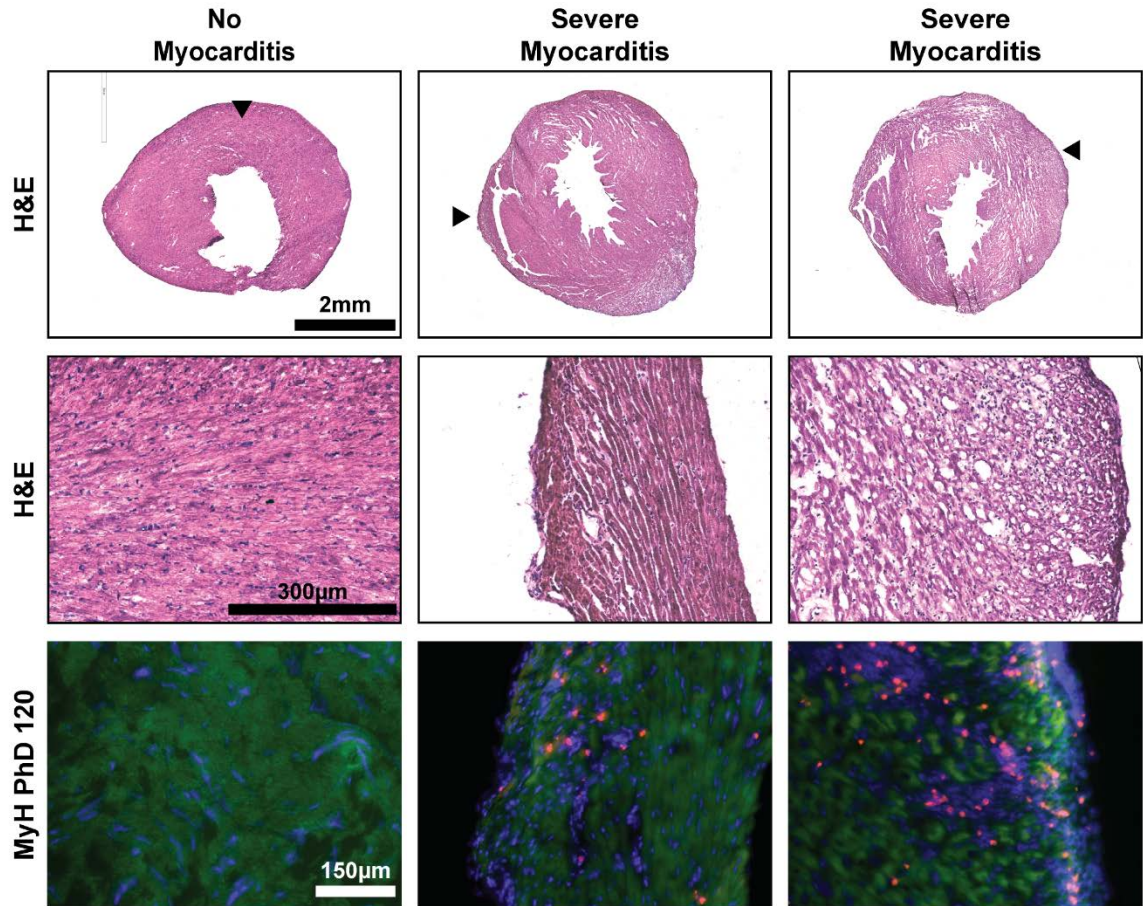


Figure 23: Representative images of hearts stained with H&E and MyH-PhD-120. Black arrowheads on the whole heart H&E images represent the approximate location of the areas that were amplified in subsequent H&E images. MyH-PhD-120 corresponds to areas of increased leukocyte infiltration in animals with myocarditis. Fluorescent imaging: 20x, Blue: DAPI (nuclei), Green: FITC (auto fluorescence), and Red: Cy5 (peptide).

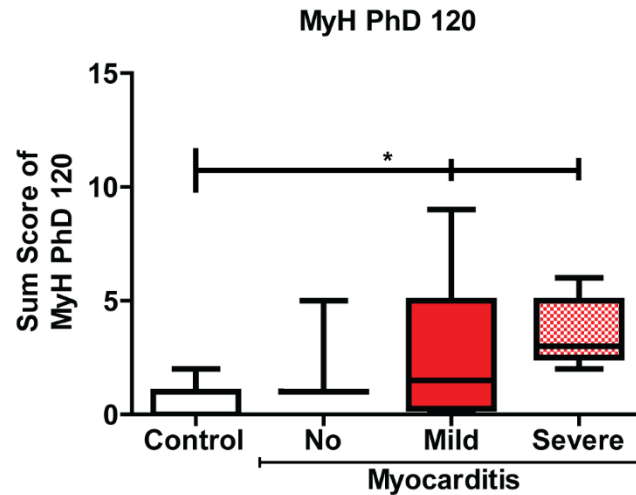


Figure 24: Quantification of *ex vivo* MyH-PhD-120 staining at 21 days. Median values (horizontal line), 25% to 75% percentiles (box), and range of values (whiskers). Control: n=15; No Myocarditis: n=3; Mild Myocarditis: n=8; Severe Myocarditis: n=5. One way ANOVA ($p < 0.05$) with Tukey multiple comparison test, $*p < 0.05$.

To verify that this increased staining was specific to the heart, off target tissue (lung, liver, spleen, kidney, thigh) in three animals with severe myocarditis were stained with MyH-PhD-05 or MyH-PhD-120. No off target binding of either MyH-PhD-05 or MyH-PhD-120 was observed (Figure 25). For future experiments, we decided to focus on exploring the targeting potential of peptide MyH-PhD-05 *in vivo*.

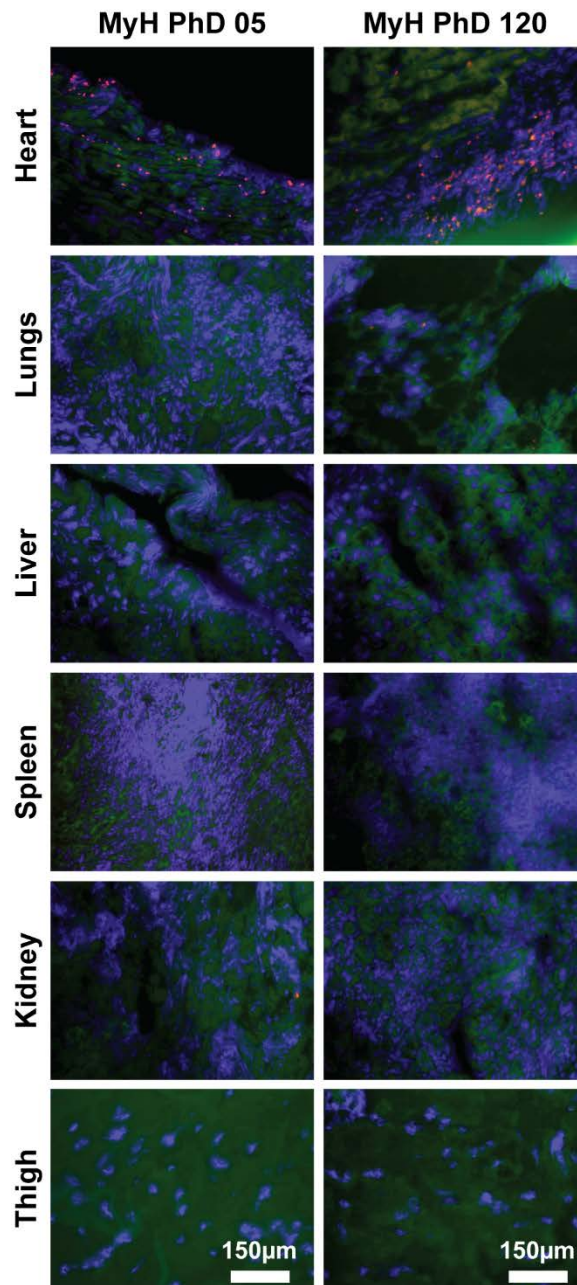


Figure 25: Representative images of organs stained with targeting peptides. The heart, lung, liver, spleen, kidney and thigh of animals with myocarditis were stained with MyH-PhD-05 or MyH-PhD-120. Both MyH-PhD-05 and MyH-PhD-120 only stained the heart in animals with severe myocarditis. Fluorescent Imaging: 20x, Blue: DAPI (nuclei), Green: FITC (auto fluorescence), and Red: Cy5 (peptide).

4.2.5: Peptide Screening in Animal Model of Myocardial Infarction

To ensure that MyH-PhD-05 was targeting inflammation specific to myocarditis, we explored the *ex vivo* targeting potential of MyH-PhD-05 in animal model of myocardial infarction (MI). Briefly, adult male C57BL/6 mice (>8 weeks old, n=2) were subjected to permanent ligation of the left anterior descending coronary artery to induce MI [100, 101]. In this model, extensive infiltration of inflammatory cells is expected around 72 hours after MI induction [101]. After allowing the animals to recover for 3 days, the animals were euthanized and the hearts were dissected and processed into frozen sections. These frozen sections were then stained with MyH-PhD-05 and imaged. As shown in Figure 26, no staining of MyH-PhD-05 was observed in the peri-infarct or the non-infarct area of the hearts of animals with MI, suggesting that MyH-PhD-05 only targets inflammation in myocarditis and not MI.

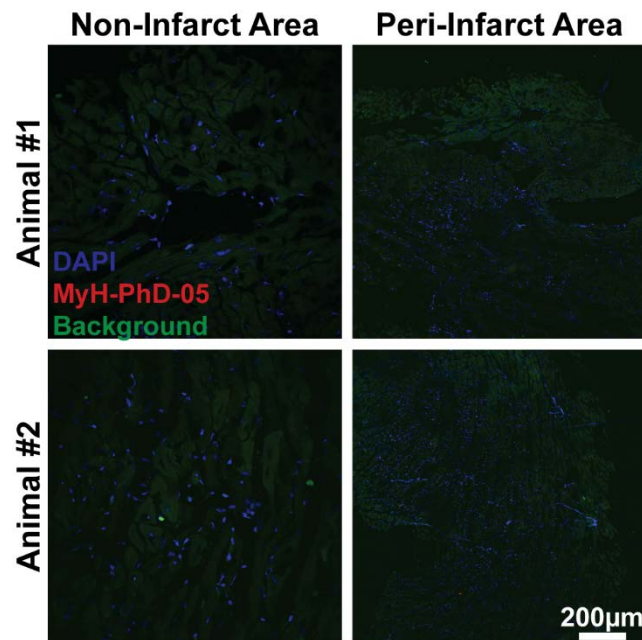


Figure 26: Representative images of hearts with MI stained with MyH-PhD-05. The non-infarct area and the peri-infarct area of two animals with myocarditis were stained with

MyH-PhD-05. No staining of MyH-PhD-05 was observed. Fluorescent Imaging: Blue: DAPI (nuclei), Green: FITC (auto fluorescence), and Red: Cy5 (peptide).

4.2.6: *In Vivo* Peptide Screening

To assess the *in vivo* targeting potential of MyH-PhD-05 and MyH-PhD-120, each biotinylated peptide was conjugated with Streptavidin DyLight 650 (Thermo Fisher Scientific). At 21 days after the induction of EAM, each animal received a tail vein IV injection containing 1100ng of one of resulting compounds, S-MyH-PhD-05 or S-MyH-PhD-120. The compound was allowed to circulate for 15 minutes after being injected, at which point animals were euthanized and the heart, lungs, liver, spleen, kidney, and thigh were dissected and immediately imaged using the In Vivo Xtreme Imaging System (Bruker). The spleen showed the lowest and least variable fluorescent signal across animals in all treatment groups, and the fold change in fluorescent signal relative to the spleen was reported for each organ of interest. A total of 63 animals were used for *in vivo* peptide screening in the following treatment groups: untreated controls (n=8), immunized with PBS/CFA (n=7), and immunized with MyH/CFA (n=48). A total of 29 out of 48 animals immunized with MyH/CFA (60.42%) developed myocarditis (mild: n=20; severe: n=9). Since we expected only 40-60% of animals immunized with MyH/CFA to develop myocarditis [62, 64, 93-99], we increased the number of animals being screened with our most promising compound S-MyH-PhD-05 (n=36) when compared with compound S-MyH-PhD-120 (n=12). For animals treated with an IV injection of S-MyH-PhD-05 (n=43), the fluorescent signal in the hearts of animals with severe myocarditis (2.05 ± 0.22 , n=7) was significantly elevated compared to the hearts of animals in the control group (1.38 ± 0.08 , $p < 0.01$, n=7), animals with no myocarditis (1.42 ± 0.06 , $p < 0.001$, n=13), and with animals with mild myocarditis (1.52 ± 0.05 , $p < 0.01$, n=16) as shown in Figure 27 and Figure 28. To determine if this trend was specific to a particular section of the heart, each

heart was excised into three different sections (the base, the midsection, and the apex) and imaged. The fluorescent signal in each of the three different sections followed a similar pattern to that observed in the whole heart. To determine if S-MyH-PhD-05 was also targeting other organs, the fluorescent signal in the lung, thigh, liver, and kidney were quantified. No significant differences between treatment groups were observed in any of these organs (Figure 29).

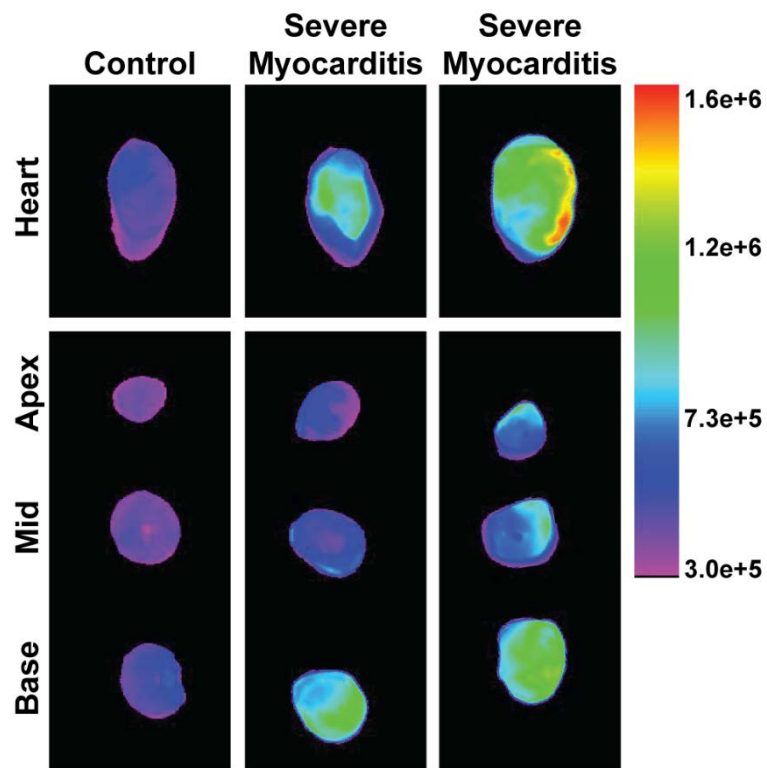


Figure 27: Representative fluorescent images of hearts treated with S-MyH-PhD-05. The hearts of animals with and without myocarditis treated with IV S-MyH-PhD-05 were dissected and fluorescently imaged at 21 days after initial immunization. The whole heart (top panels) and three different sections (bottom panels) of one control animal and two animals with severe myocarditis are shown. Scale represents relative fluorescent units.

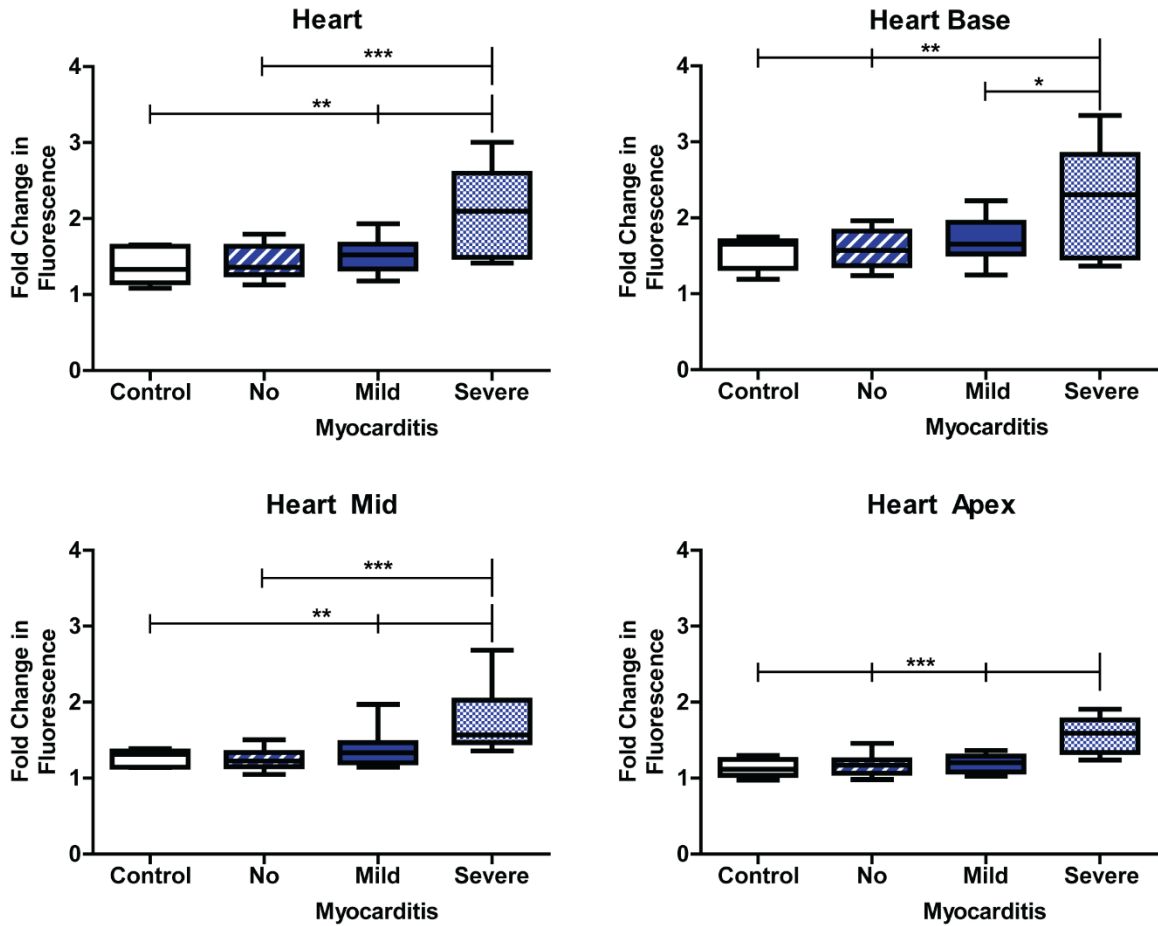


Figure 28: Quantification of S-MyH-PhD-05 signal in hearts at 21 days. The *ex vivo* fluorescent signal in the hearts of animals treated with an IV injection of S-MyH-PhD-05 at 21 days after initial immunization was quantified for the whole heart and for three different sections of the heart: the base, the midsection, and the apex. Fold change relative to spleen. Median values (horizontal line), 25% to 75% percentiles (box), and range of values (whiskers). Control: n=7; No Myocarditis: n=13; Mild Myocarditis: n=16; Severe Myocarditis: n=7. One-way ANOVA ($p < 0.05$) with Tukey's multiple comparison test, * $p < 0.05$, ** $p < 0.01$, *** $p < 0.001$.

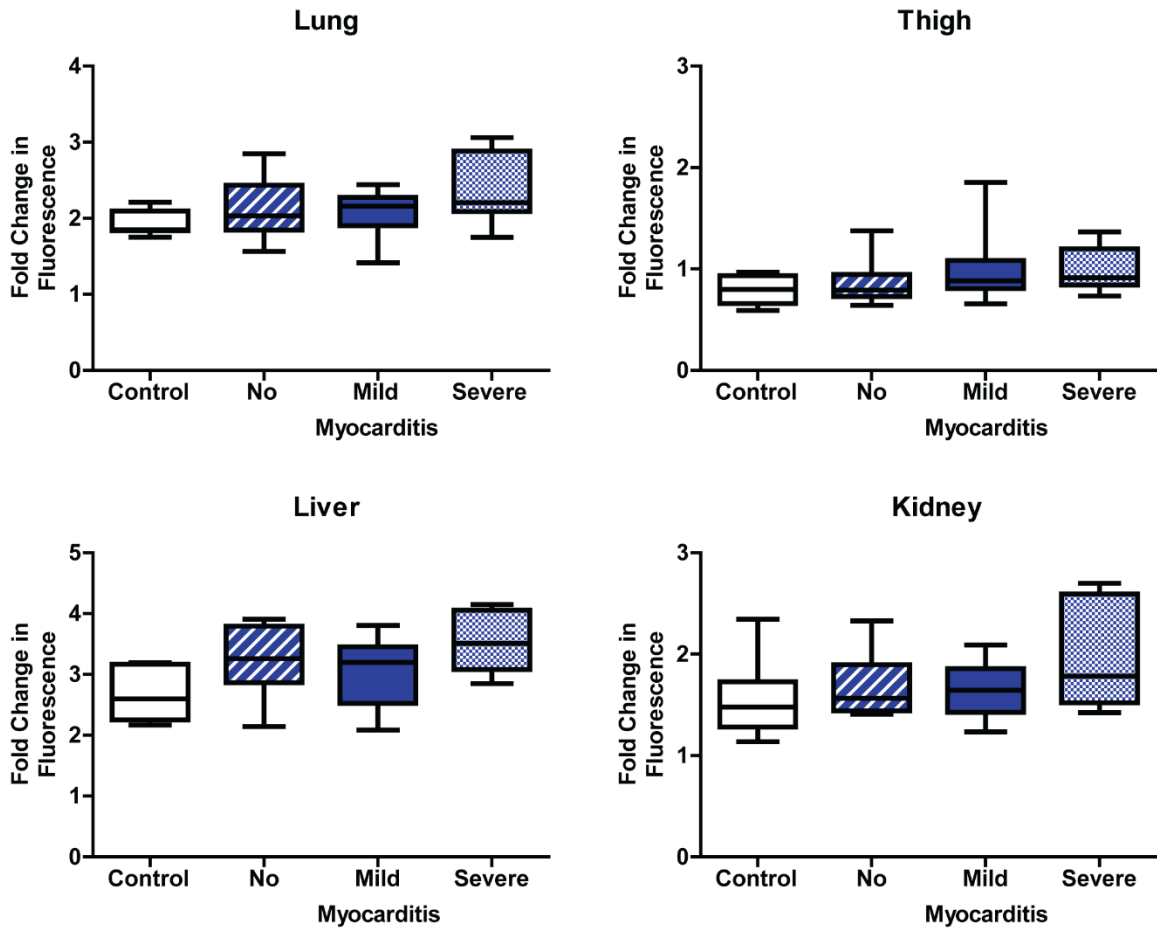


Figure 29: Quantification of S-MyH-PhD-05 signal in organs at 21 days. The *ex vivo* fluorescent signal in the lung, thigh, liver, and kidney of animals treated with an IV injection of S-MyH-PhD-05 at 21 days after initial immunization was quantified. Fold change relative to spleen. Median values (horizontal line), 25% to 75% percentiles (box), and range of values (whiskers). Control: n=7; No Myocarditis: n=13; Mild Myocarditis: n=16; Severe Myocarditis: n=7. One-way ANOVA ($p < 0.05$) not significant for any organ.

For animals treated with an IV injection of S-MyH-PhD-120 (n=20), the fluorescent signal in the hearts of animals with either mild (n=4) or severe myocarditis (n=2) were elevated compared to animals with no myocarditis (n=6) or in the control group (n=8) as shown in Figure 30. Nevertheless, a reduced number of animals were used to screen compound S-

MyH-PhD-120, resulting in inconsistent *in vivo* targeting results. It is possible that with an increased number of animals a relationship similar to that observed for S-MyH-PhD-05 would emerge for animals treated with S-MyH-PhD-120.

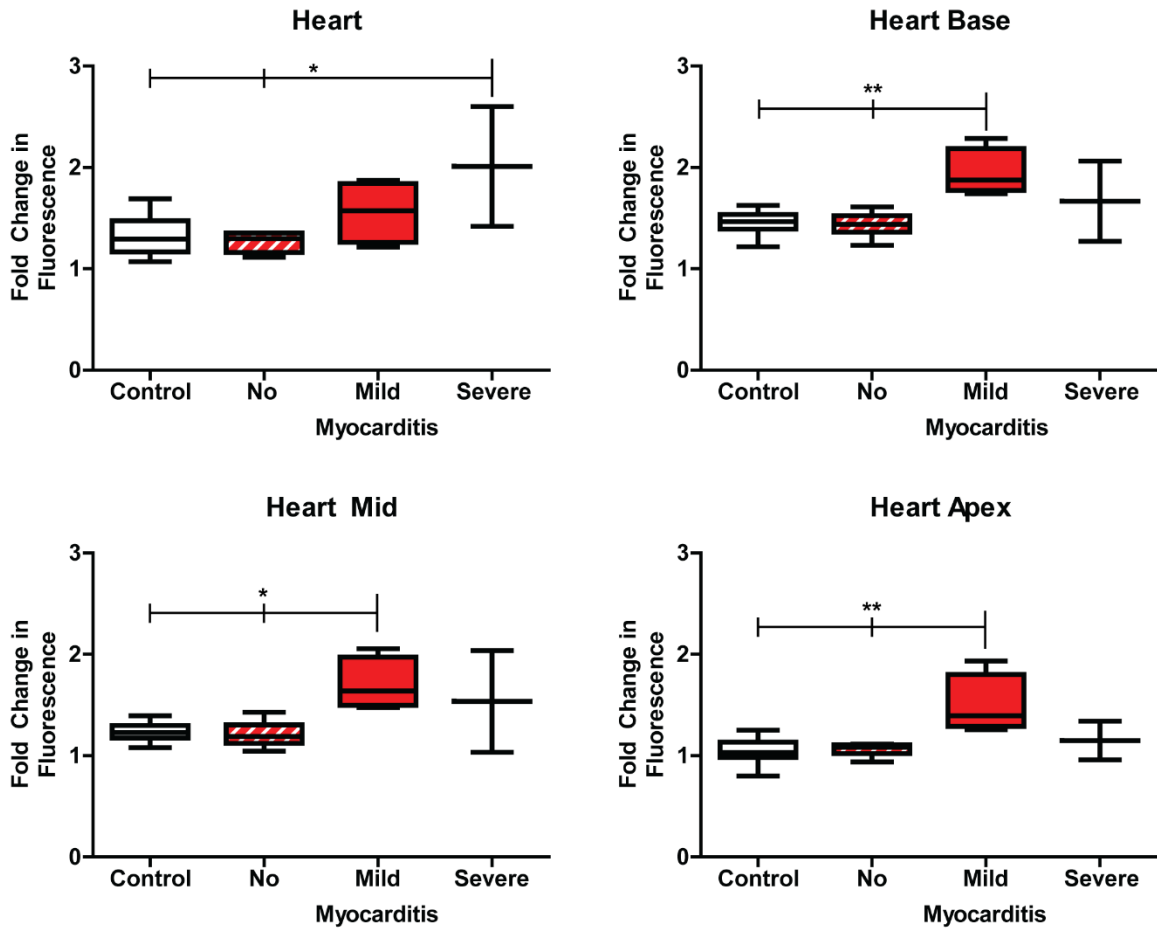


Figure 30: Quantification of S-MyH-PhD-120 signal in hearts at 21 days. The *ex vivo* fluorescent signal in the hearts of animals treated with an IV injection of S-MyH-PhD-120 at 21 days after initial immunization was quantified for the whole heart and for three different sections of the heart: the base, the midsection, and the apex. Fold change relative to spleen. Median values (horizontal line), 25% to 75% percentiles (box), and range of values (whiskers). Control: n=8; No Myocarditis: n=6; Mild Myocarditis: n=4; Severe

Myocarditis: n=2. One-way ANOVA ($p<0.05$) with Tukey's multiple comparison test, $*p<0.05$, $**p<0.01$.

It is important to reiterate that no differences in any functional parameters measured by echocardiography were observed at 21 days after initial immunization (Figure 18), demonstrating that detection of myocarditis by MyH-PhD-05 (and to a lesser extent MyH-PhD-120) is possible in the absence of functional changes. Finally, due to the nature of the study and shortcomings in fluorescent imaging, we were not able to perform longitudinal, long-term studies to determine predictive value, though that will be an important next step in future studies.

4.2.7: Immunohistochemistry

We then used immunohistochemistry to identify the cell types in inflammatory infiltrates of myocarditis and their colocalization with MyH-PhD-05. Previous studies have shown that inflammatory infiltrates in myocarditis are predominantly CD4+ T-cells; however, monocytes, macrophages, dendritic cells, and granulocytes have also been identified [62, 64]. We decided to investigate three different cell types in the inflammatory infiltrate using frozen sections of the hearts of mice with severe myocarditis (n=4). For each animal, different sections were stained with MyH-PhD-05 and either CD4 (T-cells), CD68 (macrophages), or CD11b (monocytes). Fluorescent images were acquired, and the relative fluorescence from CD4, CD68, and CD11b staining along with their colocalization with MyH-PhD-05 was measured using Fiji software. As shown in Figure 31A, the different immune markers and MyH-PhD-05 only bound to regions with inflammatory infiltrates. These infiltrates were predominantly CD4+ T cells, and MyH-PhD-05 preferentially colocalized with CD4+ T cells and monocytes (Figure 31B and Figure 31C). However, the low resolution of fluorescent microscopy (several hundred nanometers) makes it difficult

to determine if the peptide is binding to intracellular components, cell surface components or extracellular components. We decided to use proteomic analysis to identify the potential binding partners of MyH-PhD-05, although future work can focus on using other techniques such as single cell flow cytometry and multiphoton imaging.

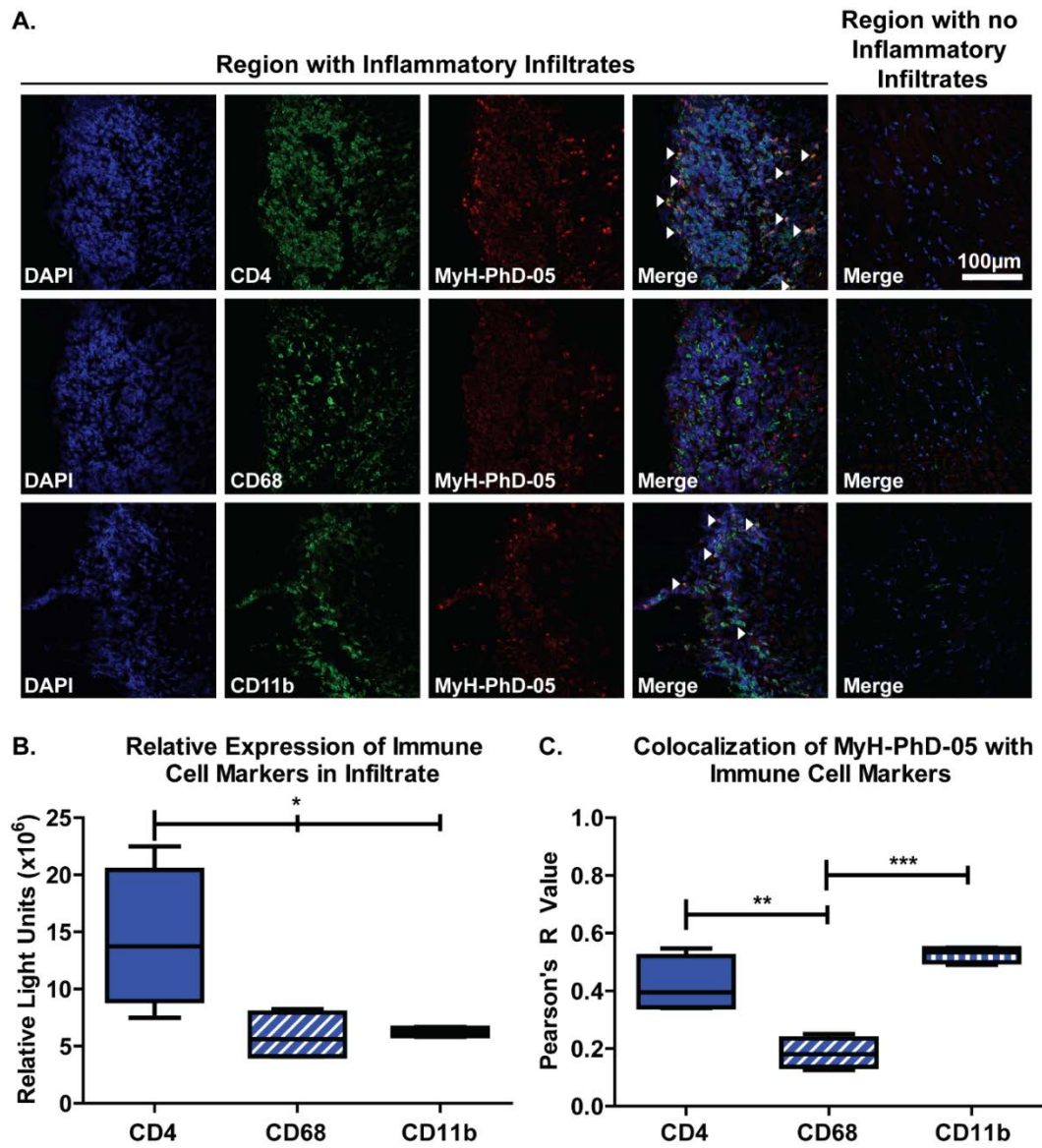


Figure 31: Representative images and quantification of immune cells in myocarditis. A. Representative images of 3 different sections of the same animal with severe myocarditis stained with CD4 (T-cells), CD68 (Macrophages), and CD11b (Monocytes) and imaged at

a region with inflammatory infiltrate and a region with no inflammatory infiltrate. B. Quantification of the relative expression each immune cell marker in the inflammatory infiltrate. C. Quantification of the colocalization of MyH-PhD-05 with each immune cell marker. Fluorescent imaging: Blue: DAPI (nuclei), Green: FITC (CD4, CD68, and CD11b), and Red: Cy5 (MyH-PhD-05). Median values (horizontal line), 25% to 75% percentiles (box), and range of values (whiskers). CD4, CD68, and CD11b: n=4. One-way ANOVA ($p < 0.05$) with Tukey's multiple comparison test, * $p < 0.05$, ** $p < 0.01$, *** $p < 0.001$.

4.2.8: Proteomic Analysis

For proteomic analysis, a total of 9 animals were used in the following treatment groups: animals immunized with MyH/CFA (n=7), and animals immunized with PBS/CFA (n=2). At 21 days after initial immunization, animals were euthanized, and the hearts were dissected and flash frozen. Each heart was then homogenized and incubated with streptavidin conjugated paramagnetic particles (MagneSphere, Promega) functionalized with biotinylated MyH-PhD-05 (New England Peptide). The resulting magnetic beads were then removed, washed with PBS, frozen, and sent to the Emory Integrated Proteomics Core for processing and analysis. All the identified genes that showed at least a two fold increase in the number of peptide spectral matches in at least two animals from the MyH/CFA treatment group when compared to the PBS/CFA treatment group average were selected for enrichment analysis with ToppGene (<https://toppgene.cchmc.org>). A total of 75 genes met the criteria for selection (Appendix Table 1). Using ToppGene, the 20 cellular components where at least 10% of the genes that met the selection criteria were present (i.e.: 8 proteins from input) were selected, and the $-\log_{10}(p \text{ value})$ for each component was reported (Figure 32). These results suggests that MyH-PhD-05 is potentially binding to several different intracellular components. This could be due to uptake of MyH-PhD-05 by different cells, although it is more likely due to the binding of

the peptide to intracellular components released into extracellular space during inflammation present in myocarditis. Several cellular components and subsets of cellular components were identified more than once in enrichment analysis, such as different mitochondrial components (n=6), or different junctional components (n=5). Given that MyH-PhD-05 has homology with cytotoxic T lymphocyte lipase, it is interesting that several cellular components have high lipid content such as the myelin sheath, the mitochondrial envelope, the mitochondrial membrane, mitochondrial inner membrane, organelle inner membrane, and the cell surface. The presence of different junctions (cell junction, cell-substrate junction, cell-substrate adherens junction, focal adhesions, adherens junctions, and anchoring junction) also suggests that MyH-PhD-05 targets proteins spanning from the cytoskeleton of the cell through the cell membrane.

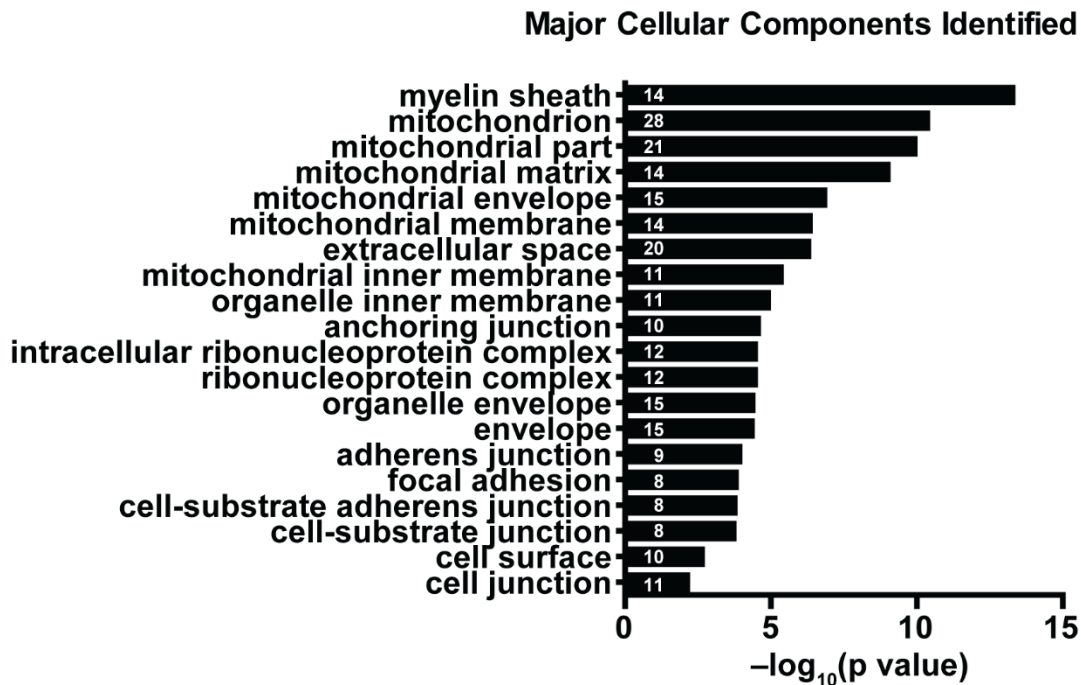


Figure 32: List of major cellular components identified through proteomic analysis. The top cellular components along the $-\log_{10}(p \text{ value})$ are provided. Numbers in bars indicate the number of identified proteins that were in each particular cellular component.

4.3: Discussion

Myocarditis is one of the most challenging diagnosis in cardiology [9, 56, 59]. The gold standard for diagnosis, EMB, is invasive and has a high risk for serious complications [9, 12, 53, 55-57, 59, 61]. Thus, there is interest in exploring noninvasive imaging modalities such as CMR, echocardiography and computerized tomography [102-107], and improvements to these imaging modalities are constantly being explored. For example, targeted molecular imaging using fluoride-19 in CMR and antibody coated microbubbles in echocardiography have shown improvements in the diagnosis of myocarditis [62, 64]. However, fluoride-19 is not specific to myocarditis and can be incorporated by macrophages and monocytes in other disease processes such as pneumonia, allograft rejection, cardiac ischemia, and cerebral ischemia; whereas the use of antibodies in therapies is limited by production costs, low tissue penetration, and host immune response to antibody [62, 63].

To address these potential limitations, we used *in vivo* phage display to identify potential targeting peptides for the diagnosis of myocarditis. Similar to other published *in vivo* phage display experiments [88-91], we performed a total of 3 pannings and identified 36 unique 12 AA peptides (Figure 20). We then selected 6 of those peptides for *ex vivo* peptide screening experiments based on either the frequency each peptide came up or on BLAST and literature review suggesting each different peptide had a homology with different cell types involved in the immune response (Table 2). After *ex vivo* screening (Figure 21-25), we selected two peptides, MyH-PhD-05 and MyH-PhD-120, for *in vivo* peptide screening. Fluorescent imaging after IV delivery of these two peptides demonstrated that MyH-PhD-05 (and to a lesser extent MyH-PhD-120) was able target animals with severe myocarditis in the absence of any functional changes (Figure 18, 27-30). We verified that MyH-PhD-

05 was targeting inflammation specific to myocarditis by testing its *ex vivo* targeting potential in animal model of MI (Figure 26). We then used immunohistochemistry on animals with severe myocarditis to demonstrate that inflammatory infiltrates are predominantly CD4+ T cells, and that MyH-PhD-05 colocalizes with CD4+ T cells and monocytes (CD11b+) (Figure 31). Finally, we used proteomic analysis to show that MyH-PhD-05 targets intracellular contents that are released to extracellular space during myocarditis (Figure 32).

The animal model of EAM is only efficient in inducing myocarditis in 40-60% of animals immunized, and those animals usually have variable disease severity as determined by the degree of infiltration observed on H&E stained sections [62, 64, 93-99] (Figure 17). To account for this, we increased the number of animals in our treatment groups. For example, in the *in vivo* peptide screening study, a total of 36 animals were immunized with MyH/CFA before treatment with S-MyH-PhD-05. It is possible that with an increased number of animals a relationship similar to that observed for S-MyH-PhD-05 would emerge for animals treated with S-MyH-PhD-120 (n=12). Additionally, the protocols that are used to score animals for myocarditis and myocarditis severity vary among different reports [62, 64, 93-99]. These protocols are also subject to inter- and intra-observer variability in addition to investigator bias. To account for this, we selected a protocol similar to the ones that have been more recently published and all scoring was conducted and analyzed by investigators blinded to the animal's treatment group [62, 64]. In keeping with prior studies, we were unable to show functional differences in cardiac function at 21 days, despite some animals having severe myocarditis. This is important as it shows that the peptide MyH-PhD-05 is able to detect myocarditis in the absence of functional changes.

In vivo phage display has been extensively used in different animal models [88-92]. Although the use of more than 3 pannings could aid in screening for peptides with stronger affinity for myocarditis, most protocols and studies suggest that using 3 pannings is appropriate. Furthermore, since only 40-60% of animals immunized with MyH/PhD were expected to develop myocarditis, we pooled together the hearts of animals for each of the four treatment groups. As a result, a total of 43 animals were used for these experiments and each additional panning would have been both resource and time intensive without necessarily providing better results. We also expected to see a preferential accumulation in the number of phages binding to the hearts of animals in the MyH PhD group in each subsequent panning when compared to the other treatment groups, but this was not observed (Table 1). This is probably due the variability present in the titrating process and the single data point present for each panning after pooling animals in the same treatment group together. Finally, only a handful of colonies were picked for sequencing for each of the four treatment groups. Of those colonies sequenced, we selected only 6 peptides for *ex vivo* screening (Table 2). It is possible that screening more colonies or selecting more peptides could have yielded other good candidates for targeting myocarditis, though screening so many candidates is both time and resource intensive.

For our *in vivo* peptide screening experiments, we were unable to measure the level of fluorescent signal in the heart of animals when these animals were being imaged *in vivo* under anesthesia. This is probably due to the low penetrance of the fluorescent signal through tissue and the low levels of peptide present in focal regions with inflammatory infiltrates in animals with myocarditis. Thus, we presented *ex vivo* fluorescent data (Figure 27-30). In future experiments, using higher concentrations of our peptide or conjugating our peptides to fluorescent molecules with higher wavelengths (i.e.: Streptavidin DyLight 800) could yield better results. Due to the nature of our studies and the shortcomings in

fluorescent imaging, we were not able to perform longitudinal, long-term studies to determine predictive value, though that is also an important next step.

While identifying the exact cell and protein that our peptides target is of great interests, it was difficult to determine using our immunohistochemistry analysis. The resolution of fluorescent microscopy is several hundred nanometers, making it difficult to determine if our peptide is binding to intracellular components, cell surface components, or extracellular components. We decided to use proteomic analysis to identify the potential binding partners of MyH-PhD-05, although future work can focus on using other techniques such as single cell flow cytometry and multiphoton imaging. Furthermore, our initial studies focused on screening for only three different cell types, CD4+ T cells, macrophage (CD68), and monocytes (CD11b). Future experiments will focus on screening for other cell types and markers that are present in inflammatory infiltrates of myocarditis, such as macrophages (F4/80), dendritic cells (CD11c), and granulocytes (Gr-1) [62, 64].

Proteomic analysis suggested that S-MyH-PhD-05 was binding to several different intracellular components. This could be due to uptake of phages containing MyH-PhD-05 by different cells, although it is more likely due to the binding of the phages to intracellular components released into extracellular space during inflammation present in myocarditis. Several cellular components and subsets of cellular components were identified more than once in enrichment analysis, such as different mitochondrial components (n=6), or different junctional components (n=5). Given that MyH-PhD-05 has homology with cytotoxic T lymphocyte lipase, it is interesting that several cellular components have high lipid content such as the myosin sheath, the mitochondrial envelope, the mitochondrial membrane, mitochondrial inner membrane, organelle inner membrane, and the cell surface. The presence of different junctions (cell junction, cell-substrate junction, cell-

substrate adherens junction, focal adhesions, adherens junctions, and anchoring junction) also suggests that MyH-PhD-05 targets proteins spanning from the cytoskeleton of the cell through the cell membrane.

In summary, we were able to use *in vivo* phage display to identify and test potential targeting peptides for myocarditis. We identified one peptide, MyH-PhD-05, that targets severe myocarditis. Future studies will focus on better identification of its potential targets. For clinical applications, MyH-PhD-05 can be conjugated to other imaging agents to improve current diagnostic and therapeutic technologies. For example, MyH-PhD-05 could be conjugated to microbubbles for echocardiography [64] or to gadolinium contrast agents for CMR, which have been used clinically in myocarditis [105, 108]. MyH-PhD-05 can also be conjugated to different dendrimers or exosomes in order to deliver novel therapies such as CD40 siRNA, CCR2 siRNA, or P2X7 receptor antagonist [94, 109-112], and improve clinical outcomes. Additionally, when considering clinical applications of MyH-PhD-05, it is important to note that MyH-PhD-05 has similar homology in humans as mice (homology: lipase, pancreatic triacylglycerol lipase precursor, ryanodine receptor) and thus future studies will examine human biopsies.

CHAPTER 5: SUMMARY AND FUTURE DIRECTIONS

Cardiovascular disease (CVD) has accounted for more deaths than any other major cause of death in the United States every year since 1900, with the exception of 1918 [1]. Despite improvements in the management of CVD, there is still a need for new and improved treatments and diagnostics. In peripheral artery disease (PAD), treatment with pro-angiogenic growth factors, such as vascular endothelial growth factor (VEGF), is currently being explored [4-6, 26]. However, there is a need to overcome limitations of this therapy, such as the growth factor's short half-life, inadequate delivery to target tissue, and inadequate retention at target tissue [5, 7, 8, 19, 26, 33-35]. In myocarditis, a large number of patients go undiagnosed due to the disease's heterogeneous etiology, pathophysiology, and clinical presentation [9, 12]. Current diagnostic techniques, such as endomyocardial biopsy and cardiac magnetic resonance, are inadequate, and there is a need for new technologies for the appropriate diagnosis and timely treatment of myocarditis. This dissertation aims to explore two different targeting techniques for the treatment and diagnosis of PAD and myocarditis.

5.1: Targeted Delivery of VEGF for the Treatment of PAD

5.1.1: Summary

In this project we explored the use of a novel targeted delivery system using a modified Hoechst compound to target extracellular DNA in an animal model of PAD and deliver VEGFmp or VEGF₁₆₅ to ischemic tissue. We successfully synthesized two different compounds, HoVEGFmp and HoVEGF₁₆₅. After conjugation, we used a permeability assay to confirm that both compounds were cell impermeable but retained the ability to bind to extracellular DNA. We then used Western blot analysis and a tube formation assay

to demonstrate that our compounds retained their angiogenic activity, but these results were inconclusive. For *in vivo* studies, we used an animal model of hindlimb ischemia (HLI). Neither of compounds showed improvements in retention or targeting when compared to controls.

5.1.2: Limitations

The major limitation of this project is the rapid breakdown of our compounds *in vivo*. Blood plasma contains a number of different proteinases that can rapidly breakdown both peptides and proteins [82, 83]. Furthermore, in sites of inflammation there is an increase in the amount of proteinases that can breakdown any circulating peptides and proteins [82, 83]. In our retention studies, an inflammatory response to the femoral ligation surgery increases the levels of proteinases present at the injury site, which in turn leads to the rapid breakdown of both peptides (HoVEGFmp) and proteins (HoVEGF₁₆₅). In our targeting studies, both of our compounds were broken down by proteinases present in blood plasma before reaching the target tissue.

A second limitation of this project is the rapid breakdown and excretion of our compound through the kidneys. Both peptides (<5kDa) and small proteins (20kDa) are efficiently cleared by the kidneys, with renal clearance ratios of 1.0 and 0.5-0.8 respectively [82, 84, 86]. Peptides are usually hydrolyzed by brush membrane proteinases, while proteins are collected in endocytic vacuoles that fuse with lysosomes and break down the proteins [82, 84, 86]. In both our retention and targeting studies, our compounds were rapidly cleared through the renal system. Interestingly, we observed fluorescent signal in the anatomical area corresponding to the bladder for animals that were treated with HoVEGFmp, but not for animals treated with HoVEGF₁₆₅. This suggests that our HoVEGFmp was being broken down in the brush border membrane of the kidneys, while HoVEGF₁₆₅ was internalized

into endocytic vacuoles, where the fluorophore was probably broken down instead of being secreted through the renal system.

Finally, for *in vivo* studies we used an animal model of HLI with BALB/c mice. BALB/c mice have been reported to have fewer or narrower collaterals when compared to C57BL/6 mice [71]. Even though we would expect more severe ischemia and necrosis in BALB/c mice, the lack of collaterals limits the amount of compound that can be delivered to areas of ischemia and necrosis.

5.1.3: Future Directions

To circumvent the limitations of our compounds, we need to explore making certain modifications that increase the stability of our compounds *in vivo*. For example, some modifications that might increase the half-life of our peptide and protein based compounds include glycosylation, PEGylation, substitution of peptide cleavage sites, modification of secondary peptides structures, and binding to carrier proteins such albumin [82-85]. Perhaps one modification that can be easily explored is the conjugation of both our modified Hoechst compound and VEGFmp or VEGF₁₆₅ to streptavidin (~50kDa). In our lab, streptavidin has been successfully conjugated to both peptides (Chapter 4) and proteins (Insulin Growth Factor-1 [23]) for *in vivo* studies.

We also need to explore modifications to our animal model. For example, using C57BL/6 mice instead BALB/c mice might provide more collaterals for our compound to be delivered to ischemic tissue. Furthermore, we can adjust the severity of ischemia by removing part of the femoral artery in order to induce more necrosis and release more DNA [113], although this might cause more inflammation at the surgery site. Finally, we

can also explore using animal models that better reflect the underlying atherosclerotic disease in patients with PAD, such as using ApoE knockout mice [114].

5.2: Identification of Targeting Peptides for the Diagnosis of Myocarditis

5.2.1: Summary

In this project, we identified a targeting peptide for the diagnosis and treatment of myocarditis. In an animal model of myocarditis, we used an *in vivo* phage display library to identify peptides that preferentially targeted diseased myocardium. We then did *ex vivo* screening on six of our potential peptides, successfully identifying two peptides whose binding correlated with disease severity. *In vivo* screening demonstrated that one peptide, MyH-PhD-05, was able to detect animals with severe myocarditis in the absence of functional changes. Immunohistochemistry was used to show that inflammatory infiltrates in myocarditis are predominantly CD4+ T cells, and that MyH-PhD-05 colocalizes with CD4+ T cells and monocytes (CD11b+). Finally, proteomic analysis was used to demonstrate that MyH-PhD-05 targets intracellular contents that are released to extracellular space during myocarditis.

5.2.2: Limitations

The animal model of myocarditis that we used is only efficient in inducing myocarditis in 40-60% of animals immunized, and those animals usually have a variable severity of myocarditis [62, 64, 93-99]. To account for this, we increased the number of animals in our treatment groups. However, there is no way to determine beforehand how many animals will develop mild myocarditis or severe myocarditis. Furthermore, the protocols that are used to score animals for myocarditis and myocarditis severity vary among different reports [62, 64, 93-99]. These protocols are subject to inter- and intra-observer

variability. To account for this, all scoring was conducted and analyzed by investigators blinded to the animal's treatment group. The cutoffs used to define mild myocarditis and severe myocarditis also vary between different reports. We used a cutoff similar to the ones employed by Steini et al and van Heeswijk et al [62, 64], although we adjusted the cutoffs to account for the fact that animals that were not immunized at all sometimes showed small foci of leukocytes between cells (i.e.: H&E Sum Score ≤ 3).

For *in vivo* phage display experiments, only a handful of colonies were picked for sequencing for each of the four treatment groups. Of those colonies sequenced, we selected only 6 peptides for *ex vivo* screening (Table 2). It is possible that screening more colonies or selecting more peptides could have yielded other good candidates for targeting myocarditis, though screening so many candidates is both time and resource intensive.

For our *in vivo* peptide screening experiments, we were unable to measure a fluorescent signal *in vivo*. Thus, all the data presented in Chapter 4 is based on the *ex vivo* imaging done 10 minutes after treatment of animals with our targeting peptides. The use of higher concentrations of our peptides or conjugating our peptides to fluorescent molecules with higher wavelengths (i.e.: Streptavidin DyLight 800) could allow us to use *in vivo* imaging instead of *ex vivo* imaging. This would allow us to do long term longitudinal studies and to reduce the amount of animals used in our future experiments.

Finally, the identification of the exact cell and protein that our peptides target is limited by the use of both immunohistochemistry and proteomic analysis. The resolution of fluorescent microscopy is several hundred nanometers, making it difficult to determine if our peptide is binding to intracellular components, cell surface components, or extracellular components. Proteomic analysis, on the other hand provides good

resolution of cellular components targeted, but not of specific proteins. Future work can focus on using other techniques such as single cell flow cytometry and multiphoton imaging that provide better resolution.

5.2.3: Future Directions

In the future, we will further explore the cells and proteins our peptides are targeting. In myocarditis, many different inflammatory cell populations play a role, such as leukocytes, T lymphocytes (helper T cells, cytotoxic T cells, Memory T cells, etc.) B-lymphocytes, macrophages, natural killer cells, and dendritic cells [54, 55, 58, 98, 115, 116]. Additionally, there is wide variety of cytokines, metalloproteases, and other proteins that are involved [94-96, 111, 112, 117]. We can use flow cytometry and multiphoton imaging to identify the cell populations and proteins that our peptides target.

We can also conjugate our peptides to improve current diagnostic technologies. For example, our peptides could be conjugated to microbubbles for echocardiography [64, 118], or to gadolinium contrast agents for MRI [108, 119, 120]. We can also conjugate our peptides to different dendrimers or exosomes in order to deliver novel therapies such as CD40 siRNA, CCR2 siRNA, or P2X7 receptor antagonist [94, 109-112].

Finally, when considering clinical applications of peptides, it is important to note that our peptide MyH-PhD-05 has similar homology in humans as mice (human homology: lipase, pancreatic triacylglycerol lipase precursor, ryanodine receptor) and thus future studies can examine the targeting potential of this peptides on human biopsies.

APPENDIX

A.1: Methods for Peripheral Artery Disease Project

A.1.1: Synthesis of Compounds

A.1.1.1: Synthesis of HoVEGFmp

VEGFmp (MW = 3166.9g/mol, Anaspec) was resuspended in deionized water to a molarity of 1nmol/ μ L. Hoechst-thiopyridyl (MW = 751.96g/mol, Niren Murthy Lab) was resuspended in deionized water to a molarity of 1.86nmol/ μ L. Equimolar amounts of each compound were mixed together in addition to PBS/EDTA to the final desired molarity. For example, 25nmol of each reagent plus PBS/EDTA were mixed to a final volume of 50 μ L to synthesize a compound with a molarity of 0.5nmol/ μ L. The reaction was allowed to proceed for 3 hours at room temperature. Using a Slide-A-Lyzer Mini Dialysis Unit with a 2kDa molecular weight cut off (Thermo Scientific #69580), the resulting compound was then dialyzed three times in 50mL of PBS/EDTA. The first two dialysis were for 2 hours at room temperature, and the third dialysis was overnight in a cold room (2-8°C). A Bradford Assay was used to determine the final concentration.

A.1.1.2: Synthesis of HoVEGF₁₆₅

Human recombinant VEGF₁₆₅ (MW = 19,165g/mol, Cell Signaling #8065) was resuspended in sterile PBS to a final concentration of 1000 μ g/mL. The DyLight 800 Microscale Antibody Labelling Kit (Thermo Scientific #53063) was then used as instructed to fluorescently label the protein (VEGF₁₆₅-Dy). We then used a Bradford Assay to determine our protein yield (i.e.: in one batch, the yield was 88.53% with a VEGF₁₆₅ concentration of 995.45 μ g/mL and a VEGF₁₆₅-Dy concentration of 881.25 μ g/mL). For

further conjugation calculations, we assumed VEGF₁₆₅-Dy was conjugated to at least one fluorophore (MW=1050g/mol) and had a MW of 20,215g/mol. Hoechst-thiopyridyl (MW = 751.96g/mol) was resuspended in deionized water to a molarity of 0.337nmol/μL. For every 1nmol of VEGFG₁₆₅-Dy, 20nmol of Hoechst-thiopyridyl were added in addition to PBS/EDTA to a final molarity of 0.0109nmol/μL. The reaction was allowed to proceed for 3 hours at room temperature. Using a Slide-A-Lyzer Mini Dialysis Unit with a 2kDa molecular weight cut off (Thermo Scientific #69580), the resulting compound was then dialyzed three times in 50mL of PBS/EDTA. The first two dialysis were for 2 hours at room temperature, and the third dialysis was overnight in a cold room (2-8°C). A Bradford Assay was used to determine the final concentration.

A.1.2: Methods for *In Vitro* Studies

A.1.2.1: Permeability Assay

A.1.2.1.1: HoVEGFmp

Cardiomyocyte progenitor cells were isolated from the hearts of adult male Sprague-Dawley rats by selection of c-Kit⁺ cells with anti-cKit antibody (H-300, Santa Cruz) coated magnetic beads (Dyna) as previously described [121]. CPC growth media consisted of Ham's F12 media, 10% Fetal Bovine Serum (FBS), basic Fibroblast Growth Factor (10ng/mL), Leukemia Inhibitory Factor (10ng/mL), Penicillin/Streptomycin (100 Units/mL, 100μg/mL), and L-Glutamine (2mM). 10,000 cells were plated on 4 different wells of a 96 well plate and allowed to grow for 2 days. For fixed cells (2 wells), 100μL of ice cold methanol was added to each well for 10 minutes. The methanol was then removed and each well (including 2 wells with live cells) was washed with 100μL of CPC growth media. A total of 100μL of treatment (2.00 x 10⁻⁶M of either Hoechst-thiopyridyl or HoVEGFmp in

CPC growth media) was then added to each respective well for 20 minutes. Treatments were then removed, and 50µL of Hank's Balanced Salt Solution was added to each well. Each well was then imaged using fluorescent microscopy with a DAPI filter.

A.1.2.1.2: HoVEGF₁₆₅

Immortalized mouse aortic endothelial cells (iMAECs) were received from the Hanjoong Jo Lab. iMAEC growth media consisted of DMEM, ECGS (Sigma #E2759, 50µg/mL), MNEAA (GIBCO #11140-050), 10% FBS, and Penicillin/Streptomycin (100Units/mL, 100µg/mL). 50,000 cells were plated on 6 different wells of a 24 well plate and allowed to grow for 2 days. For fixed cells (3 wells), 200µL of ice cold methanol was added to each well for 10 minutes. The methanol was then removed and each well (including 3 wells with live cells) was washed with 200µL of iMAEC growth media. A total of 200µL of treatment (2000ng/mL of Hoechst 33258, 2000ng/mL of Hoechst-thiopyridyl or 500ng/mL of HoVEGF₁₆₅ in iMAEC growth media) was then added to each respective well for 20 minutes. Treatments were then removed, and 200µL of Hank's Balanced Salt Solution was added to each well. Each well was then imaged using fluorescent microscopy with a DAPI filter.

A.1.2.2: Western Blot Analysis

iMAECs were received from the Hanjoong Jo Lab. iMAEC growth media consisted of DMEM, ECGS (Sigma #E2759, 50µg/mL), MNEAA (GIBCO #11140-050), 10% FBS, and Penicillin/Streptomycin (100Units/mL, 100µg/mL). Once confluent, cells were starved for 5-6 hours in starving media, which includes DMEM, MNEAA, and Penicillin/Streptomycin. Treatments of HoVEGFmp and VEGFmp were made to a final molarity of 1.00×10^{-6} in starving media. After 5-6 hours, starving media was removed and replaced with the appropriate treatment of either HoVEGFmp or VEGFmp. At the appropriate time point (1,

5, 10, or 30 minutes after treatment), the treatment was removed, and cell lysis buffer was added. Lysates were then removed from each well, pipetted into an Eppendorf tube and placed in the cold room overnight. Bradford was performed to determine the protein concentration of each lysate. For Western Analysis, 40µg of protein were loaded into each lane, and a standard protocol was followed. Antibodies for pERK1/2 (Cell Signaling #9101S) and ERK1/2 (Cell Signaling #9102S) were used and bands were analyzed using ImageJ.

A.1.2.3: Tube Formation

Rat Cardiac endothelial cells (CECs) were thawed from previous stocks in the Davis Lab. CEC growth media was made using the Complete Rat Endothelial Cell Media Kit (Cell Biologics #M1266). Growth media consisted of suggested ratios of kit contents: EGF, FBS (2%), L-Glutamate, Antibiotic/Antimycotic, and CEC Base Media. After the cells were confluent, they were placed in starving media (0.4% FBS) overnight. All treatments (500ng/mL of VEGF₁₆₅, VEGF₁₆₅-Dy, and HoVEGF₁₆₅) were made in Insulin Transferrin Selenium (ITS) media, which included the same components of growth media but ITS was used to replace FBS. The starving media was replaced with the appropriate treatment (1mL per well in a 6 well plate) for 24 hours. After treatment, the cells were removed and from their respective wells using TrypLE (Thermo Scientific), and 30,000 cells/cm² were placed on each well of a 96 well plate covered with Geltrex (Thermo Scientific). After six hours, 50µL of 4µM Calcein was added to each well and left to incubate for 15 minutes. Fluorescent images was performed.

A.1.3: Animal Models

A.1.3.1: Hindlimb Ischemia

Male BALB/c mice were anesthetized with 1-3% isoflurane, intubated, and placed on a heating pad (37°C). Hair was removed from both hindlimbs using Nair hair removal lotion. On the left hindlimb, a small incision (5mm) was made beginning at the inguinal crease along the femoral vessels that are visible through the skin. At the origin of the deep femoral artery, the nerve, artery, and vein were gently separated to avoid injury. The first ligation of the femoral artery was done at this site. Similar procedure was used to separate the femoral nerve, artery, and vein at the knee level of the exposed hindlimb, where the saphenous artery originates. A second ligation of the femoral artery was done at this site. Animals were allowed to recover for 1 day before undergoing Laser Doppler Perfusion Imaging for functional assessment or receiving appropriate treatments.

A.1.3.2: Myocardial Infarction

Myocardial infarction was performed on male C57BL/6 mice. Briefly, mice were anaesthetized (1-3% isoflurane), intubated and heat exposed by separation of ribs. The left anterior descending (LAD) coronary artery was ligated for 30 minutes. Animals were then closed and allowed to recover for 1 day before receiving appropriate treatments.

A.1.4: Methods for *In Vivo* Studies

A.1.4.1: SYBR Gold Nucleic Assay Gel Stain

Blood was extracted from each animal (20µL) by nicking their tail and collecting blood in sterile capillary tubes containing EDTA at different time points (2, 24, and 48 hours after surgery). After 30-60 minutes, samples were spun at 2,000 x g for 5 minutes and the

supernatant (serum) was removed and placed in a new Eppendorf tube. SYBR Gold Nucleic Acid Gel Stain (Thermo Fisher Scientific #S11494) was used as indicated to measure DNA concentrations using a plate reader (Excitation / Emission: 485nm/528nm) and a single stranded DNA standard.

A.1.4.2: Fluorescent Imaging

In vivo and *ex vivo* Fluorescent imaging was performed using either the Xenogen IVIS 100 imaging system or the In Vivo Xtreme Imaging system. For *in vivo* imaging, animals were anesthetized using 1-3% isoflurane, and each individual mouse was imaged using appropriate filters and exposures. For *ex vivo* imaging, organs were imaged immediately after dissection using appropriate filters and exposures. Fold change in fluorescent signal relative to control tissue was reported for each region of interest. In animals undergoing hindlimb ischemia, the contralateral hindlimb was used as the control tissue. In animals with EAM, the spleen was used as the control tissue.

A.1.4.3: Homogenization of Tissue

We weighed the tissue to be homogenized. For every 1mg of tissue, 3-5mL of lysis buffer (with protease and phosphatase inhibitors) were added. Tissue was homogenized and left in the cold room overnight. The next day samples were centrifuged at 13,000 x g for 10 minutes, and the supernatant was removed and placed in a new Eppendorf Tube. Bradford was performed to determine the protein concentration.

A.1.4.4: Immunoprecipitation

For immunoprecipitation, 100µg of protein were incubated with VEGFR-2 Antibody overnight in a cold room. 20µL of appropriate microbeads were then added to each samples, and the samples were incubated for 2 hours. Samples were then centrifuged at

2,500 x g for 5 minutes, and the supernatant was removed. To elute the proteins, 30 μ L of Laemeli dye was used and Westerns were run using VEGFR-2 and p-tyrosine kinase antibodies.

A.1.5: Statistical Analysis

All statistical analysis were performed using GraphPad Prism 5. All data are expressed as Mean \pm SEM. To determine significance, either a One-way or Two-way analysis of variance (ANOVA) were performed, followed by Tukey multiple comparisons test or Bonferroni post hoc test. For correlations, a linear regression was done followed by a Pearson's correlations method. For all tests, a p-value <0.05 was considered significant.

A.2: Methods for Myocarditis Project

A.2.1: Animal Models

A.2.1.1: Animal Model of Experimental Autoimmune Myocarditis

All animal experiments were performed with the approval of the Emory University Institutional Animal Care and Use Committee. A total of 146 male BALB/c mice (6-8 weeks old) were used in this study and were divided as follows: 43 Animals for phage display, 31 for *ex vivo* analysis, 63 for *in vivo* analysis and immunohistochemistry, and 9 for proteomic analysis. To induce experimental autoimmune myocarditis (EAM), mice were anesthetized using 1-3% isoflurane (Piramal) and injected subcutaneously at 0 and 7 days with 150µg of myosin heavy-chain α peptide (MyH: Ac-SLKLMATLFSTYASAD-OH, New England Peptide) dissolved in 100µL of PBS and emulsified with 100µL of complete Freund's adjuvant (CFA, Sigma) [62, 64, 93-99]. For control animals, animals were either injected subcutaneously at 0 and 7 days with 100µL of PBS emulsified in 100 µL of CFA, or received no treatment. In this model, 40-60% of animals develop myocarditis with variable severity [62, 64, 93-99]. This phenotype is characterized by the presence of inflammation within 10 days after initial immunization, which peaks around day 21 and is cleared by day 56 [55, 99].

Each treatment dose was prepared the day before by mixing the MyH or PBS with CFA, capping the mixture tightly, and vortexing it overnight in the cold room. One the day of treatment, the emulsion was drawn up using glass syringes and 18-G needles and thoroughly mixed. After removing the air, the 18-G needles were replaced with a 25-G needle, and emulsion was injected subcutaneously onto the back of anesthetized animals.

A.2.1.2: Animal Model of Myocardial Infarction

All animal experiments were performed with the approval of the Emory University Institutional Animal Care and Use Committee. A total of 2 adult male C57BL/6 mice (>8 weeks old) were subjected to myocardial infarction (MI) in this study. Briefly, the animals were anesthetized using 1-3% isoflurane (Piramal), and after tracheal intubation, the hearts were exposed by separation of the ribs. Myocardial infarction was induced by the permanent ligation of the left anterior descending coronary artery [100, 101]. The chest was then closed and the animals were allowed to recover. After 3 days, when extensive infiltration of inflammatory cells is expected [101], the hearts were removed and processed into frozen sections for immunohistochemistry and immunofluorescence as described below.

A.2.2: *In Vivo* Phage Display

A total of 43 animals were used for *in vivo* phage display. The experimental setup is similar to what has been previously described and is shown in Figure 20 [88-91]. A total of 3 cycles or pannings were performed, similar to other published *in vivo* phage display experiments.[88-91] Briefly, at day 21 after induction of EAM, animals were anesthetized using 1-3% isoflurane (Piramal) and received an intravenous (IV) injection through the tail vein with either a linear 12 amino acid (AA) peptide phage library (Ph.D. 12 Phage Display Peptide Library Kit, New England BioLabs, #E8110S) or an empty phage (M13KE, New England BioLabs, #EN0316S) at a concentration of 1×10^9 plaque-forming units (pfu)/ μL of PBS (110 μL total volume). For each panning, animals were divided into the following treatment groups: MyH PhD: immunized with MyH/CFA and injected with the phage library (n=5 per panning); MyH Cont: immunized with MyH/CFA and injected with the control phage (n=4-5 per panning); PBS PhD: immunized with PBS/CFA and injected with the phage library (n=2-3 per panning); and PBS Cont: immunized with PBS/CFA and injected

with the control phage (n=2 per panning). After allowing the phage to circulate for 10 minutes, animals were euthanized with CO₂ and the hearts were excised, washed extensively in PBS and flash frozen.

A.2.2.1: Phage Amplification

The hearts for each of the four treatment groups were then weighed, pooled together, and homogenized in DMEM (Sigma) with protease inhibitors (Sigma) and phosphatase inhibitors (Sigma) at 1g of tissue per 1-4mL of DMEM solution. Each homogenate was then centrifuged at 2400xg and the pellet was re-suspended in DMEM solution.

ER2738 Bacteria was streaked out on LB plates with tetracycline, and incubated at 37°C overnight. For phage amplification, 20mL of LB medium were placed in an Erlenmeyer flask and inoculated with a single ER2738 colony for each treatment group. Bacteria was allowed to grow until early-log (~2 hours). A total 400µL of the homogenate for each treatment group was added to each corresponding Erlenmeyer flask, and the bacteria was allowed to grow until mid-log (~4 hours). The resulting culture was placed in a centrifuge tube and spun for 10 minutes at 12,000 x g at 4°C. The resulting supernatant was transferred to fresh centrifuge tube and spun for 10 minutes at 12,000 x g at 4°C. The pellet was discarded and the supernatant was mixed with 1/6 volume of 20%PEG/2.5M NaCl and incubated overnight in the cold room in order to precipitate the phage.

The resulting solution for each treatment group was spun at 12,000g for 15 minutes at 4°C. The supernatant was discarded and the remaining pellet was resuspended in 1mL of TBS. The solution was re-spun and precipitated with 20%PEG/2.5M NaCl one more time in order to ensure no contamination was found. At the end, the resulting pellet was resuspended in 200µL of TBS.

A.2.2.2: Phage Titering

For phage titering, 5-10mL of LB were inoculated with a single colony of ER2738 Bacteria and allowed to grow for 4-8 hours. For each treatment group, serial dilutions of the purified phage in LB were made ranging from 10^3 to 10^{11} . A total of 200 μ L of ER2730 were infected with 10 μ L of each phage dilution for each treatment group and incubated for 5 minutes. The infected cells were then placed in tubes containing 45°C Top Agar and poured on pre-wared LB/IPTG/Xgal plates. The plates were incubated overnight at 37°C. The next day, blue plaques were counted on plates with at least 100 blue plaques, and the resulting number was multiplied by the dilution factor to give us the total number of plaque forming unites (pfu) per 10 μ L. For each subsequent panning, you want to make sure that each animal is injected with a similar number of pfu intravenously. The phages isolated in panning 1 were injected at 1×10^9 pfu/ μ L of PBS (110 μ L total volume) to animals in the same treatment group in panning 2, and the phages isolated in panning 2 were injected at 1×10^9 pfu/ μ L of PBS (110 μ L total volume) to animals in the same treatment group in panning 3.

A.2.2.3: DNA sequencing

After panning 3, a total of 110 colonies for MyH PhD, 16 colonies for MyH Cont, 110 colonies for PBS PhD, and 16 colonies for PBS Cont were selected for DNA sequencing. Each colony was amplified by polymerase chain reaction (PCR) using unique primers based on the sequence of M13KE: (1) forward/sense: CACCGTTCATCTGTCCTCTTTC, and (1) reverse/antisense: TCACCGTACTCAGGAGGTTTAG (Integrated DNA Technologies). The sequence for each 12 amino acid linear peptide was found in the amplicon created by this primers. Colonies for each treatment group were picked by tapping them with a 10 μ L tip and pipetting up and down into 40 μ L of sterile water. The resulting colonies were then incubated at 95°C for 5 minutes, and spun at 3800 x g for 10

minutes. A total of 1µL each colony solution was amplified for 30-40 cycles using PCR and the primers described above. The presence of the amplicon was verified using a 1% agarose gel with SYBER Safe DNA Gel Stain (Invitrogen). The PCR products were then cleaned up with a QIAquick 96 PCR Purification Kit (Qiagen) according to manufacturer's instructions. Nanodrop 2000c (Thermo Fisher Scientific) was used to quantify the DNA concentration of each amplicon, and the DNA sequence was generated by a DNA sequencer (Eurofins). The peptide sequences were determined using BioEdit Sequence Alignment Editor and further analyzed for homology to known proteins by searching NIH online databases.

A.2.3: Histology, Immunohistochemistry, and Immunofluorescence

At day 21 after induction of EAM, animals were euthanized using CO₂ and the following organs were dissected: heart, lungs, liver, spleen, kidney, and thigh muscle. Similarly, at 3 days after induction of MI, animals were euthanized using CO₂ and the hearts were dissected. To make frozen sections, immediately after dissection samples were placed in OCT compound, frozen with liquid nitrogen, and stored at -80°C. Each sample was then sliced (8µm sections) and the resulting sections were stored at -80°C until use. Before any staining was performed, frozen sections were fixed with ice cold acetone for 5 to 10 minutes. Only frozen sections were made for both animals that underwent MI. To make paraffin embedded sections, immediately after dissection samples were placed in 10% Formalin for 24 hours, and then in 70% ethanol at 4°C for 5 to 7 days until they were paraffin embedded. Each sample was then sliced (5µm sections) and the resulting sections were stored at room temperature until use. Before any staining, two 5 minute Histoclear washes were used to remove the paraffin, and the tissue was then rehydrated through serial 2 minute washes in decreasing concentrations of ethanol (100%, 90%, 70%, 50%, and de-ionized water).

For the assessment of myocarditis severity, frozen and paraffin embedded heart sections were stained with hematoxylin (Thermo Fisher Scientific) and eosin (Thermo Fisher Scientific) (H&E) and mounted with Cytoseal. Each section was then imaged using NanoZoomer SQ (Hamamatsu) and scored for disease severity by investigators blinded to each animal's treatment group in a manner similar to previous reports [62, 64]. Briefly, the left ventricle (LV) was divided into four quadrants. Each quadrant and the right ventricle (RV) were then scored on a scale of 0 to 4, with 0 representing no inflammatory infiltrates, 1 representing small foci of leukocytes between cells, 2 representing larger foci of > 100 leukocytes, 3 representing >10% of the quadrant cross section involved with inflammatory infiltrates, and 4 representing >30% of the quadrant cross section involved with inflammatory infiltrates. The sum of the scores for each LV quadrant and the RV (H&E Sum Score) was then used to classify the severity of myocarditis as follows: no myocarditis: H&E Sum Score ≤ 3 ; mild myocarditis: $4 \leq$ H&E Sum Score ≤ 7 ; and severe myocarditis: H&E Sum Score ≥ 8 .

For assessment of the targeting potential of the peptides identified, custom peptides of each sequence (Table 1) were made with the following modifications: an LC Biotin on the N-terminus, and an amide on the C-terminus (New England Peptide). After fixation with acetone, frozen sections were incubated with proteinase K (5 μ g/mL in PBS, Thermo Fisher Scientific) for 15 minutes at room temperature, blocked with 5% bovine serum albumin (BSA) for 1 hour at room temperature, incubated with biotinylated peptides (10 μ g/mL in PBS, New England Peptide) for 1 hour at room temperature, and incubated with Streptavidin DyLight 650 (10 μ g/mL in PBS, Thermo Fisher Scientific) for 1 hour at room temperature in the dark. Nuclei were then stained with DAPI (1 μ g/mL in PBS) for 10 minutes at room temperature before mounting using Prolong Gold Antifade Reagent

(Invitrogen). Fluorescent imaging of each section was then performed using an Olympus IX71 fluorescent microscope. Each section was then scored for the presence of targeting peptides by investigators blinded to each animal's treatment group in a similar fashion to the H&E disease severity scoring previously described. Briefly, the LV was divided into four quadrants. Each quadrant and the RV were then scored on a scale of 0 to 3, with 0 representing no stained cells, 1 representing few scattered stained cells, 2 representing the presence of a few stained foci, and 3 representing the continuous presence of stained tissue. The sum of the scores for each LV quadrant and the RV (Sum Score of peptide) was used to assess the degree of staining of each peptide, with a Sum Score of peptide > 2 being considered as positive staining.

For assessment of inflammatory infiltrate cell types and the colocalization of these cell types with peptide MyH-PhD-05, frozen sections of the hearts of mice with severe myocarditis were used. After fixation with acetone, frozen sections were incubated with proteinase K (5µg/mL in PBS, Thermo Fisher Scientific) for 15 minutes at room temperature, blocked with 5% BSA for 1 hour at room temperature, and incubated with either CD4 (1:100 dilution in 5% BSA, Bio-Rad Laboratories, MCA4635), CD68 (1:100 dilution in 5% BSA, Bio-Rad Laboratories, MCA1957), or CD11b (1:100 dilution in 5% BSA, eBioscience, 14-0112-81) at 4°C overnight. All sections were then incubated in Goat Anti-Rat Alexa Fluor 488 secondary antibody (1:200 dilution in 5% BSA, Thermo Fisher Scientific, A-11006) for one hour at room temperature in the dark, blocked with 5% BSA for 1 hour at room temperature in the dark, incubated with MyH-PhD-05 biotinylated peptide (100µg/mL in 5% BSA, New England Peptide) for 1 hour at room temperature in the dark, and incubated with Streptavidin DyLight 650 (10µg/mL in 5% BSA, Thermo Fisher Scientific) for 1 hour at room temperature in the dark. Nuclei were then stained with DAPI (1µg/mL in PBS) for 10 minutes at room temperature before mounting using Prolong

Gold Antifade Reagent (Invitrogen). Fluorescent images were acquired using an Olympus IX70 fluorescent microscope. Relative fluorescence from CD4, CD68, and CD11b labeling within inflammatory cell infiltrate of similar sections was measured using Fiji software (Version 1.51n) to calculate the sum of the pixel values and presented as relative light units (RLU). Colocalization analyses between each inflammatory cell marker and MyH-PhD-05 were performed with Fiji software (Version 1.51n) using the Coloc2 function to obtain the Pearson's R value. For each animal, 2 to 3 different fields were analyzed and the average value was reported.

Finally, for the assessment of the targeting potential of MyH-PhD-05 to animals with MI, the frozen sections of the hearts of two animals that underwent MI were used. After fixation with acetone, frozen sections were incubated with proteinase K (5 μ g/mL in PBS, Thermo Fisher Scientific) for 15 minutes at room temperature, blocked with 5% BSA for 1 hour at room temperature, incubated with MyH-PhD-05 biotinylated peptide (100 μ g/mL in 5% BSA, New England Peptide) for 1 hour at room temperature, and incubated with Streptavidin DyLight 650 (10 μ g/mL in 5% BSA, Thermo Fisher Scientific) for 1 hour at room temperature in the dark. Nuclei were then stained with DAPI (1 μ g/mL in PBS) for 10 minutes at room temperature before mounting using Prolong Gold Antifade Reagent (Invitrogen). Fluorescent imaging of each section was then performed using an Olympus IX70 fluorescent microscope.

A.2.4: Peptide Conjugation for *In Vivo* Delivery

To assess the *in vivo* targeting potential of peptides identified, either biotinylated MyH-PhD-05 (New England Peptide, MW = 1762g/mol, 1 μ g/ μ L) or biotinylated MyH-PhD-120 (New England Peptide, MW = 1791g/mol, 1 μ g/ μ L) were incubated with Streptavidin DyLight 650 (Thermo Fisher Scientific, MW = 55,649g/mol, 1 μ g/ μ L) at a 5:1 molar ratio in

PBS at 37°C for 3 hours in the dark. Assuming that four biotinylated peptides bound to each streptavidin, our target for each conjugation reaction was to produce 400µL of compound at a concentration of 400µg/mL. Using a dialysis unit with a 10kDa molecular weight cutoff (Microcon Ultracel), the resulting compound was then dialyzed three times for one hour in 500mL of PBS. Nanodrop 2000c (Thermo Fisher Scientific) was used to determine the final concentration of each resulting compound: S-MyH-PhD-05, and S-MyH-PhD-120. Compounds were stored at -20°C until use.

A.2.5: Ex Vivo Fluorescent Imaging

A total of 63 animals were used for *ex vivo* fluorescent imaging. Briefly, 21 days after induction of EAM, each animal received an IV tail vein injection containing 1100ng of either S-MyH-PhD-05 (n=43) or S-MyH-PhD-120 (n=20) in a total volume of 110µL of PBS. Fifteen minutes after IV injection, animals were euthanized by CO₂, and the heart, lungs, liver, spleen, kidney, and thigh were dissected and immediately imaged using the In Vivo Xtreme Imaging System (Bruker). Fold change in fluorescent signal relative the spleen was reported for each organ of interest.

A.2.6: Echocardiography

Animals were anesthetized using 1-3% isoflurane (Piramal). To assess cardiac function, echocardiography (Vevo 3100 with a MX550D, 22-55MHz probe) was performed prior to sacrifice. All functional evaluations were conducted and analyzed by investigators blinded to the animal's treatment group.

A.2.7: Proteomic Analysis

A total of 9 animals were used in the following treatment groups: animals immunized with MyH/CFA (n=7), and animals immunized with PBS/CFA (n=2). At 21 days, animals were

ethanized using CO₂ and the hearts were dissected and flash frozen. Each heart was then weighted and homogenized in NP40 buffer (Thermo Fisher Scientific) with protease inhibitors (Sigma) and phosphatase inhibitors (Sigma) at 1g of tissue per 1-4mL of NP40 solution. The homogenate was then centrifuged, the pellet discarded, and the concentration measured using a Bradford protein assay (Bio-Rad). Streptavidin conjugated paramagnetic particles (SA-PMPs) (Magnesphere, Promega) were then functionalized with biotinylated MyH-PhD-05 (New England Peptide) according to manufacturer's instructions to a final concentration of 1mg/mL in NP40. For each homogenate, 1000µg of protein were incubated with 100µg of functionalized SA-PMPs for 1.5 hours. After 2 washes with NP40 buffer and 1 wash with PBS, the beads were frozen and sent to Emory Integrated Proteomics Core.

At the Proteomics Core, samples were first homogenized as follows. All samples were vortexed in 300 µL of urea lysis buffer (8M urea, 100 mM NaHPO₄, pH 8.5), including 3 µL (100x stock) HALT protease and phosphatase inhibitor cocktail (Pierce). Next, the samples were briefly centrifuged for 1 minute at 12000 g. Each solution was then treated with 1 mM dithiothreitol (DTT) at 25°C for 30 minutes, followed by 5 mM iodoacetimide (IAA) at 25°C for 30 minutes in the dark. Protein was then digested with 1:50 (w/w) lysyl endopeptidase (Wako) at 25°C overnight. Samples were further digested overnight with 1:50 (w/w) trypsin (Promega) at 25°C. Resulting peptides were desalted with a Sep-Pak C18 column (Waters) and dried under vacuum.

Derived peptides were then resuspended in 10 µL of loading buffer (0.1% formic acid, 0.03% trifluoroacetic acid, 1% acetonitrile). Peptide mixtures (2 µL) were separated on a self-packed C18 (1.9 µm Dr. Maisch, Germany) fused silica column (25 cm x 75 µm internal diameter (ID); New Objective) by a Water's NanoAcquity and monitored on a Q-

Exactive Plus Orbitrap (Thermo Fisher Scientific). Elution was performed over a 100 minute gradient at a rate of 250 nL/minute with buffer B ranging from 3% to 80% (buffer A: 0.1% formic acid in water, buffer B: 0.1 % formic in acetonitrile, both with 5% DMSO). The mass spectrometer (MS) cycle was programmed to collect at the top 10 mode. The MS scans (300-1800 m/z range, 1,000,000 AGC, 100 ms maximum ion time) were collected at a resolution of 70,000 at m/z 200 in profile mode and the HCD MS/MS spectra (17,500 at m/z 200, 2 m/z isolation width, 30% collision energy, 50,000 AGC target, 50 ms maximum ion time). Dynamic exclusion was set to exclude previous sequenced precursor ions for 30 seconds within a 10 ppm window. Precursor ions with +1, and +8 or higher charge states were excluded from sequencing.

Spectra were searched using Proteome Discoverer 2.1 against mouse Uniprot database (53,289 target sequences). Searching parameters included fully tryptic restriction and a parent ion mass tolerance (± 20 ppm) and a product mass tolerance of 0.05 dalton. Methionine oxidation (+15.99492 Da), asparagine and glutamine deamidation (+0.98402 Da) and protein N-terminal acetylation (+42.03670) were variable modifications (up to 3 allowed per peptide); cysteine was assigned a fixed carbamidomethyl modification (+57.021465 Da). Percolator was used to filter the peptide spectrum matches to a false discovery rate of 1%.

All genes that showed at least a two fold increase in the number of peptide spectral matches in at least two animals from the MyH/CFA treatment group when compared to the PBS/CFA treatment group average were selected for enrichment analysis (Appendix Table 1). Enrichment analysis was performed with TopGene (<https://toppgene.cchmc.org>).

A.2.7.1: List of Genes for Enrichment Analysis

Appendix Table 1: List of genes used for enrichment analysis.

#	Protein
1	ACADL (acyl-CoA dehydrogenase, long chain)
2	ACOT1 (acyl-CoA thioesterase 1)
3	ACOT2 (acyl-CoA thioesterase 2)
4	ADH5 (alcohol dehydrogenase 5 (class III), chi polypeptide)
5	AKR1B1 (aldo-keto reductase family 1 member B)
6	ANXA6 (annexin A6)
7	APOA1 (apolipoprotein A1)
8	CKB (creatine kinase B)
9	CMYA5 (cardiomyopathy associated 5)
10	COX7C (cytochrome c oxidase subunit 7C)
11	CPSF6 (cleavage and polyadenylation specific factor 6)
12	CPT2 (carnitine palmitoyltransferase 2)
13	CRAT (carnitine O-acetyltransferase)
14	CSRP1 (cysteine and glycine rich protein 1)
15	DDX46 (DEAD-box helicase 46)
16	DEC1 (2,4-dienoyl-CoA reductase 1)
17	DES (desmin)
18	EDC4 (enhancer of mRNA decapping 4)
19	ENO1 (enolase 1)
20	ENO3 (enolase 3)
21	ETFDH (electron transfer flavoprotein dehydrogenase)
22	FABP3 (fatty acid binding protein 3)
23	FABP4 (fatty acid binding protein 4)
24	FGA (fibrinogen alpha chain)
25	FGG (fibrinogen gamma chain)
26	GDI2 (GDP dissociation inhibitor 2)
27	GLO1 (glyoxalase I)

#	Protein
28	GNAI2 (G protein subunit alpha i2)
29	GNB1 (G protein subunit beta 1)
30	GOT2 (glutamic-oxaloacetic transaminase 2)
31	GSTM2 (glutathione S-transferase mu 2)
32	HADH (hydroxyacyl-CoA dehydrogenase)
33	HIBADH (3-hydroxyisobutyrate dehydrogenase)
34	HNRNPA3 (heterogeneous nuclear ribonucleoprotein A3)
35	HNRNPH2 (heterogeneous nuclear ribonucleoprotein H2)
36	HPX (hemopexin)
37	HSPG2 (heparan sulfate proteoglycan 2)
38	IVD (isovaleryl-CoA dehydrogenase)
39	KRT10 (keratin 10)
40	KRT13 (keratin 13)
41	KRT2 (keratin 2)
42	KRT5 (keratin 5)
43	KRT75 (keratin 75)
44	KRT77 (keratin 77)
45	LUC7L (LUC7 like)
46	MACROD1 (MACRO domain containing 1)
47	MRPL2 (mitochondrial ribosomal protein L2)
48	MRPL40 (mitochondrial ribosomal protein L40)
49	MSN (moesin)
50	MT-CO1 (cytochrome c oxidase subunit I)
51	MYH9 (myosin heavy chain 9)
52	NDUFA3 (NADH:ubiquinone oxidoreductase subunit A3)
53	OAT (ornithine aminotransferase)
54	PDIA3 (protein disulfide isomerase family A member 3)
55	PEBP1 (phosphatidylethanolamine binding protein 1)
56	PGAM1 (phosphoglycerate mutase 1)
57	PGAM2 (phosphoglycerate mutase 2)

#	Protein
58	PGM1 (phosphoglucomutase 1)
59	PGM2 (phosphoglucomutase 2)
60	PPA1 (pyrophosphatase (inorganic) 1)
61	PPIA (peptidylprolyl isomerase A)
62	PRDX3 (peroxiredoxin 3)
63	PRSS1 (protease, serine 1)
64	RBM39 (RNA binding motif protein 39)
65	RPL23A (ribosomal protein L23a)
66	RPL26 (ribosomal protein L26)
67	RPS27A (ribosomal protein S27a)
68	SFRP1 (secreted frizzled related protein 1)
69	SOD2 (superoxide dismutase 2)
70	TF (transferrin)
71	TFAM (transcription factor A, mitochondrial)
72	TNNC1 (troponin C1, slow skeletal and cardiac type)
73	U2AF1 (U2 small nuclear RNA auxiliary factor 1)
74	U2AF2 (U2 small nuclear RNA auxiliary factor 2)
75	UBA1 (ubiquitin like modifier activating enzyme 1)

A.2.8: Statistical Analysis

All data were analyzed with GraphPad Prism 5. Data are represented as a box and whiskers, with median values represented by the horizontal line, 25% to 75% percentiles by the box, and the range of values by the whiskers. Where appropriate, a two-way ANOVA, one-way ANOVA, or unpaired t-test was performed. Values in the text are expressed as mean \pm standard error of the mean.

REFERENCES

1. Mozaffarian, D., et al., *Heart disease and stroke statistics--2015 update: a report from the American Heart Association*. Circulation, 2015. **131**(4): p. e29-322.
2. Go, A.S., et al., *Heart disease and stroke statistics--2014 update: a report from the American Heart Association*. Circulation, 2014. **129**(3): p. e28-e292.
3. Krishna, S.M., J.V. Moxon, and J. Golledge, *A review of the pathophysiology and potential biomarkers for peripheral artery disease*. International Journal of Molecular Sciences, 2015. **16**(5): p. 11294-322.
4. Germani, A., et al., *Regenerative therapy in peripheral artery disease*. Cardiovascular Therapeutics, 2009. **27**(4): p. 289-304.
5. Hughes, G.C. and B.H. Annex, *Angiogenic Therapy for Coronary Artery and Peripheral Artery Disease*. Expert Review of Cardiovascular Therapy, 2005. **3**(3): p. 521-535.
6. Attanasio, S. and J. Snell, *Therapeutic angiogenesis in the management of critical limb ischemia: current concepts and review*. Cardiology in Review, 2009. **17**(3): p. 115-20.
7. Zachary, I. and R.D. Morgan, *Therapeutic angiogenesis for cardiovascular disease: biological context, challenges, prospects*. Heart, 2011. **97**(3): p. 181-9.
8. Epstein, S.E., et al., *Angiogenesis Therapy : Amidst the Hype, the Neglected Potential for Serious Side Effects*. Circulation, 2001. **104**(1): p. 115-119.
9. Biesbroek, P.S., et al., *Diagnosis of myocarditis: Current state and future perspectives*. International Journal of Cardiology, 2015. **191**: p. 211-9.
10. Han, L., et al., *Experimental drugs for treatment of autoimmune myocarditis*. Chinese Medical Journal, 2014. **127**(15): p. 2850-9.
11. Hazebroek, M., R. Dennert, and S. Heymans, *Virus infection of the heart--unmet therapeutic needs*. Antiviral Chemistry and Chemotherapy, 2012. **22**(6): p. 249-53.

12. Levine, M.C., D. Klugman, and S.J. Teach, *Update on myocarditis in children*. *Current Opinion in Pediatrics*, 2010. **22**(3): p. 278-83.
13. Aggarwal, S., R.S. Loomba, and R. Arora, *Preventive aspects in peripheral artery disease*. *Therapeutic Advances in Cardiovascular Disease*, 2012. **6**(2): p. 53-70.
14. Aggarwal, S., et al., *Rehabilitation Therapy in Peripheral Arterial Disease*. *Canadian Journal of Cardiology*, 2016. **32**(10S2): p. S374-S381.
15. Peach, G., et al., *Diagnosis and management of peripheral arterial disease*. *BMJ*, 2012. **345**(aug14 1): p. e5208-e5208.
16. Thiruvoipati, T., C.E. Kielhorn, and E.J. Armstrong, *Peripheral artery disease in patients with diabetes: Epidemiology, mechanisms, and outcomes*. *World Journal of Diabetes*, 2015. **6**(7): p. 961-9.
17. Lippi, G., M. Franchini, and G. Targher, *Arterial thrombus formation in cardiovascular disease*. *Nature Reviews Cardiology*, 2011. **8**(9): p. 502-12.
18. Badimon, L. and G. Vilahur, *Thrombosis formation on atherosclerotic lesions and plaque rupture*. *Journal of Internal Medicine*, 2014. **276**(6): p. 618-32.
19. Scott, R.C., et al., *Targeting VEGF-encapsulated immunoliposomes to MI heart improves vascularity and cardiac function*. *The FASEB Journal*, 2009. **23**(10): p. 3361-7.
20. Anversa, P., *Myocyte Death in the Pathological Heart*. *Circulation Research*, 2000. **86**(2): p. 121-124.
21. Dasari, M., et al., *Hoechst-IR: An Imaging Agent That Detects Necrotic Tissue in Vivo by Binding Extracellular DNA*. *Organic Letters*, 2010. **12**(15): p. 3300-3303.
22. van der Meer, F.J., et al., *Apoptosis- and necrosis-induced changes in light attenuation measured by optical coherence tomography*. *Lasers in Medical Science*, 2010. **25**(2): p. 259-67.
23. Khan, R.S., et al., *Targeting extracellular DNA to deliver IGF-1 to the injured heart*. *Scientific Reports*, 2014. **4**: p. 4257.

24. Ye, Z., et al., *An electronic medical record-linked biorepository to identify novel biomarkers for atherosclerotic cardiovascular disease*. *Global Cardiology Science and Practice*, 2013. **2013**(1): p. 82-90.
25. Shimony, A., et al., *Cell free DNA detected by a novel method in acute ST-elevation myocardial infarction patients*. *Acute Cardiac Care*, 2010. **12**(3): p. 109-11.
26. Webber, M.J., et al., *Supramolecular nanostructures that mimic VEGF as a strategy for ischemic tissue repair*. *Proceedings of the National Academy of Sciences of the United States of America*, 2011. **108**(33): p. 13438-13443.
27. Borselli, C., et al., *Functional muscle regeneration with combined delivery of angiogenesis and myogenesis factors*. *Proceedings of the National Academy of Sciences of the United States of America*, 2010. **107**(8): p. 3287-92.
28. Patel, M.R., et al., *Evaluation and treatment of patients with lower extremity peripheral artery disease: consensus definitions from Peripheral Academic Research Consortium (PARC)*. *Journal of the American College of Cardiology*, 2015. **65**(9): p. 931-41.
29. Shishehbor, M.H., et al., *Critical Limb Ischemia: An Expert Statement*. *Journal of the American College of Cardiology*, 2016. **68**(18): p. 2002-2015.
30. Mac Gabhann, F., et al., *Systems biology of pro-angiogenic therapies targeting the VEGF system*. *Wiley Interdisciplinary Reviews: Systems Biology and Medicine*, 2010. **2**(6): p. 694-707.
31. Lederman, R.J., et al., *Therapeutic angiogenesis with recombinant fibroblast growth factor-2 for intermittent claudication (the TRAFFIC study): a randomised trial*. *The Lancet*, 2002. **359**(9323): p. 2048-2050.
32. Vera Janavel, G.L., et al., *Effect of vascular endothelial growth factor gene transfer on infarct size, left ventricular function and myocardial perfusion in sheep after 2 months of coronary artery occlusion*. *The Journal of Gene Medicine*, 2012. **14**(4): p. 279-87.
33. Zhang, J., et al., *Collagen-targeting vascular endothelial growth factor improves cardiac performance after myocardial infarction*. *Circulation*, 2009. **119**(13): p. 1776-84.

34. Takahashi, S., *Vascular Endothelial Growth Factor (VEGF), VEGF Receptors and Their Inhibitors for Antiangiogenic Tumor Therapy*. Biological and Pharmaceutical Bulletin, 2011. **34**(12): p. 1785-1788.
35. Zisa, D., et al., *Intramuscular VEGF repairs the failing heart: role of host-derived growth factors and mobilization of progenitor cells*. American Journal of Physiology: Regulatory, Integrative and Comparative Physiology, 2009. **297**: p. R1503-R1515.
36. Silva, E.A. and D.J. Mooney, *Spatiotemporal control of vascular endothelial growth factor delivery from injectable hydrogels enhances angiogenesis*. Journal of Thrombosis and Haemostasis, 2007. **5**: p. 590-598.
37. Mulyasmita, W., et al., *Avidity-controlled hydrogels for injectable co-delivery of induced pluripotent stem cell-derived endothelial cells and growth factors*. Journal of Controlled Release, 2014.
38. Kim, P.H., et al., *Injectable multifunctional microgel encapsulating outgrowth endothelial cells and growth factors for enhanced neovascularization*. Journal of Controlled Release, 2014.
39. Lee, J., et al., *Active blood vessel formation in the ischemic hindlimb mouse model using a microsphere/hydrogel combination system*. Pharmaceutical Research, 2010. **27**(5): p. 767-74.
40. Xie, J., et al., *Induction of angiogenesis by controlled delivery of VEGF using nanoparticles*. Cardiovascular Therapeutics, 2012.
41. Seshadri, G., et al., *The delivery of superoxide dismutase encapsulated in polyketal microparticles to rat myocardium and protection from myocardial ischemia-reperfusion injury*. Biomaterials, 2010. **31**(6): p. 1372-9.
42. Isner, J.M., et al., *Arterial Gene Therapy for Therapeutic Angiogenesis With Peripheral Artery Disease*. Circulation, 1995. **91**(11): p. 2687-2692.
43. White, C.J. and W.A. Gray, *Endovascular therapies for peripheral arterial disease: an evidence-based review*. Circulation, 2007. **116**(19): p. 2203-15.
44. Post, M.J., et al., *Therapeutic angiogenesis in cardiology using protein formulations*. Cardiovascular Research, 2001. **49**: p. 522-531.

45. Koch, S., et al., *Signal transduction by vascular endothelial growth factor receptors*. Biochemical Journal, 2011. **437**(2): p. 169-83.
46. Keyt, B.A., et al., *Identification of Vascular Endothelial Growth Factor Determinants for Binding KDR and FLT-1 Receptors*. The Journal of Biological Chemistry, 1996. **271**(10): p. 5638-5646.
47. Takahashi, T., et al., *A single autophosphorylation site on KDR/Flk-1 is essential for VEGF-A-dependent activation of PLC-gamma and DNA synthesis in vascular endothelial cells*. The EMBO Journal, 2001. **20**(11): p. 2768-78.
48. Mebratu, Y. and Y. Tesfaigzi, *How ERK1/2 activation controls cell proliferation and cell death: Is subcellular localization the answer?* Cell Cycle, 2009. **8**(8): p. 1168-75.
49. Neidle, S., *DNA minor-groove recognition by small molecules (up to 2000)*. Natural Product Reports, 2001. **18**(3): p. 291-309.
50. Patel, S.R., et al., *Phase I-II study of pibenzimol hydrochloride (NSC 322921) in advanced pancreatic carcinoma*. Investigational New Drugs, 1991. **9**: p. 53-57.
51. Kraut, E.H., et al., *Phase II study of pibenzimol in pancreatic cancer*. Investigational New Drugs, 1991. **9**: p. 95-96.
52. Cooper, L.T., Jr., et al., *The global burden of myocarditis: part 1: a systematic literature review for the Global Burden of Diseases, Injuries, and Risk Factors 2010 study*. Global Heart, 2014. **9**(1): p. 121-9.
53. Fung, G., et al., *Myocarditis*. Circulation Research, 2016. **118**(3): p. 496-514.
54. Epelman, S., P.P. Liu, and D.L. Mann, *Role of innate and adaptive immune mechanisms in cardiac injury and repair*. Nature Reviews Immunology, 2015. **15**(2): p. 117-29.
55. Cihakova, D. and N.R. Rose, *Pathogenesis of myocarditis and dilated cardiomyopathy*. Advances in Immunology, 2008. **99**: p. 95-114.
56. Bergmann, K.R., A. Kharbada, and L. Haveman, *Myocarditis And Pericarditis In The Pediatric Patient: Validated Management Strategies*. Pediatric Emergency Medicine Practice, 2015. **12**(7): p. 1-22; quiz 23.

57. Das, B.B., *Role of endomyocardial biopsy for children presenting with acute systolic heart failure*. Pediatric Cardiology, 2014. **35**(2): p. 191-6.
58. Maisch, B. and S. Pankuweit, *Standard and etiology-directed evidence-based therapies in myocarditis: state of the art and future perspectives*. Heart Failure Reviews, 2013. **18**(6): p. 761-95.
59. May, L.J., D.J. Patton, and D.S. Fruitman, *The evolving approach to paediatric myocarditis: a review of the current literature*. Cardiology in the Young, 2011. **21**(3): p. 241-51.
60. Luetkens, J.A., et al., *Comprehensive Cardiac Magnetic Resonance for Short-Term Follow-Up in Acute Myocarditis*. Journal of the American Heart Association, 2016. **5**(7).
61. Pophal, S.G., et al., *Complications of endomyocardial biopsy in children*. Journal of the American College of Cardiology, 1999. **34**(7): p. 2105-10.
62. van Heeswijk, R.B., et al., *Selective in vivo visualization of immune-cell infiltration in a mouse model of autoimmune myocarditis by fluorine-19 cardiac magnetic resonance*. Circulation Cardiovascular Imaging, 2013. **6**(2): p. 277-84.
63. Chames, P., et al., *Therapeutic antibodies: successes, limitations and hopes for the future*. British Journal of Pharmacology, 2009. **157**(2): p. 220-33.
64. Steinl, D.C., et al., *Noninvasive Contrast-Enhanced Ultrasound Molecular Imaging Detects Myocardial Inflammatory Response in Autoimmune Myocarditis*. Circulation Cardiovascular Imaging, 2016. **9**(8).
65. Leslie-Barbick, J.E., et al., *The promotion of microvasculature formation in poly(ethylene glycol) diacrylate hydrogels by an immobilized VEGF-mimetic peptide*. Biomaterials, 2011. **32**(25): p. 5782-9.
66. D'Andrea, L.D., et al., *Targeting Angiogenesis: Structural Characterization and Biological Properties of a de novo Engineered VEGF Mimicking Peptide*. Proceedings of the National Academy of Sciences of the United States of America, 2005. **102**(40): p. 14215-14220.
67. Santulli, G., et al., *In vivo properties of the proangiogenic peptide QK*. Journal of Translational Medicine, 2009. **7**: p. 41.

68. Dasari, M., et al., *Hoechst-IR: An Imaging Agent That Detects Necrotic Tissue in Vivo by Binding Extracellular DNA*. *Organic Letters*, 210. **12**(15): p. 3300-3303.
69. Ebright, Y.W., et al., *S-[2-(4-Azidosalicylamido)ethylthio]-2-thiopyridine: Radioiodinatable, Cleavable, Photoactivatable Cross-Linking Agent*. *Bioconjugate Chemistry*, 1996. **7**(3): p. 380-384.
70. Olson, E.S., et al., *Activatable cell penetrating peptides linked to nanoparticles as dual probes for in vivo fluorescence and MR imaging of proteases*. *Proceedings of the National Academy of Sciences of the United States of America*, 2010. **107**(9): p. 4311-6.
71. Chalothorn, D., et al., *Collateral density, remodeling, and VEGF-A expression differ widely between mouse strains*. *Physiological Genomics*, 2007. **30**(2): p. 179-191.
72. Couffignal, T., et al., *Mouse model of angiogenesis*. *American Journal of Pathology*, 1998. **152**(6): p. 1667-1679.
73. Hodara, R., et al., *Overexpression of catalase in myeloid cells causes impaired postischemic neovascularization*. *Arteriosclerosis, Thrombosis, and Vascular Biology*, 2011. **31**(10): p. 2203-9.
74. Limbourg, A., et al., *Evaluation of postnatal arteriogenesis and angiogenesis in a mouse model of hind-limb ischemia*. *Nature Protocols*, 2009. **4**(12): p. 1737-46.
75. Czeiger, D., et al., *Measurement of circulating cell-free DNA levels by a new simple fluorescent test in patients with primary colorectal cancer*. *American Journal of Clinical Pathology*, 2011. **135**(2): p. 264-70.
76. Lin, K.T., et al., *Bp5250 inhibits vascular endothelial growth factor-induced angiogenesis and HIF-1 α expression on endothelial cells*. *Naunyn-Schmiedeberg's Archives of Pharmacology*, 2012. **385**(1): p. 39-49.
77. Vaishya, R., et al., *Long-term delivery of protein therapeutics*. *Expert Opinion on Drug Delivery*, 2015. **12**(3): p. 415-40.
78. Schmidt, J., et al., *Alginate Sulfates Mitigate Binding Kinetics of Proangiogenic Growth Factors with Receptors toward Revascularization*. *Molecular Pharmaceutics*, 2016. **13**(7): p. 2148-54.

79. Arnaoutova, I. and H.K. Kleinman, *In vitro angiogenesis: endothelial cell tube formation on gelled basement membrane extract*. Nature Protocols, 2010. **5**(4): p. 628-35.
80. Waters, R.E., et al., *Preclinical models of human peripheral arterial occlusive disease: implications for investigation of therapeutic agents*. Journal of Applied Physiology, 2004. **97**(2): p. 773-80.
81. Jazwa, A., et al., *Limb ischemia and vessel regeneration: Is there a role for VEGF?* Vascular Pharmacology, 2016. **86**: p. 18-30.
82. Bocci, V., *Catabolism of therapeutic proteins and peptides with implications for drug delivery*. Advanced Drug Delivery Reviews, 1989. **4**: p. 149-169.
83. Katsila, T., A.P. Siskos, and C. Tamvakopoulos, *Peptide and protein drugs: the study of their metabolism and catabolism by mass spectrometry*. Mass Spectrometry Reviews, 2012. **31**(1): p. 110-33.
84. Mahmood, I. and M.D. Green, *Pharmacokinetic and Pharmacodynamic Considerations in the Development of Therapeutic Proteins*. Clinical Pharmacokinetics, 2005. **44**(4): p. 331-347.
85. Fosgerau, K. and T. Hoffmann, *Peptide therapeutics: current status and future directions*. Drug Discovery Today, 2015. **20**(1): p. 122-8.
86. Mahmood, I., *Pharmacokinetic Considerations in Designing Pediatric Studies of Proteins, Antibodies, and Plasma-Derived Products*. American Journal of Therapeutics, 2016. **23**: p. e1043-e1056.
87. Shah, D.K., *Pharmacokinetic and pharmacodynamic considerations for the next generation protein therapeutics*. Journal of Pharmacokinetics and Pharmacodynamics, 2015. **42**(5): p. 553-71.
88. Hofmeister, L.H., et al., *Phage-display-guided nanocarrier targeting to atheroprone vasculature*. ACS Nano, 2015. **9**(4): p. 4435-46.
89. Kanki, S., et al., *Identification of targeting peptides for ischemic myocardium by in vivo phage display*. Journal of Molecular and Cellular Cardiology, 2011. **50**(5): p. 841-8.

90. Kelly, K.A., et al., *In vivo phage display selection yields atherosclerotic plaque targeted peptides for imaging*. *Molecular Imaging and Biology*, 2006. **8**(4): p. 201-7.
91. Babickova, J., et al., *In vivo phage display--a discovery tool in molecular biomedicine*. *Biotechnology Advances*, 2013. **31**(8): p. 1247-59.
92. Han, Z., et al., *EDB Fibronectin Specific Peptide for Prostate Cancer Targeting*. *Bioconjugate Chemistry*, 2015.
93. Yuan, J., et al., *Autophagy contributes to IL-17-induced plasma cell differentiation in experimental autoimmune myocarditis*. *International Immunopharmacology*, 2014. **18**(1): p. 98-105.
94. Zempo, H., et al., *A P2X7 receptor antagonist attenuates experimental autoimmune myocarditis via suppressed myocardial CD4 T and macrophage infiltration and NADPH oxidase 2/4 expression in mice*. *Heart and Vessels*, 2014.
95. Tada, Y., et al., *Neovascularization induced by hypoxia inducible transcription factor is associated with the improvement of cardiac dysfunction in experimental autoimmune myocarditis*. *Expert Opinion on Investigational Drugs*, 2014. **23**(2): p. 149-62.
96. Su, Z., et al., *Up-regulated HMGB1 in EAM directly led to collagen deposition by a PKCbeta/Erk1/2-dependent pathway: cardiac fibroblast/myofibroblast might be another source of HMGB1*. *Journal of Cellular and Molecular Medicine*, 2014. **18**(9): p. 1740-51.
97. Pummerer, C.L., et al., *Identification of cardiac myosin peptides capable of inducing autoimmune myocarditis in BALB/c mice*. *Journal of Clinical Investigation*, 1996. **97**(9): p. 2057-62.
98. Ong, S., et al., *Natural killer cells limit cardiac inflammation and fibrosis by halting eosinophil infiltration*. *American Journal of Pathology*, 2015. **185**(3): p. 847-61.
99. Myers, J.M., et al., *Autoimmune myocarditis, valvulitis, and cardiomyopathy*. *Current Protocols in Immunology*, 2013. **Chapter 15**: p. Unit 15 14 1-51.
100. Ahn, D., et al., *Induction of myocardial infarcts of a predictable size and location by branch pattern probability-assisted coronary ligation in C57BL/6 mice*. *American Journal of Physiology: Heart and Circulatory Physiology*, 2004. **286**(3): p. H1201-7.

101. Wang, J., et al., *A simple and fast experimental model of myocardial infarction in the mouse*. Texas Heart Institute Journal, 2006. **33**(3): p. 290-3.
102. Bami, K., et al., *Noninvasive imaging in acute myocarditis*. Current Opinion in Cardiology, 2016. **31**(2): p. 217-23.
103. Brett, N.J., W.E. Strugnell, and R.E. Slaughter, *Acute myocarditis demonstrated on CT coronary angiography with MRI correlation*. Circulation Cardiovascular Imaging, 2011. **4**(3): p. e5-6.
104. Hsiao, J.F., et al., *Speckle tracking echocardiography in acute myocarditis*. International Journal of Cardiovascular Imaging, 2013. **29**(2): p. 275-84.
105. Friedrich, M.G. and F. Marcotte, *Cardiac magnetic resonance assessment of myocarditis*. Circulation Cardiovascular Imaging, 2013. **6**(5): p. 833-9.
106. Schumm, J., et al., *Cardiovascular magnetic resonance risk stratification in patients with clinically suspected myocarditis*. Journal of Cardiovascular Magnetic Resonance, 2014. **16**(14).
107. Mavrogeni, S., G. Markousis-Mavrogenis, and G. Kolovou, *How to approach the great mimic? Improving techniques for the diagnosis of myocarditis*. Expert Review of Cardiovascular Therapy, 2016. **14**(1): p. 105-15.
108. Kolodziej, A.F., et al., *Peptide optimization and conjugation strategies in the development of molecularly targeted magnetic resonance imaging contrast agents*. Methods in Molecular Biology, 2014. **1088**: p. 185-211.
109. Liu, J., et al., *Novel peptide-dendrimer conjugates as drug carriers for targeting nonsmall cell lung cancer*. International Journal of Nanomedicine, 2011. **6**: p. 59-69.
110. Xitong, D. and Z. Xiaorong, *Targeted therapeutic delivery using engineered exosomes and its applications in cardiovascular diseases*. Gene, 2016. **575**(2 Pt 2): p. 377-84.
111. Gong, X., et al., *Attenuation of Experimental Autoimmune Myocarditis by si-RNA Mediated CD40 Silencing*. International Heart Journal, 2014. **55**(6): p. 539-45.
112. Leuschner, F., et al., *Silencing of CCR2 in myocarditis*. European Heart Journal, 2014.

113. Krishna, S.M., S.M. Omer, and J. Golledge, *Evaluation of the clinical relevance and limitations of current pre-clinical models of peripheral artery disease*. *Clinical Science*, 2016. **130**(3): p. 127-50.
114. Pellegrin, M., et al., *Experimental peripheral arterial disease: new insights into muscle glucose uptake, macrophage, and T-cell polarization during early and late stages*. *Physiology Reports*, 2014. **2**(2): p. e00234.
115. Basso, C., et al., *Classification and histological, immunohistochemical, and molecular diagnosis of inflammatory myocardial disease*. *Heart Failure Reviews*, 2013. **18**(6): p. 673-81.
116. Eriksson, U., et al., *Dendritic cell-induced autoimmune heart failure requires cooperation between adaptive and innate immunity*. *Nature Medicine*, 2003. **9**(12): p. 1484-90.
117. Hendry, R.G., L.M. Bilawchuk, and D.J. Marchant, *Targeting matrix metalloproteinase activity and expression for the treatment of viral myocarditis*. *Journal of Cardiovascular Translational Research*, 2014. **7**(2): p. 212-25.
118. Villanueva, F.S., *Molecular imaging of cardiovascular disease using ultrasound*. *Journal of Nuclear Cardiology*, 2008. **15**(4): p. 576-86.
119. Caravan, P., et al., *Collagen-targeted MRI contrast agent for molecular imaging of fibrosis*. *Angewandte Chemie International Edition*, 2007. **46**(43): p. 8171-3.
120. Overoye-Chan, K., et al., *EP-2104R: a fibrin-specific gadolinium-Based MRI contrast agent for detection of thrombus*. *Journal of the American Chemical Society*, 2008. **130**(18): p. 6025-39.
121. Beltrami, A.P., et al., *Adult cardiac stem cells are multipotent and support myocardial regeneration*. *Cell*, 2003. **114**(6): p. 763-76.